



**GEOLOGICAL SURVEY OF CANADA
COMMISSION GÉOLOGIQUE DU CANADA**

Open File 3220

**PETROGRAPHIC AND GEOCHEMICAL
ANALYSES OF BEAUFORT-MACKENZIE
BASIN SHALES**

J. Bloch
and
D.R. Issler

Geological Survey of Canada (Calgary)
3303 33 Street N.W.
Calgary, Alberta
T2L 2A7

FEBRUARY 1996

Although every effort has been made to ensure accuracy, this Open File Report has not been edited for conformity with Geological Survey of Canada standards.

TABLE OF CONTENTS

TABLE OF CONTENTS	2
LIST OF FIGURES	3
EXECUTIVE SUMMARY	4
INTRODUCTION	5
METHODS	6
RESULTS.....	7
PETROGRAPHY.....	7
Normally Pressured Samples	8
Overpressured Samples	11
GEOCHEMISTRY	13
Organic Matter and Maturity Trends.....	13
Inorganic Geochemistry and Mineralogy	15
DISCUSSION.....	18
CONCLUSIONS	20
REFERENCES	22
FIGURES.....	24
APPENDIX A.....	41
APPENDIX B.....	65

LIST OF FIGURES

Figure 01 - A) Pseudo Van Krevelen diagram and B) C-S data	24
Figure 02 - T_{\max} versus Depth A) present, B) maximum	25
Figure 03 - T_{\max} (A) and Depth (B) versus PI	26
Figure 04A - Diffractograms of O09061 ($<2\mu\text{m}$)	27
Figure 04B - Diffractograms of A06071 ($<2\mu\text{m}$)	28
Figure 05 - Calculated clay abundances	29
Figure 06 - Whole-rock diffractograms	30
Figure 07 - Calculated quartz abundances	31
Figure 08 - Calculated siderite and pyrite abundances	32
Figure 09 - Mineral abundances versus Depth	33
Figure 10 - Fe - S systematics (A) and Fe- minerals vs. Depth (B)	34
Figure 11 - $\%K_2O$ versus Depth	35
Figure 12 - Element ratio diagram (K/Al vs. Si/Al)	36
Figure 13 - Porosity versus Depth	37
Figure 14 - XRD characteristics of I/S with depth	38
Figure 15 - Porosity versus Density	39
Figure 16 - Fe-mineral abundance vs. Matrix Density	40

EXECUTIVE SUMMARY

This reports records the results of a petrographic and geochemical investigation of 41 shale core samples from the Beaufort - Mackenzie Basin. This work was carried out in conjunction with other investigations to evaluate controls on porosity and permeability trends within hydrocarbon bearing zones of the Beaufort - Mackenzie Basin. The data presented herein will be used to better calibrate wireline data that may then be used in hydrocarbon exploration and exploitation strategies.

This report contains extensive petrographic documentation of Beaufort - Mackenzie shale fabrics and geochemical data that includes bulk, mineralogical and organic matter compositions. Results of this investigation indicate that the shales of the Beaufort - Mackenzie Basin are relatively homogeneous and that diagenetic effects are minor. Sorting and rate of deposition of sediments are controlling factors in the subsequent compaction behaviour and resulting porosity loss. Sample density and porosity characteristics are controlled primarily by compaction with minimal diagenetic effects.

INTRODUCTION

With recent advances in basin modeling techniques, the need for data to calibrate model variables is increasing dramatically. Shales comprise the bulk of most basin fill but our knowledge regarding shale composition and compactional behaviour lags behind that of coarser clastics and carbonates. Determination of the petrophysical properties of shales is commonly done indirectly using wireline log data and sediment compaction trends have been shown to be variable from basin to basin (e.g. Rieke and Chilingarian, 1974; Gallagher, 1989; Gautier and Schmoker, 1989). Wireline signatures may be compositionally sensitive, particularly with respect to organic matter (Passey et al., 1990), and therefore direct measurement of shale compositions, porosity and permeability are necessary to calibrate wireline data.

A recent study of the log-derived compaction characteristics of Beaufort - Mackenzie basin shales identified a significant correlation between compaction trends and sedimentation rate, overpressuring, and overburden removal (Issler, 1992). Follow-up studies (Katsube and Issler, 1993; Issler and Katsube, 1994) are in progress to measure the porosity, permeability, sonic velocity, electrical and thermal conductivity and composition of the same Beaufort - Mackenzie basin shales. This report documents chemical and mineralogical trends within the thick sequence of overpressured and normally pressured shales studied by Issler (1992). In addition, extensive petrographic data are presented to clarify compaction and diagenetic effects on rock fabric and porosity and permeability trends.

In this study, the term shale is used as a *class* name to define a group of rock types that contain greater than 50% of terrigenous and/or argillaceous material less than 0.062 mm in size (Potter et al., 1980). Shales may be further subdivided according to the silt and clay content as follows: siltstone - contains greater than

65% silt-sized material (0.004 to 0.062 mm), mudstone - contains between 33 and 65% silt-sized material, and claystone - contains less than 33% silt-sized material.

METHODS

Forty-one samples from nine drill cores were selected for chemical, petrophysical and petrographic analyses. Samples were selected to represent the different compaction zones of the Beaufort-Mackenzie basin as described by Issler (1992). Core locations are given in Issler and Katsube (1994).

Total organic carbon (TOC) content was determined by Rock-Eval pyrolysis (Espitalié et al., 1977; Peters, 1986). This method also provides estimates of organic matter maturity (pyrolysis temperature of maximum hydrocarbon generation - T_{max} and production index - PI) and type (hydrogen index - HI and oxygen index - OI). Bulk mineralogy was characterized by powder X-ray diffraction (XRD). Clay mineralogy was characterized by XRD on oriented $< 2\mu m$ separates using standard treatments (Moore and Reynolds, 1989). Major element chemistry was determined by X-ray fluorescence (XRF). Total carbon and sulphur analyses were determined by combustion. Major element chemistry by XRF was also done on $< 2\mu m$ separates to determine clay mineral compositions. Details of the analytical procedures and precision are given elsewhere (Baedeker, 1987; Bloch, 1994).

Petrographic analysis was done on a Cambridge 150 scanning electron microscope with a 2 kV threshold backscatter detector at 30 kV and a working distance of 13 mm. Samples were epoxy impregnated, polished, and carbon coated. Qualitative mineral identification was done by energy dispersive X-ray (EDX) analysis.

Mineral modes were calculated from the bulk chemical data using the program LPNORM (Caritat et al., 1994a). This method uses linear programming

and an objective function that maximizes mineral yield and minimizes residual amounts of the constituent oxides. Maximizing the abundance of a particular mineral(s) may also be included as an additional constraint. Iterative calculations are performed and mineral compositions may be altered to achieve maximum mineral yields and minimize residuals.

Linear programming requires the composition of a mineral as input and this presents problems for mixtures of minerals with variable compositions, particularly clay minerals. Unless pure clay mineral separates are analyzed, clay mineral compositions must be estimated from mixtures. Beaufort - Mackenzie clay fractions (<2 micrometers in size) generally contain four mineral phases, two of which (mixed-layer I/S and chlorite) have variable compositions. Quartz and kaolinite are usually the other mineral phases present and their compositions are considered ideal SiO_2 and $\text{Al}_2\text{Si}_2\text{O}_5(\text{OH})_4$, respectively. Minor amounts of illite and muscovite may also be present. Initially, to approximate mixed-layer clay compositions, chemical data from Ko (1992) was used. These data comprise elemental abundances of the <0.05 micrometer fraction, which may not be representative of the entire clay fraction of the rock.

RESULTS

Data presentation is divided into two sections describing petrographic and geochemical characteristics. Because of the large number of SEM photomicrographs (96), they have been placed in an appendix (Appendix A). Data tables (6) are in Appendix B.

PETROGRAPHY

The textural characteristics of Beaufort - Mackenzie shales may be determined by, 1) primary compositional variations that include grain size

distribution and sorting, mineralogy and the degree of bioturbation, 2) diagenetic processes that produce neoformed minerals, primarily as cement and discrete authigenic phases, and 3) compaction effects. The effect of these controls on porosity, permeability and density of these rocks are evaluated by examining a suite of samples that includes normally pressured and overpressured shales from present burial depths of about 1500 to over 4800 m. Porosity, permeability and density data are from Issler and Katsube (1994).

Normally Pressured Samples

Two representative samples at less than 2000 m present burial depth show a wide range of fabrics with minimal compaction effects. Samples D27042 (1469 m) and O09031 (1765 m) have measured porosities of 12 % and about 30 % and bulk densities of 2.34 and 1.78 g/cm³, respectively. D27042 is a framework-supported siltstone (Plate 1). Framework grains are dominantly coarse silt- to fine sand-sized angular to sub-angular quartz and chert (Plate 1A) with minor amounts of K-feldspar, organic matter (1B) and possibly bioclasts (1C) (foraminifera?). Matrix components include clay-sized quartz, illite, kaolinite and authigenic siderite (1D). Siderite is preferentially nucleated about organic stringers or "clasts" (1B). Detrital micas commonly show a uniform, dull reflectance and low K content (as determined by EDX) that are interpreted to be the result of weathering (1C and 1D).

Large areas of sample O09031 have a poor polish and are badly plucked (2A). This may result from a compositional or textural control and the images obtained from this sample may not be completely representative. However, where good quality images are obtained, they show the fine-grained and texturally homogeneous nature of this sample and compaction effects are minimal (Plates 2 and 3). Maximum grain-size is fine silt and the silt/clay ratio is much lower than in sample D27042 (Plates 1A and 2A) indicating that O09031 is a claystone. Silt

grains are angular to sub-rounded, fairly well-sorted, and matrix supported (Plates 2 and 3). Similar to D27042, most mica grains have a dull reflectance and are interpreted to be weathered to an illitic composition (Plates 2 and 3). The organic matter content is much higher than in D27042 (Plate 2). Rock-Eval data indicate that the TOC content of this sample is anomalously high (Table 1) and primarily Type III in origin. Petrographic evidence of Type III organic matter includes sideritized rootlets (Plate 3C and D).

Samples G33101 and G33102 (Plates 4 - 6) are characterized as framework (Plate 4) to matrix (Plate 6) supported mudstones. With increasing depth, framework grains, particularly micas, develop a compaction induced, bedding-parallel fabric (Plates 4, 5 and 6). Commonly, grains show tangential (Plate 4B) or concavo-convex contacts (Plate 5A) and detrital micas show a distinct, bedding-parallel orientation (Plate 4A). Exceptions to this occur where sand-size grains are present (Plates 5A and 6B). Within fine silt- to clay-sized matrix, detrital clay or mica laths show preferred orientation (Plates 4 and 6) but with decreasing grain size, laths tend to become less well oriented (Plates 6C and D). Density in these samples (G33101 and G33102, 2460 and 2461 m depth, respectively) increases to approximately 2.50 g/cm³ and measured porosities decrease to between 7 and 10%.

With the exception of abundant pyrite (Plates 4 - 6), these samples are similar in composition to those at shallower depths. The pyrite is largely framboidal indicating authigenesis from sulphate reduction. The homogeneous distribution suggests relatively low rates of sedimentation.

Kaolinite cement that occurs within sand laminations shows no evidence of compaction (Plates 5A and 5B) which suggests a relatively late period of formation or recrystallization. Fractures with no infilling material are observed (Plates 5C, 5D and 6A) and are interpreted to be induced. These fractures are largely bedding

parallel or sub-parallel and therefore most likely result from pressure release during drilling and core extraction.

At depths up to about 3100 m (sample F24011 - 3106 m depth) densities are similar to those at about 2400 m (2.50 g/cm^3) but measured porosities are higher (~12 - 14%). The increased porosity may result from a high silt content and the resulting framework supported fabric. Compare the number and type of grain contacts in F24011 (Plate 7) with those of samples G33101 and G33102 (Plates 4, 5C and 6C). Sample F24011 is characterized as a framework supported siltstone.

Textural interpretations are complicated by bioturbation in sample F24021 (Plate 8). Moderate to intense bioturbation reorients framework grains, homogenizes the sediment (Plate 8A) and creates a matrix supported fabric (Plate 8). Bioturbation also introduces an organic mucous in digested sediment that may foster microbially mediated cement formation, principally siderite (Plates 8B and 8D). Siderite formation may also occur in sediments where refractory (Type III) organic matter inhibits sulphate reduction thereby leaving Fe available for siderite formation during methanogenesis. This bioturbated sample also has a slightly lower porosity (10-12%) than the laminated sample from a similar depth (F24011). Reduced porosity could result from either the rearrangement of the sediment fabric, a mechanical effect, or from an increase in biologic activity which induces cement formation (a chemical effect), or both.

Sample F24041 (3341 m depth) is a well-laminated, framework to matrix supported siltstone (Plate 9) with an intermediate density value (2.44 g/cm^3) and somewhat lower porosity (9-10%). Framework grains appear to be less well oriented, more poorly sorted, and more angular than those in sample F24011.

At depths of 3100 to 3350 m, fecal pellets exhibit significant compaction effects and a bedding parallel orientation (Plate 7B). Bioclasts are also commonly replaced by siderite (Plates 7 and 9). Chert dissolution is also observed (Plates 9C

and 9D). Poor sorting appears to affect grain contacts - poorly sorted grains show more point contacts (Plates 7 and 9) than better sorted material (Plate 4).

Overpressured Samples

Overpressuring in the Beaufort - Mackenzie Basin may begin at about 1200 m depth, depending on the location within the basin, but generally is below 2200 m depth (Issler, 1992). The shallowest overpressured sample selected for petrographic analysis is from about 2400 m present burial depth. The composition of overpressured and normally pressured shales is similar (Table 5). Silt-sized material is dominantly quartz with minor chert, plagioclase (albite and K-feldspar), and trace amounts of muscovite and pyrite. Silt grains are angular to sub-rounded.

Sample D27141 (2421 m) is a matrix supported mudstone containing medium to fine-grained silt (Plate 10). This sample has porosity (~8%) and density (~2.48 g/cm³) characteristics similar to normally pressured samples from the same depth (see above). The development of bedding parallel compaction fabric is not as pronounced, however, and fine-grained matrix shows minimal compaction effects. Matrix porosity appears to be high (Plate 10D).

Within this sample is a network of natural fractures unlike those seen in other samples. These fractures are filled with bitumen (Plates 10 - 12) and may originate at organic "clasts" (Plate 11). The bitumen-filled fractures commonly contain some pyrite (Plates 12B and 12C). These fractures are dominantly parallel or sub-parallel to bedding. Where the fractures narrow or may be restricted (Plate 12), it appears that fracture direction changes and may be at a high angle to bedding (Plates 10A and 12A). It is not clear whether the fractures form prior to bitumen saturation, or in response to bitumen generation and migration.

A poorly developed compaction fabric persists to 2700 m depth (Plates 13 - 15). Sample D27161 is a matrix supported siltstone that shows an extreme range of grain sizes, from medium sand to clay (Plate 14). Detrital micas are poorly

aligned (Plate 14D) and the matrix fabric shows little evidence of compaction (Plates 13 A and 13B). These characteristics suggest rapid or episodic deposition. Porosity for this sample is about 11 % and the bulk density is 2.48 g/cm³. Most micas appear weathered (Plates 12 - 14), in some cases even kaolinized (Plate 14C). It cannot be determined from petrographic data alone to what degree the "kaolinization " of micas has occurred in situ. Detrital chlorite is present (Plate 15C) and commonly appears well-preserved.

Sample A06071 (3215 m) has a porosity of about 6.0 % and a density of 2.61 g/cm³. The increased density is probably due, in part, to the pervasive siderite cement that is disseminated within the matrix (Plate 16). Flattened fecal pellets (Plate 16C) and carbonate clasts (Plate 16B) are common. This siltstone is framework supported and noticeably more coarse grained than many other samples.

With increasing depth, compaction fabric remains poorly developed. Sample E90011 (3452 m) is a poorly sorted, matrix supported siltstone with a porosity of approximately 14 % and a density of 2.40 g/cm³. The density is anomalously low for a sample at this depth. The poor sorting and grain orientation (Plate 17A) again suggests rapid to episodic deposition that may inhibit a well-developed compaction fabric. Poor sorting may also account for the persistent high porosity. At this depth however, some evidence of compaction induced grain orientation is present (Plates 17B and 18C) in the coarser fraction. In some laminations, the long axis of silt-sized grains are aligned (Plate 17B) and concavo-convex grain contacts are observed (Plates 17A, 17B and 17C). The clay-sized material however, remains poorly oriented (Plates 17D and 18D).

Secondary porosity is present in this sample. Porosity is created by dissolution of framework grains (Plate 9C) and the mechanical deformation of

detrital micas (Plate 18B). Some of this pore space is occluded with siderite cement.

At approximately 3500 m present burial depth, significant compaction effects are observed in overpressured samples. Sample A06081 is a coarse grained siltstone to fine grained sandstone. It is predominantly framework supported and has a high clast to matrix ratio (Plates 19-21). Porosity is approximately 6 % and bulk density is 2.61 g/cm³. Framboidal pyrite and disseminated siderite are present. Bioclasts, primarily sideritized fecal pellets, are abundant (Plates 19B, 20A and 21A). Grain-grain contacts, primarily concavo-convex, show the effects of compaction (Plates 19A, 20B, 20C and 21A). However, the matrix fabric remains poorly oriented because of the framework supported nature of the sample. (Plates 21B - D).

The deepest overpressured sample is from 4861 m (#O09091). The porosity and bulk density of this matrix supported siltstone are approximately 12% and 2.50 g/cm³, respectively. This sample is finer grained than the other overpressured samples and appears to be generally matrix supported (Plates 22A, 22B and 24C). Compaction effects are pronounced with micas and long grain edges generally oriented parallel to bedding (Plates 22-24). Grain contacts are dominantly concavo-convex but minor suturing is observed (Plates 23 B). Bitumen-filled fractures, similar to those seen in sample D27141, are present (Plates 22 and 24) but generally much smaller in diameter. Flattened, pyrite-bearing organic "clasts" are also present (Plate 24C).

GEOCHEMISTRY

Organic Matter and Maturity Trends

Rock-Eval data are shown in Table 1 (Appendix B). A pseudo Van Krevelen plot (Fig. 1a) indicates that the organic matter in Beaufort - Mackenzie shales is

dominantly Type III and, in conjunction with petrographic data, most likely of terrestrial origin. The very high OI values ($> 250 \text{ mgCO}_2/\text{gOC}$) suggest the presence of some refractory Type IV organic matter. High OI values may result as an analytical artifact when TOC values approach 0.5 wt%. TOC values are generally less than 2 wt% (Fig. 1b) with most samples exhibiting values of between 1 and 2 wt%.

Maturity generally increases with depth with maximum T_{max} values approaching 440°C (Fig. 2a). Some of the scatter in this plot is due to differential erosion and uplift. Issler (1992) indicated that erosion in more proximal areas of the Beaufort - Mackenzie delta was significant and could be estimated from shale compaction curves. Measured (from Kelly Bushing) depths are corrected in two wells (Mallik A06 and Reindeer D27, see Table 1) by adding the amount of eroded sediment suggested by Issler for these wells. A plot of corrected depths shows a better correlation with T_{max} (Fig. 2B) because the sediment maturity reflects maximum burial conditions. Corrected depths are used in subsequent plots.

A plot of Production Index (PI) versus T_{max} indicates that most samples show a normal maturity trend where PI increases to values greater than 0.1 at a T_{max} value of about 430 to 435°C (Fig. 3A). In wells where there is good vertical sample control, a normal maturity trend is observed that indicates the onset of maturation at about 3500 m depth (Fig. 3B). There are a number of samples however that have very high PI values at low maturity (T_{max} less than 435°C). These characteristics may be caused by a number of factors that include weathering or in situ oxidation of organic matter, contamination by drilling lubricants, or the presence of migrated hydrocarbons (Peters, 1986). Organic contaminants and migrated hydrocarbons increase the HI. None of the samples in question show elevated HI values (Table 1) suggesting that the organic matter in these samples is highly weathered or oxidized. This is also consistent with the very high ($> 200 \text{ mgCO}_2/\text{gOC}$) OI values

(Fig. 1A). Petrographic data indicate the common presence of sideritized plant debris (i.e. Plate 3) and marine organic detritus (i.e. Plate 16). Siderite is a common oxidation product of organic matter. Although this study has not directly measured the character of organic matter (fluorescence microscopy), the common occurrence of weathered micas suggests that detrital organic matter may also have undergone significant oxidation prior to deposition.

Inorganic Geochemistry and Mineralogy

Clay fraction chemistry is shown in Table 2 and whole-rock chemistry in Table 3. Mixed-layer illite/smectite (I/S) was identified by XRD (Fig. 4A) and I/S compositions, as determined by linear programming, are given in Table 4. These compositions were determined using a chamosite composition ($\text{Fe}_{2.90}\text{Mg}_{0.37}\text{Al}_{2.29}\text{Si}_{3.33}\text{O}_{10}(\text{OH})_8$), consistent with XRD data (Fig. 4A), that indicate an Fe-rich chlorite, and data from Ko (1992) on the <0.05 micrometer fraction. The initial fine-fraction composition was altered to reduce residuals, particularly K, and increase mineral totals. The calculated compositions used in subsequent whole-rock calculations differ in composition from Ko's data in that they are more K-rich and show no significant variation in K content with depth (Table 4). Petrographic data indicate that the < 2 μm fraction does contain some detrital illite and, in some cases, muscovite and therefore the composition of this coarser fraction is a "bulk" composition that includes these impurities. Discrete smectite is also present in this size fraction in some samples (Fig. 4B). Because the compositions of the discrete phases are so similar, it is not possible in all cases to calculate individual abundances nor is it possible to physically separate these phases within the < 2 μm fraction. The presence of discrete illite also precludes an accurate determination of the expandability of the mixed-layer phase (Srodon, 1980). Therefore, the calculated I/S compositions should be considered as a

physical mixture of discrete illite, I/S, and trace amounts of muscovite with the indicated "bulk" composition (Table 4).

Clay mineral abundances were calculated using two different sets of constraints. A comparison of the results is shown in Figure 5. In mode 1, the objective function was defined to minimize the residual oxide values and maximize mineral yield. In mode 2, the objective function was defined to minimize residuals and maximize the abundance of I/S. The values determined using mode 2 are preferred because the mineral totals are generally higher and the residual values lower than mode 1. Figure 5 indicates that for most samples, the deviation between the two methods is about 10% relative. A few samples show a significant deviation in the abundance of chamosite and I/S. This is due to the presence of Fe-oxides. If the excess Fe is used to "make" chlorite, as mode 1 does, then erroneously high abundances of this mineral will result, and erroneously low abundances of I/S are also calculated. These samples contain abundant Fe (expressed as Fe_2O_3 in Table 2). The calculated mineral abundances in the $< 2 \mu\text{m}$ fraction are given in Table 5.

Whole-rock mineralogy is initially determined from bulk XRD (Fig. 6) and petrographic data. I/S compositions, as determined by mode 2 (Table 4), and a chamosite (see above) of fixed composition are used to calculate whole-rock mineral modes (Table 6). It is generally difficult to estimate non-clay mineral abundances from bulk XRD measurements without the addition of internal standards (see Bloch, 1994). However, in the case of quartz, a good agreement is seen between the calculated quartz abundances and the intensity of the 0.426 nm peak (Fig 7) from whole rock XRD patterns (Fig. 6). A much poorer correlation is seen for siderite and pyrite (Fig. 8), primarily because of the low abundances of these minerals (Moore and Reynolds, 1989; Bloch, 1994).

A plot of silicate mineral abundance with depth (Fig. 9) shows no significant trends and the relative abundance of individual minerals is variable. I/S and quartz are the most abundant minerals ranging from about 30 to 55% and 25 to 58%, respectively. Below about 3000 m, I/S abundance increases and quartz decreases. Plagioclase (dominantly albite with minor K-feldspar) abundance is less than 2 wt% and chlorite abundance varies from 2 to 7 wt%. Kaolinite varies from 2 to 11 wt% and shows no significant variation with depth (Fig. 9). The non-silicate fraction comprises dominantly siderite and pyrite with accessory minerals (Table 6). The low abundance of sulphur (Fig. 10A) suggests that most of the Beaufort-Mackenzie shales sampled were deposited in brackish water or that the low reactivity of organic carbon limited sulphate reduction. Siderite and pyrite abundances are somewhat antithetic (10B) and the large amount of siderite relative to that of pyrite further suggests that refractive, Type III organic matter may have limited sulfate reduction.

Mineralogical trends with depth are not obvious (Fig. 9) but there is an apparent increase in bulk K_2O content with depth below about 2800 m (Fig. 11). This trend is more pronounced in the $< 2\mu m$ fraction and the covariation of the bulk and clay K_2O trends suggests that the bulk K abundance is controlled largely by the abundance of I/S in the clay-sized fraction. I/S is the dominant phase in the clay fraction ($< 2.0 \mu m$ in size) but this cannot be resolved petrographically using backscattered electron microscopy. Illite, some muscovite and probably K-feldspar are also present in this size fraction.

The bulk composition of the clay-sized fraction, plotted on an element ratio diagram (Fig. 12), indicates a mixture of an illitic clay and kaolinite for both the measured and calculated bulk clay compositions. A regression through the measured clay fraction compositions intersects both the kaolinite and illite compositional fields. The illitic clay is a mixture of phases that comprises a small

amount of muscovite, discrete illite, mixed layer I/S and, in some samples, discrete smectite. This bulk clay fraction has a mean Si/Al value of 1.77 and K/Al value of 0.26 (Fig 12 and Table 4). The absence of any significant offset in K/Al values between the whole rock and clay fraction compositions indicates that quartz (and to a lesser degree plagioclase) is the dominant silt-sized constituent and this is confirmed by petrographic analysis. K-feldspar is present in minor to trace amounts (see below).

DISCUSSION

Over the thick interval of Cretaceous and Tertiary shales of the Beaufort - Mackenzie Basin, shale composition is relatively homogeneous (Fig. 6 and Tables 3 and 6). However, compaction characteristics and porosity and permeability trends are variable across the basin (Issler, 1992). Measured porosity values (Issler and Katsube, 1994) are generally less than approximately 12% below 2500 m, with the exception of some overpressured samples (Fig 13). Petrographic data indicate that poorly sorted, silt-rich samples appear to maintain unoriented fabrics and more intergranular porosity to greater burial depths. Poor sorting is characteristic of rapidly or episodically deposited sediments in environments where wave, current or storm energy is higher. The high silt content results in a framework supported fabric that inhibits further matrix compaction. These observed textural characteristics are consistent with Issler's interpretation that overpressuring is caused by rapid sedimentation.

Overpressuring may also be caused by thermal maturation of organic matter and/or I/S diagenesis (Powers, 1967; Burst, 1969). Figure 3 indicates that in the Beaufort-Mackenzie Basin, the onset of maturation occurs at about 3500 m, well within the overpressured zone. In addition, the top of the overpressured zone is variable across the basin, ranging from approximately 1200 to 3300 m depth

(Issler, 1992 and unpublished data). Therefore, maturation appears to have little correlation with the development of overpressure.

In a study of the $<0.05\ \mu\text{m}$ fraction, Ko indicated that the illitization of I/S was "accelerated" in overpressured zones as a result of high water/rock ratios inferred to occur there (Ko, 1992; Ko and Hesse, 1992). This interpretation contrasts with Gulf Coast studies that suggest that the illitization of smectite or I/S, a reaction that releases water, is a causative factor in overpressure development. The present study does not directly address the extent or role of I/S diagenesis in basin evolution, but the bulk chemical and mineralogical data do not indicate any significant trends that may result from extensive illitization of smectite or I/S (Fig. 12 and Table 6). The apparent increase in illite content of the mixed-layer phase with depth (Fig. 14) may be interpreted to indicate that illitization of I/S has occurred. The K_2O in both clay and bulk samples does increase systematically with depth below about 2800 m (Fig. 11) and Ko (1992) indicates that illitization of the $<0.05\ \mu\text{m}$ fraction does occur within this sequence. However, discrete smectite persists to depths of 3200 m (Fig. 4B) in some wells suggesting that the illitization of smectite may not be a pervasive reaction. In addition, this depth marks a major sequence boundary between the Kugmallit and Richards sequences and this zone also marks a distinct change in porosity trends (Fig. 13) where below about 2500 m, porosity values level off at about 10 %. A recent study of Cretaceous shales in the Western Canada Sedimentary Basin (Caritat et al., 1994b) indicates that the distribution of detrital illite and I/S, controlled by depositional facies, can mimic diagenetic trends identified by XRD, as above. Therefore, it is difficult to determine the extent of I/S diagenesis within this sequence and the possible effects on porosity and permeability distributions. Additional work to determine the compositional variation of discrete clay minerals is required address this complex problem.

With the exception of one anomalous sample, porosity, particularly helium porosity (see Issler and Katsube, 1994 for analytical details), shows an excellent correlation with sample density (Fig. 15) suggesting that compaction induced porosity loss is the primary control on sample density. This is confirmed by examining the effect of mineralogy on sample density. Authigenic siderite (Plates 16, 18, 19, and 23) occludes intergranular, matrix, and secondary porosity. With a specific gravity of 3.96, the presence of a few weight per cent siderite should significantly affect bulk density. Minor pyrite (s.g. = ~ 5.0) is also present. However, when Fe-mineral abundances are plotted against matrix density (bulk density minus porosity)(Fig. 16), there is no correlation. These observations indicate that Beaufort - Mackenzie shale density is controlled primarily by compaction and that diagenetic effects are minimal.

CONCLUSIONS

Petrographic and chemical analyses of whole-rock and clay separate samples of Beaufort - Mackenzie Basin shales indicate that the bulk chemistry and clay mineral compositions are relatively homogeneous through the studied Cretaceous - Tertiary interval. Quartz and mixed - layer I/S are the dominant mineral constituents. Kaolinite, chlorite, plagioclase, siderite, calcite, dolomite and pyrite are also commonly present. TOC is generally less than 2 wt% and the organic matter is dominantly Type III and of terrestrial origin. The organic matter is characterized by low HI and high OI values indicating that significant oxidation or weathering of organic matter has occurred. Detrital micas also show significant degradation and potassium loss consistent with weathering prior to deposition.

Petrographic observations suggest that sorting and deposition rate affect subsequent compaction behaviour and porosity loss. Overpressured samples that are poorly sorted and have a high silt content (characteristic of rapid deposition) do

not develop significant compaction characteristics until 3500m burial depth. Normally pressured samples generally develop significant compaction effects, including grain reorientation and concavo-convex contacts, at about 2500 m.

Helium porosities and density measurements correlate well and suggest that porosity loss is the primary control on bulk sample density. The abundance of the authigenic iron minerals pyrite and siderite shows no correlation with matrix density although matrix porosity appears reduced in samples with disseminated siderite cement. Extensive siderite cementation occurs predominantly in bioturbated samples.

Maturity trends (T_{max} and PI values) indicate that maturation of organic matter begins at between 3000 to 3500 m burial depth. Petrographic data indicate that evolved bitumen migrates predominantly in bedding parallel fractures but may move in a cross formational direction when porosity and/or permeability restrict fluid movement. The onset of hydrocarbon generation occurs just prior to or at a burial depth of about 3000 m where porosity is reduced to less than 15 % and sample density increases significantly.

REFERENCES

- Baedecker, P.A., 1987. Methods for geochemical analysis. United States Geological Survey Bulletin #1770.
- Bloch, J., 1994, The methods and results of geochemical analyses of Cretaceous Colorado Group shales from the Western Canada Sedimentary Basin. Geological Survey of Canada, Open File Report #2810.
- Burst, J.F., 1969. Diagenesis of Gulf Coast clayey sediments and its possible relation to petroleum migration. Bulletin of the American Association of Petroleum Geologists, 53, pp. 73-93.
- Caritat, P. de., Bloch, J. and Hutcheon, I.E., 1994a. LPNORM: A linear programming normative analysis code. Computers & Geosciences, 20, pp. 313-347.
- Caritat, P. de, Bloch, J., Hutcheon, I.E. and Longstaffe, F.J., 1994b. Compositional trends of a Cretaceous foreland basin shale (Belle Fourche Formation, Western Canada Sedimentary Basin): diagenetic and depositional controls. Clay Minerals, 29, pp. 503-526.
- Espitalié, J., Laporte, J.L., Madec, M., Marquis, F., Leplat, P., Paulet, J. & Boutefeu, A., 1977. Méthode rapide de caractérisation des roches de mères de leur potentiel pétrolier et de leur degré d'évolution. Revue de l'Institut Français Pétrolier, 32, pp. 23-42.
- Gallagher, K., 1989. An examination of some uncertainties associated with estimates of sedimentation rates and tectonic subsidence. Basin Research, 2, pp. 97-114.
- Gautier, D.L. and Schmoker, J.W., 1989. Evaluation of sandstone porosity from thermal maturity information. In Short Course in Burial Diagenesis. Mineralogical Association of Canada, Short Course #15. Hutcheon, I.E. (ed.). pp. 135-160.
- Issler, D.R., 1992. A new approach to shale compaction and stratigraphic restoration, Beaufort - Mackenzie Basin and Mackenzie corridor, northern Canada. American Association of Petroleum Geologists Bulletin, 76, pp. 1170-1189.
- Issler, D.R., and Katsube, T.J., 1994. Effective porosity of shale samples from the Beaufort - Mackenzie Basin, northern Canada. In Current Research, 1994-B, Geological Survey of Canada, pp. 19-26.
- Katsube, T.J., and Issler, D.R., 1993. Pore-size distributions of shales from the Beaufort - Mackenzie Basin, northern Canada. In Current Research, Part E, Geological Survey of Canada Paper 93-1E, pp. 123-132.

- Ko, J., 1992. Illite/smectite diagenesis in the Beaufort - Mackenzie Basin, Arctic Canada. unpubl. Ph.D. thesis: McGill University, Montreal, Canada.
- Ko, J., and Hesse, R., 1992. Illite/smectite diagenesis in overpressured and normally pressured environments, Beaufort - Mackenzie Basin, Arctic Canada. Proceedings of the 7th International Symposium on Water - Rock Interaction, Park City, Utah. v. 2, Kharaka, Y.K and Meast, A.S. (eds.). pp. 1173 - 1176.
- Moore, D.M., and Reynolds, R.C., Jr., 1989. X-ray Diffraction and the Identification and Analysis of Clay Minerals. Oxford University Press, New York. 332p.
- Passey, Q.R., Creaney, S., Kulla, J., Moretti, F., and Stroud, J. 1990. A practical model for organic richness from porosity and resistivity logs. American Association of Petroleum Geologists Bulletin, 74, pp. 1777-1794.
- Peters, K.E., 1986. Guidelines for evaluating petroleum source rock using programmed pyrolysis. American Association of Petroleum Geologists Bulletin, 70, pp. 318-329.
- Potter, P.E., Maynard, J.B., & Pryor, W.A., 1980. Sedimentology of Shale. Springer-Verlag, New York, 306p.
- Powers, M.C., 1967. Fluid-release mechanisms in compacting marine mudrocks and their importance in oil exploration. American Association of Petroleum Geologists Bulletin, 51, pp. 1240-1254.
- Rieke, H.H. & Chilingarian, G.V., 1974. Compaction of Argillaceous Sediments. Developments in Sedimentology #16. Elsevier Scientific, New York, 424p.
- Srodon, J., 1980. Precise identification of illite/smectite interstratifications by X-ray powder diffraction. Clays and Clay Minerals, 28, pp. 401-411.

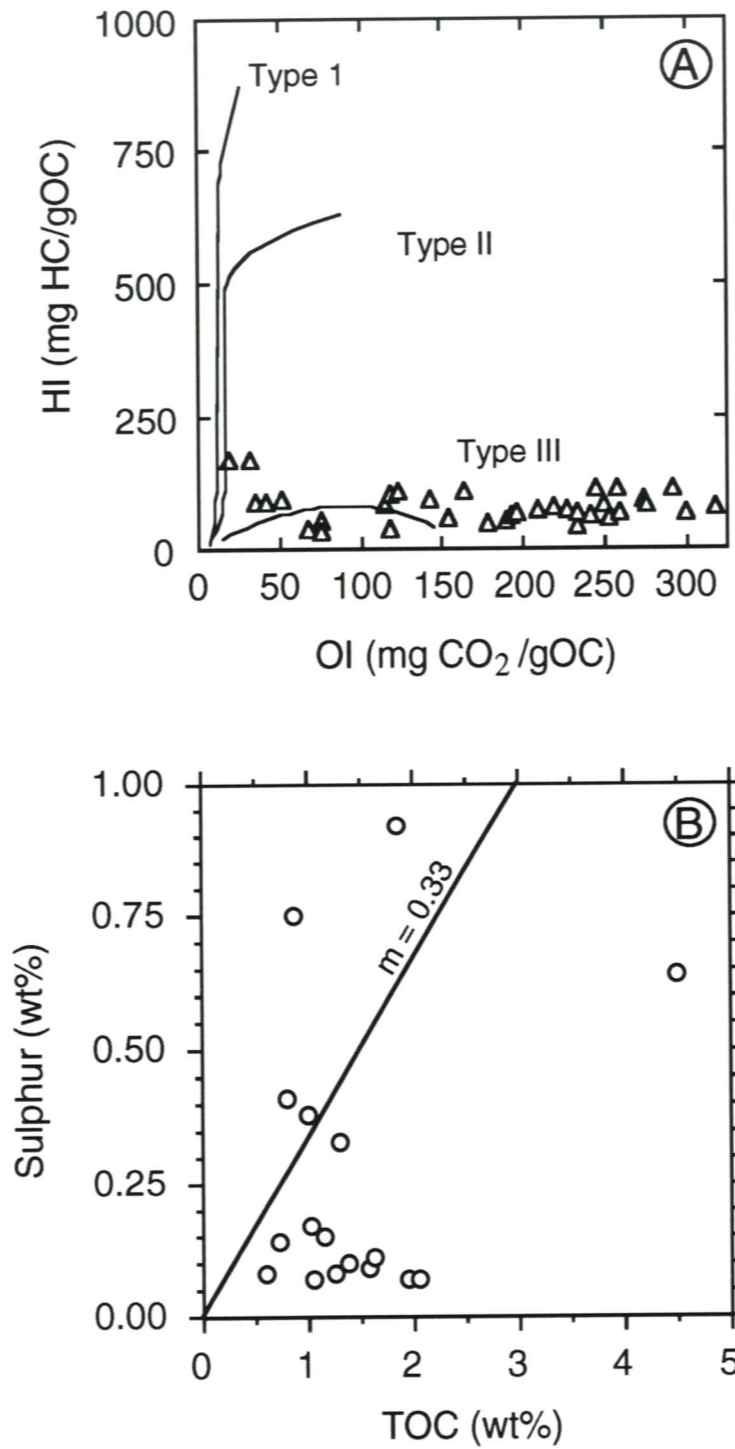


Figure 1 - Pseudo Van Krevelen diagram (A) and C-S data (B). Line in B with slope (m) of 0.33 represents normal marine S/C values.

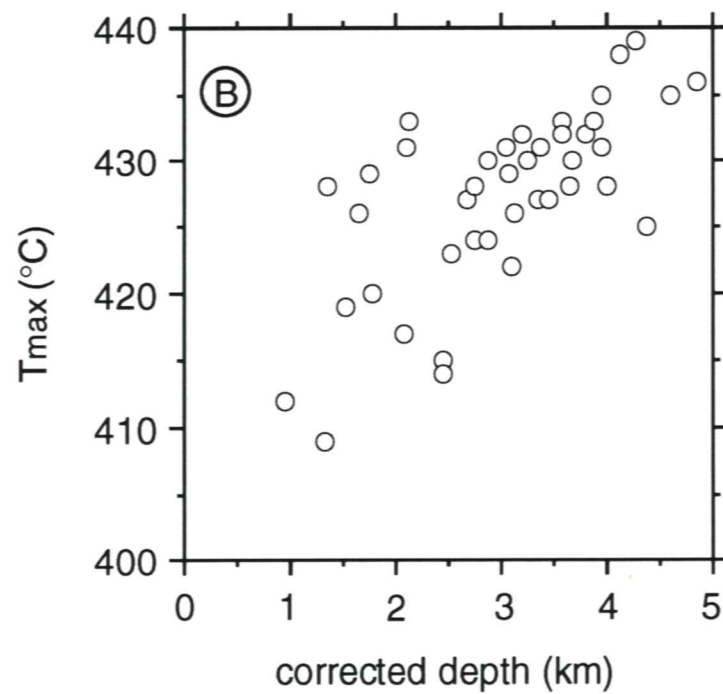
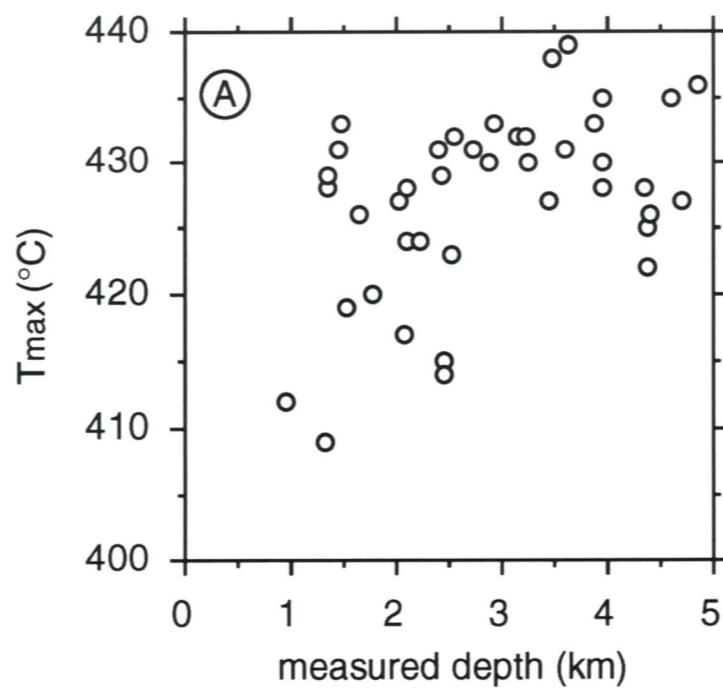


Figure 2 - T_{max} versus measured (present burial)(A) and corrected (maximum) (B) depth.

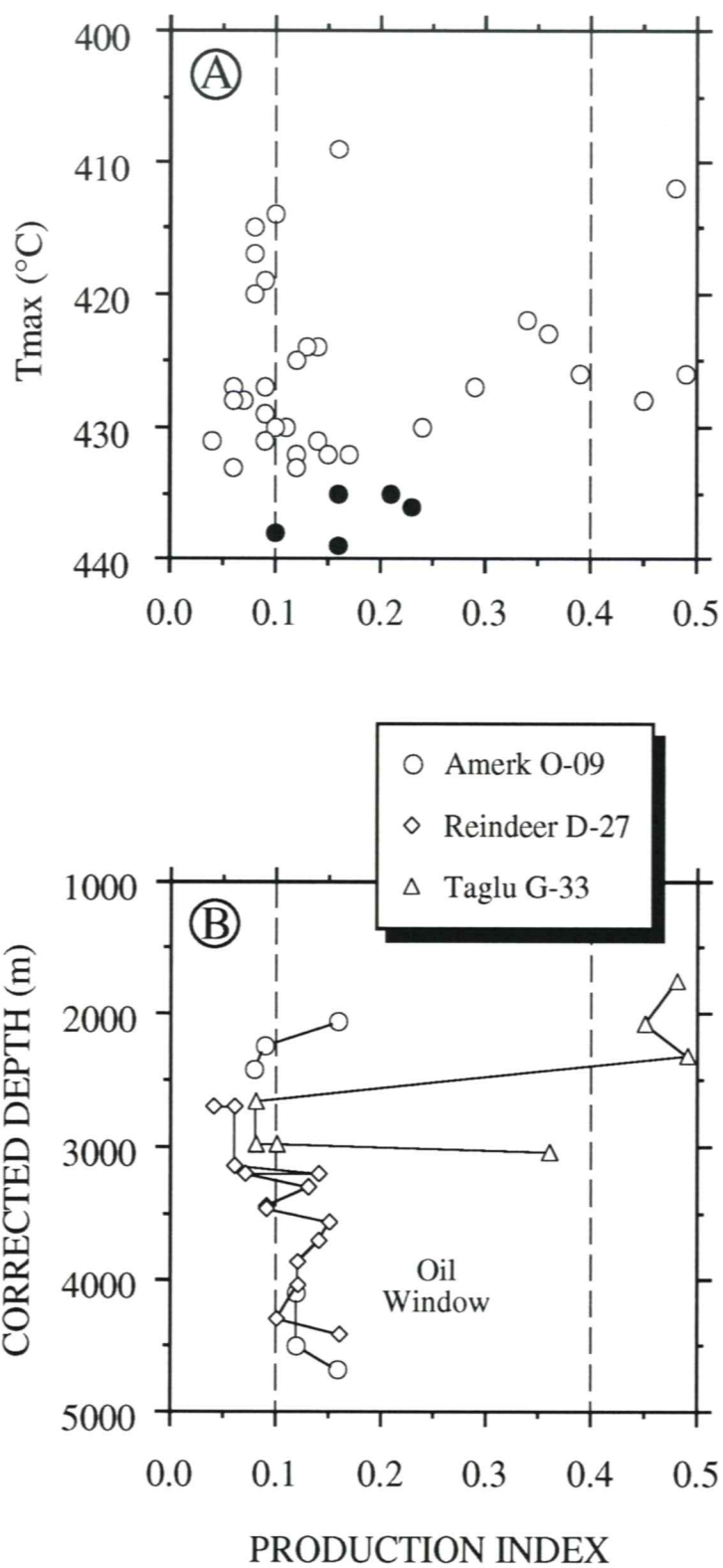


Figure 3 - T_{max} (A) and Corrected Depth (B) versus PI. Filled circles in A are samples that are thermally mature ($T_{max} \geq 435^{\circ}C$).

Sample O09061 (3866 m pbd)

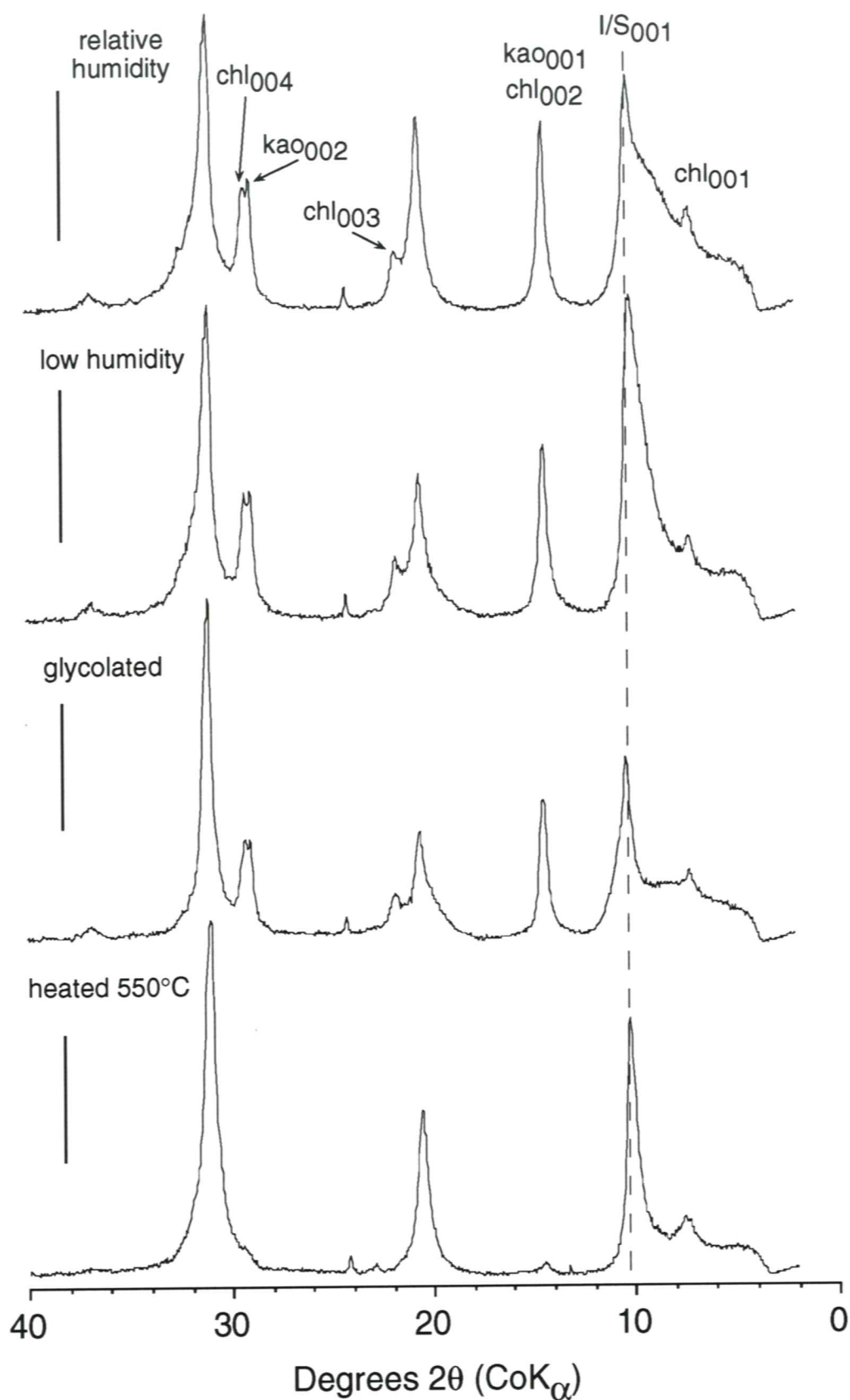


Figure 4A - Diffraction patterns from < 2 μ m oriented sample (O09061). Pbd = present burial depth (measured). Diagnostic peaks are labeled. Vertical scale bars = 2000 counts.

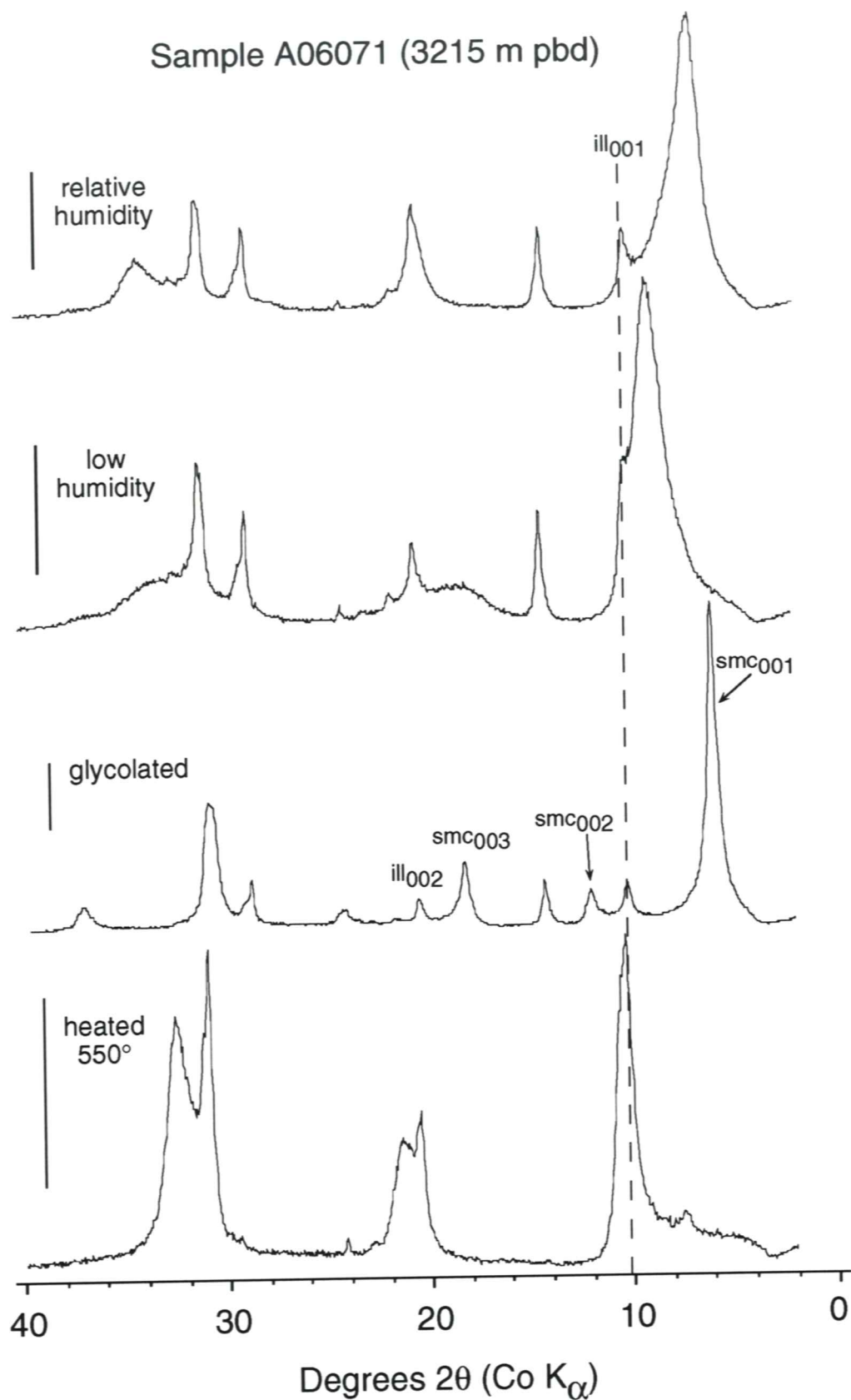


Figure 4B - Diffraction patterns from $< 2\mu\text{m}$ oriented sample (A06071). Pbd = present burial depth (measured). Diagnostic peaks are labeled. Vertical scale bars = 2000 counts.

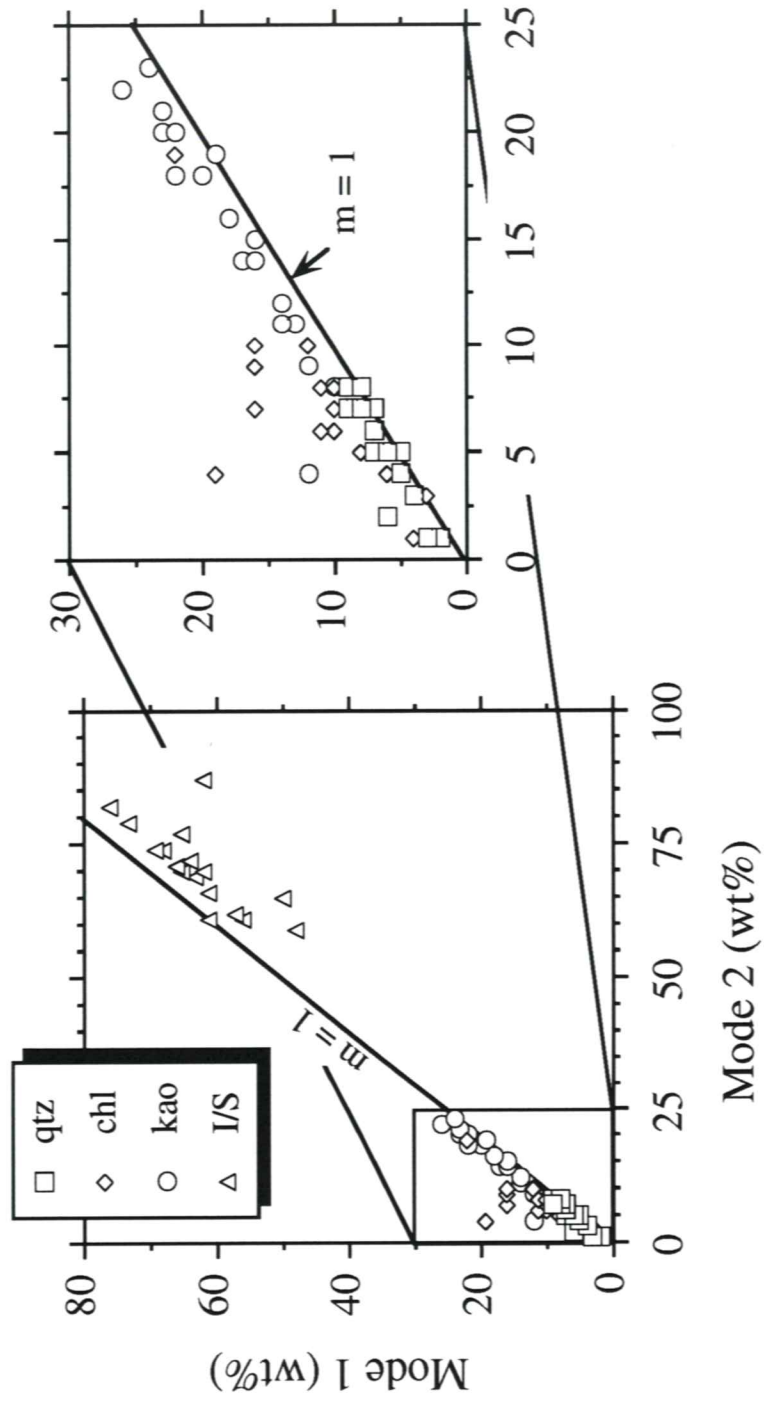


Figure 5 - Calculated clay abundances comparing two different sets of calculation conditions. See text for discussion.

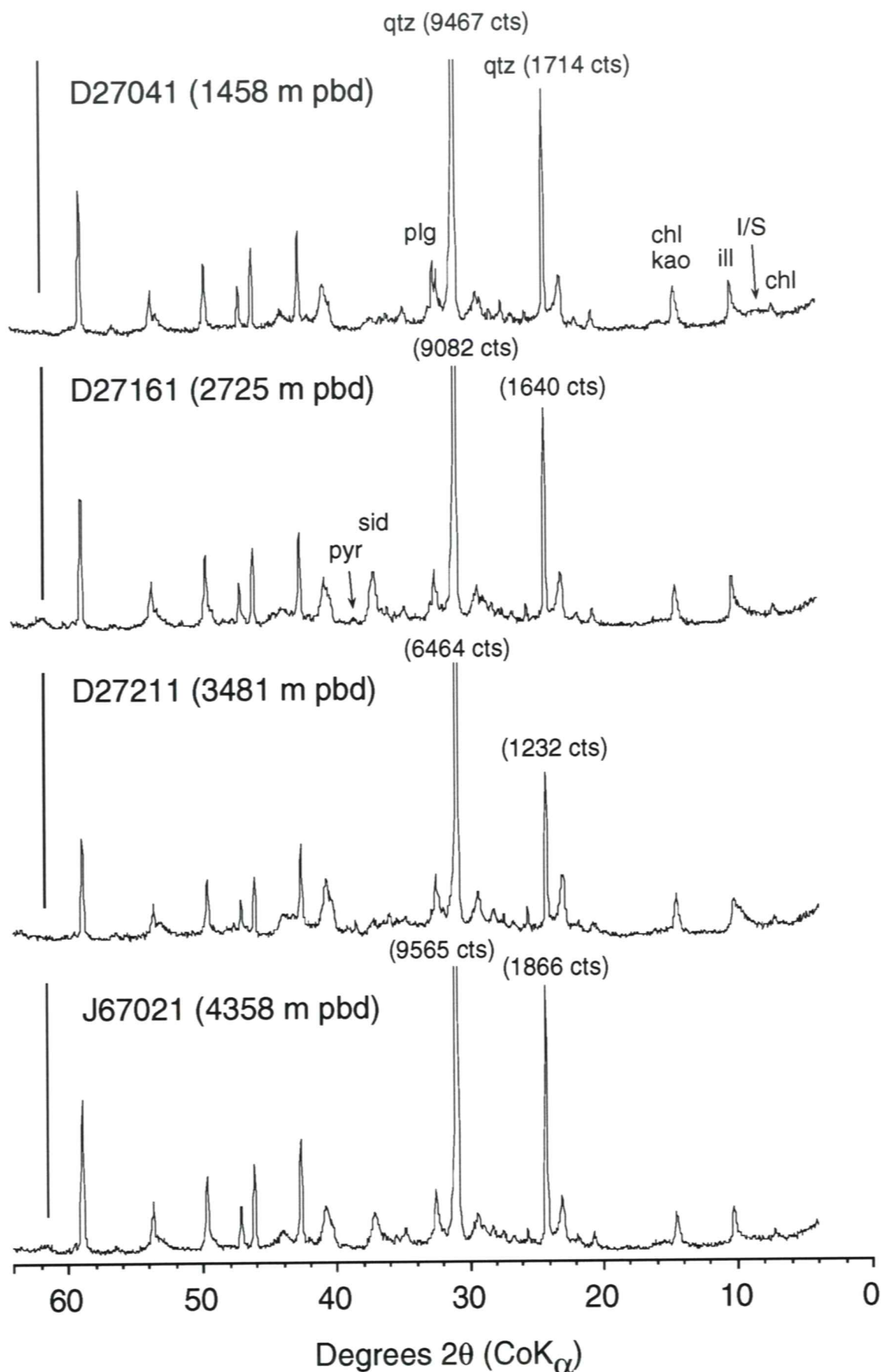


Figure 6 - Whole - rock diffractograms. Vertical scale bars = 2000 counts.
Major quartz peaks are labeled with count values

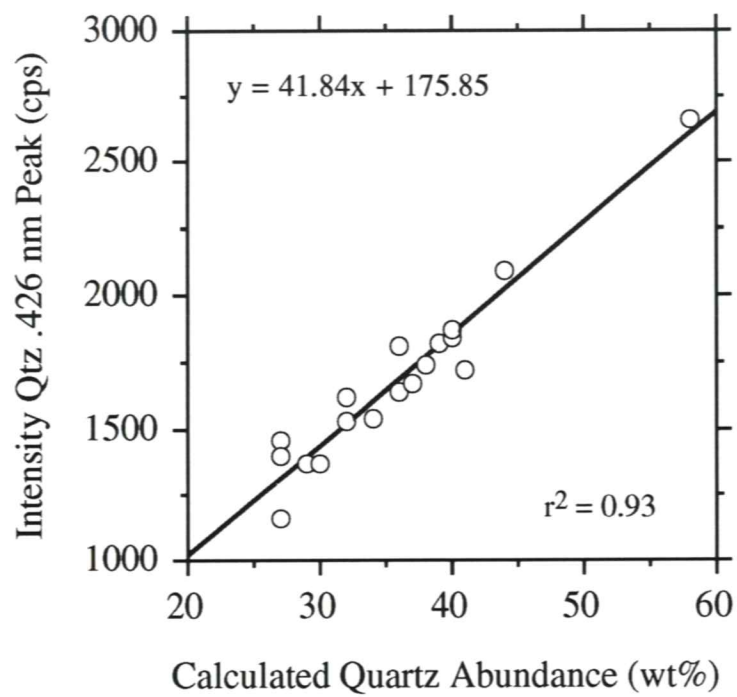


Figure 7 - Calculated quartz abundance versus the 0.426 nm intensity (see Fig. 6)

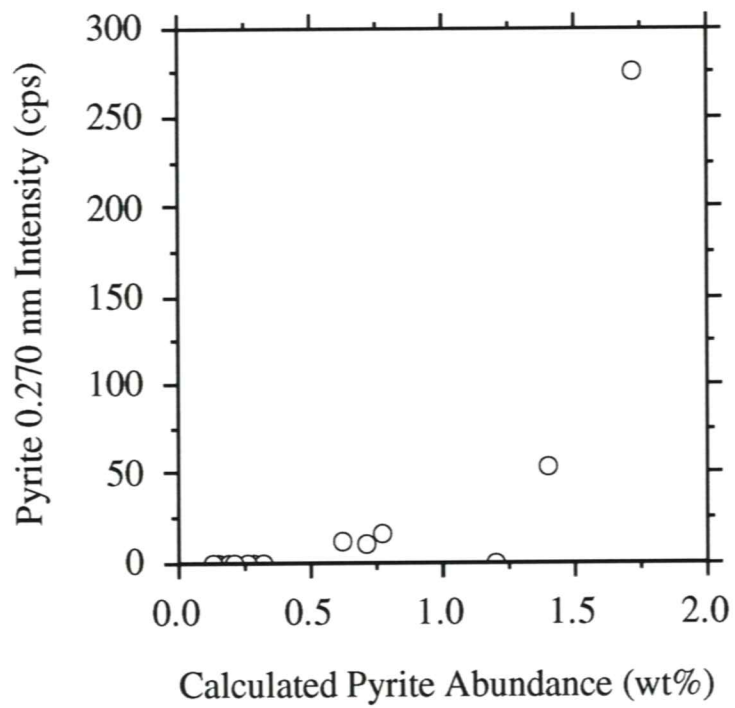
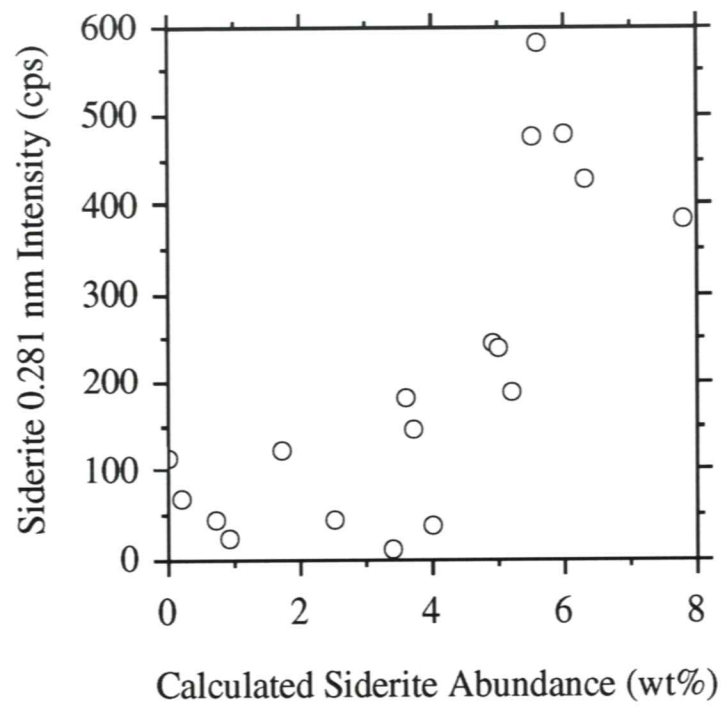


Figure 8 - Calculated siderite and pyrite abundances versus XRD peak intensities.

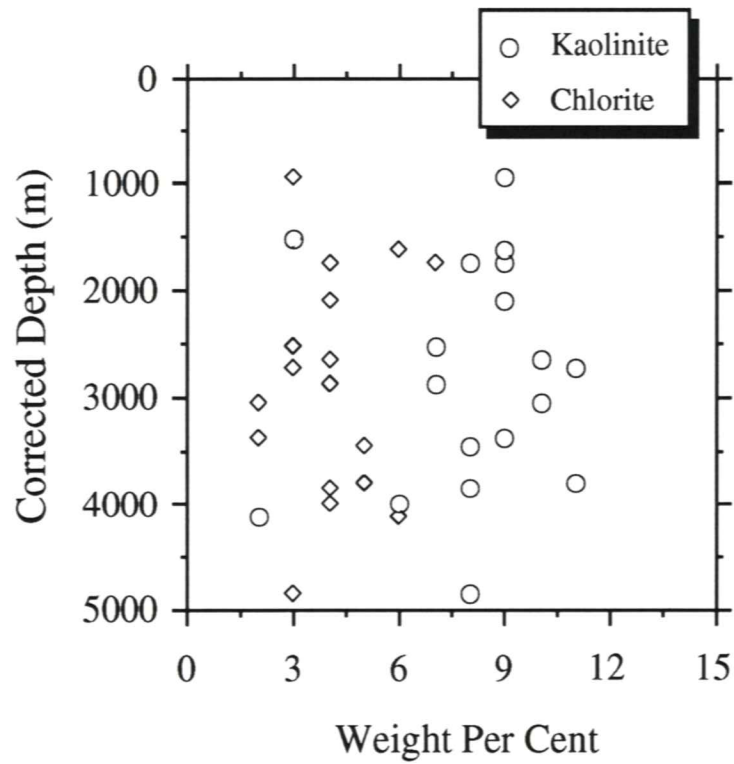
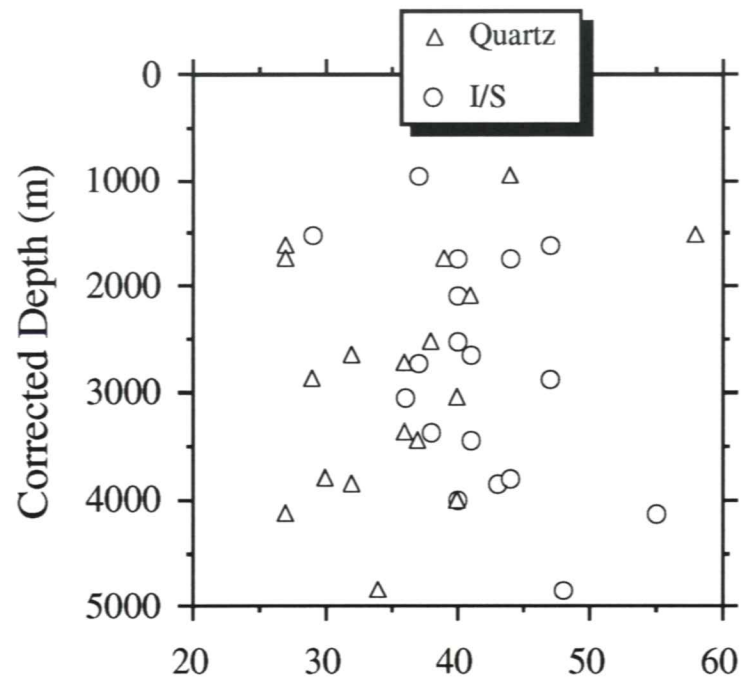


Figure 9 - Mineral abundances versus depth

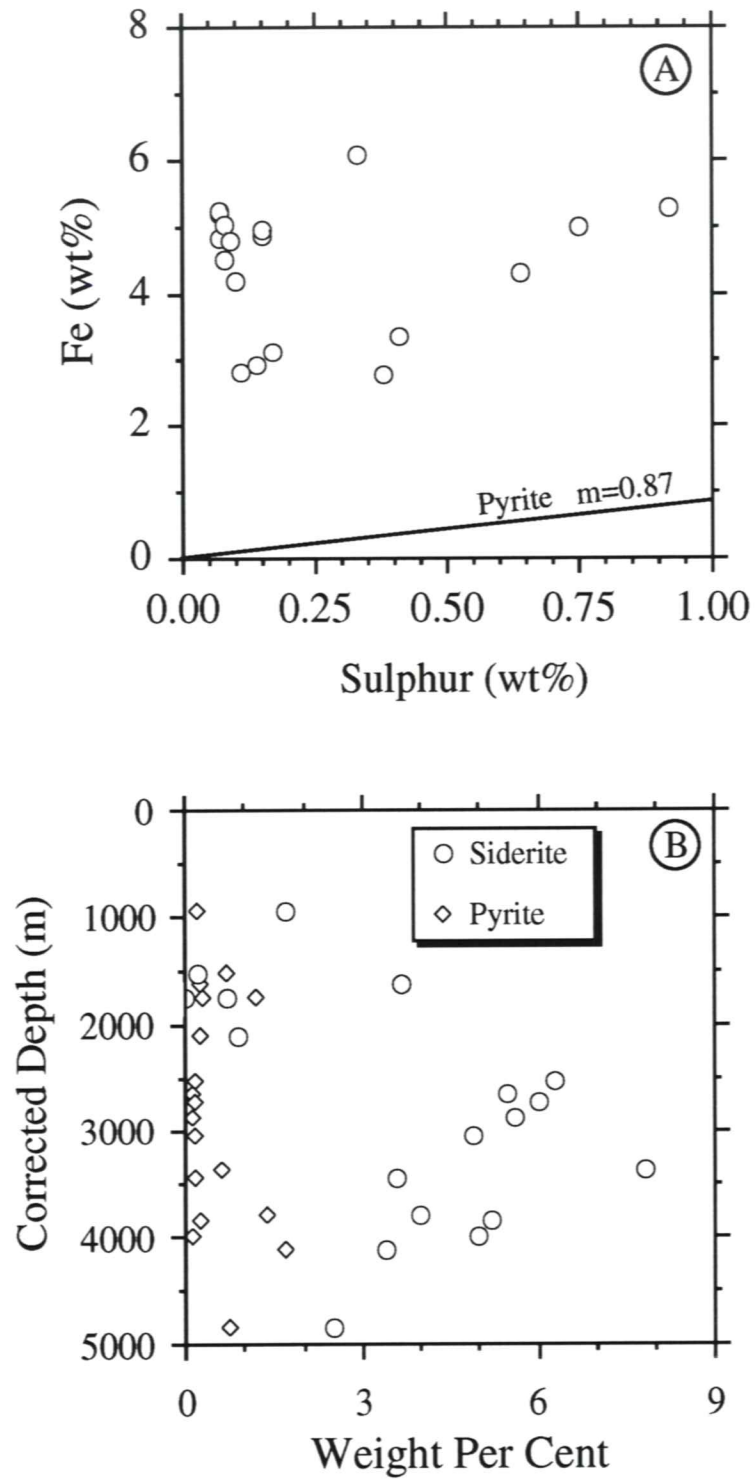


Figure 10 - Fe - S systematics (A) and Fe - minerals versus depth (B).

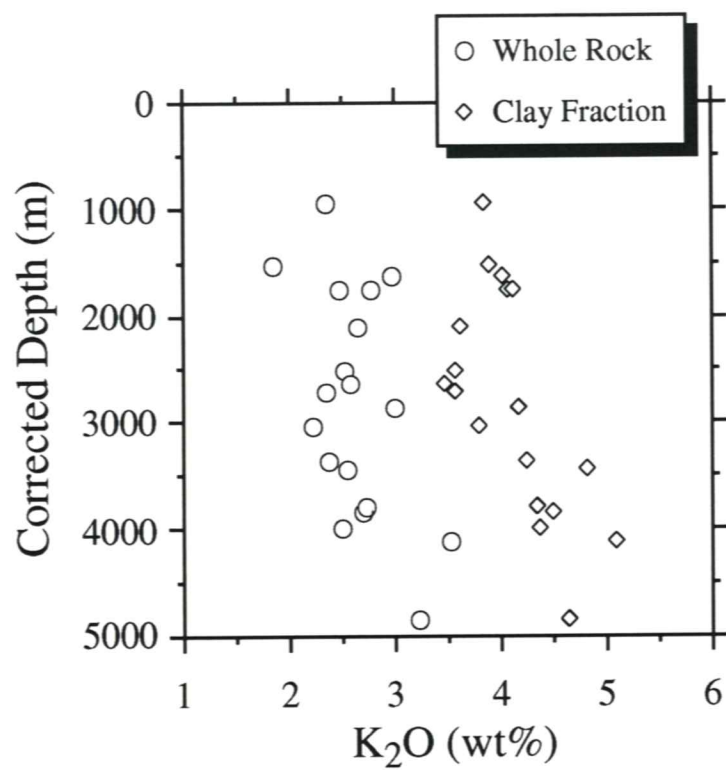


Figure 11 - Weight per cent K₂O versus corrected depth

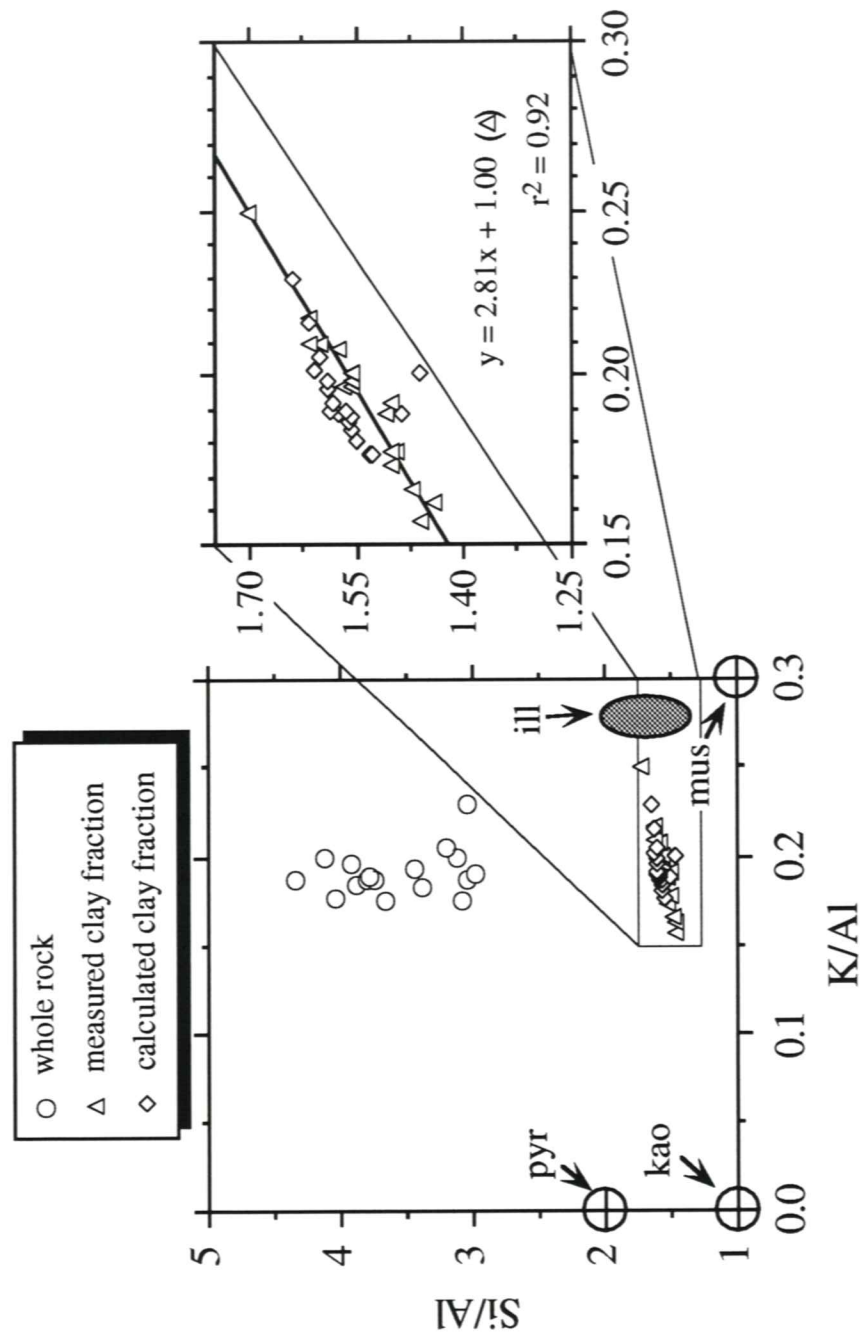


Figure 12 - Element ratio diagram. Regression in blow-up is for measured clay fraction only. Regression intercepts are the kaolinite and illite compositional fields shown on the left.

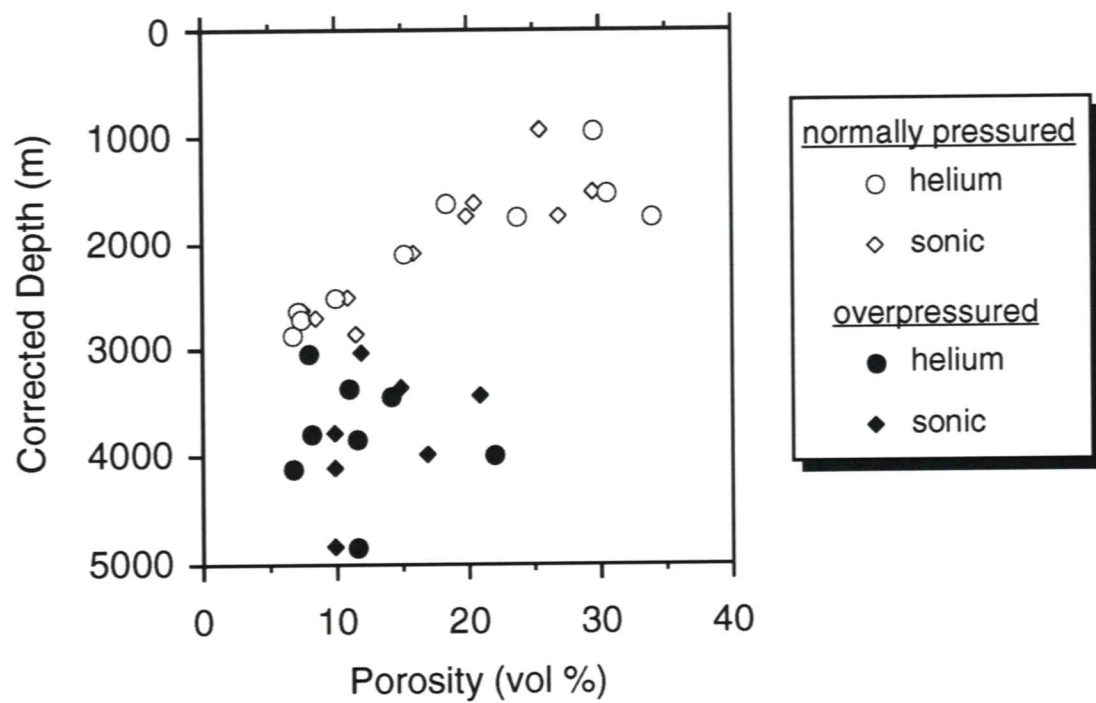


Figure 13 - Porosity versus corrected (maximum) depth

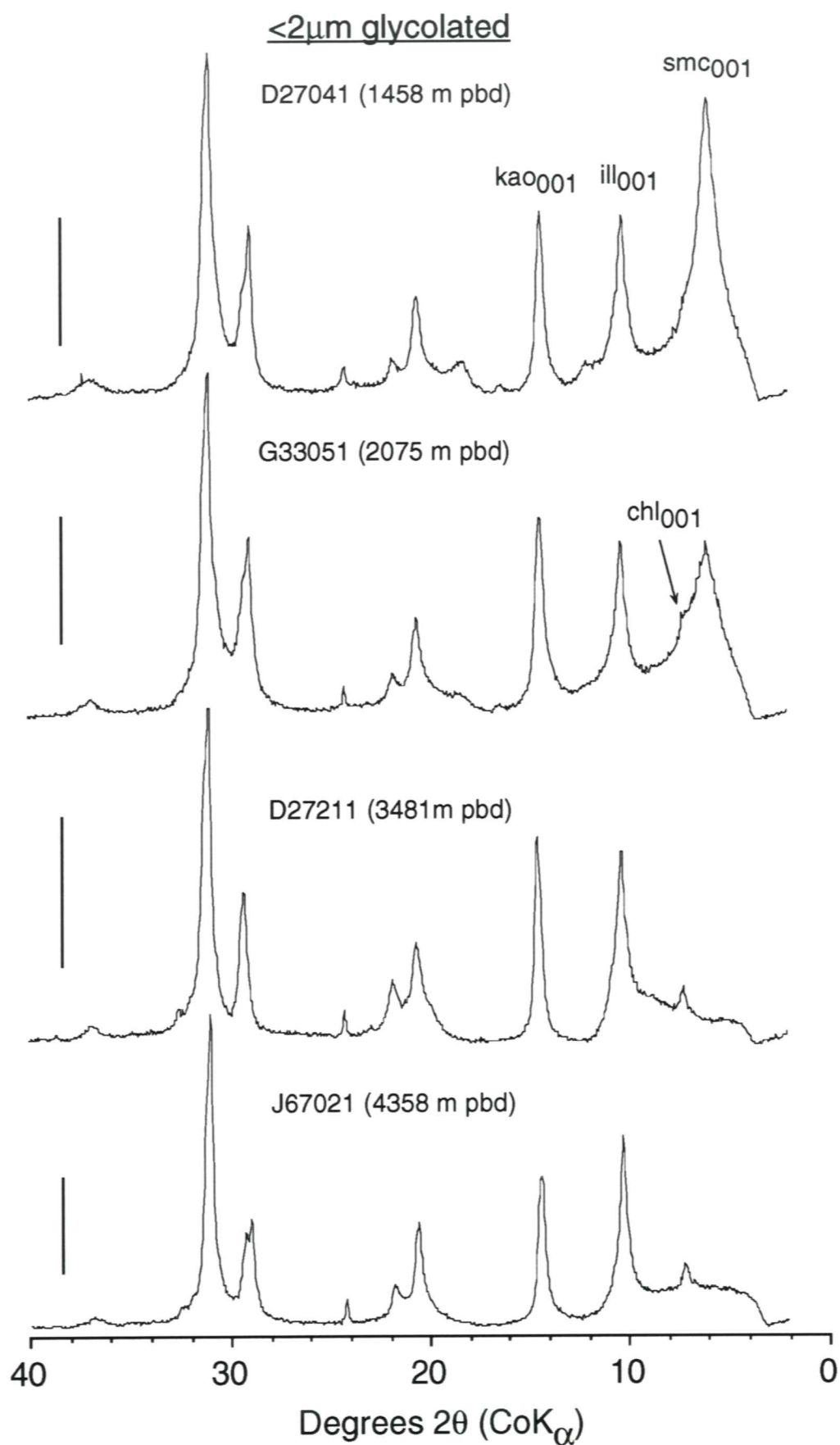


Figure 14 - XRD characteristics of I/S with depth

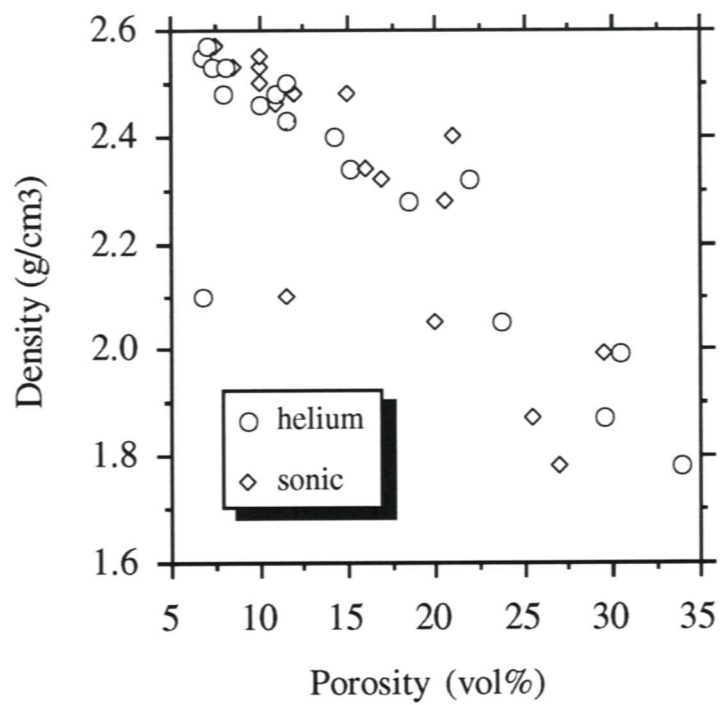


Figure 15 - Sonic and helium porosity versus density. Data from Issler and Katsube (1994).

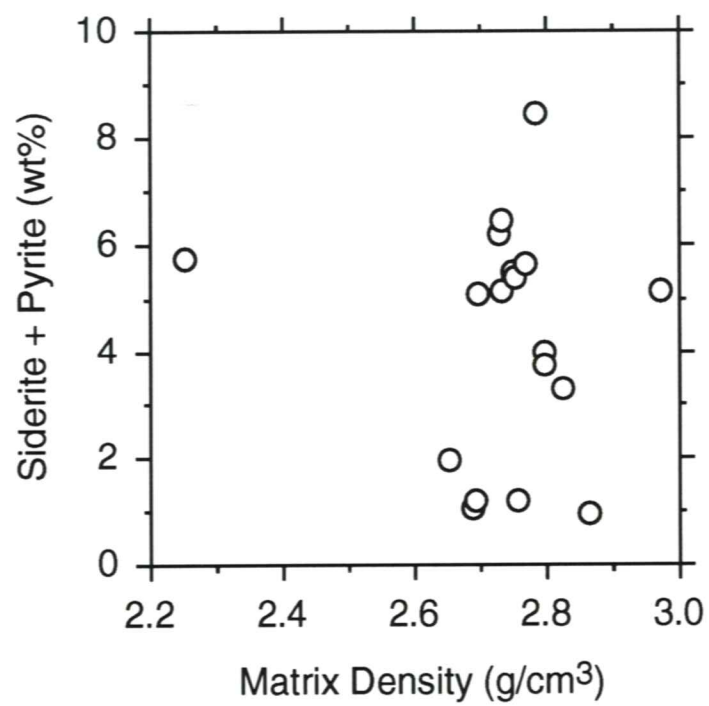


Figure 16 - Fe - mineral abundances versus matrix density (minus porosity).

APPENDIX A

Plates 1 - 24

Plate 1 - Sample D27042 or BRE-2 - 1469m, normally pressured, ~ 12% measured porosity, 15-17% sonic porosity, bulk density = 2.34 g/cm³. A) fractured K-feldspar (K) and extensively dissolved K-feldspar (arrow) in quartz-rich siltstone. Note numerous point - edge contacts. Matrix comprises clay-sized quartz, illite, kaolinite and siderite. Framework grains have relief above plucked matrix resulting in edge effects (bright grain edges). B) siderite (bright material) nucleated about an organic "clast". C) partially dissolved calcareous foraminifera. D) siltstone matrix comprising illitic clay (arrow), quartz (Q) and siderite (bright areas).

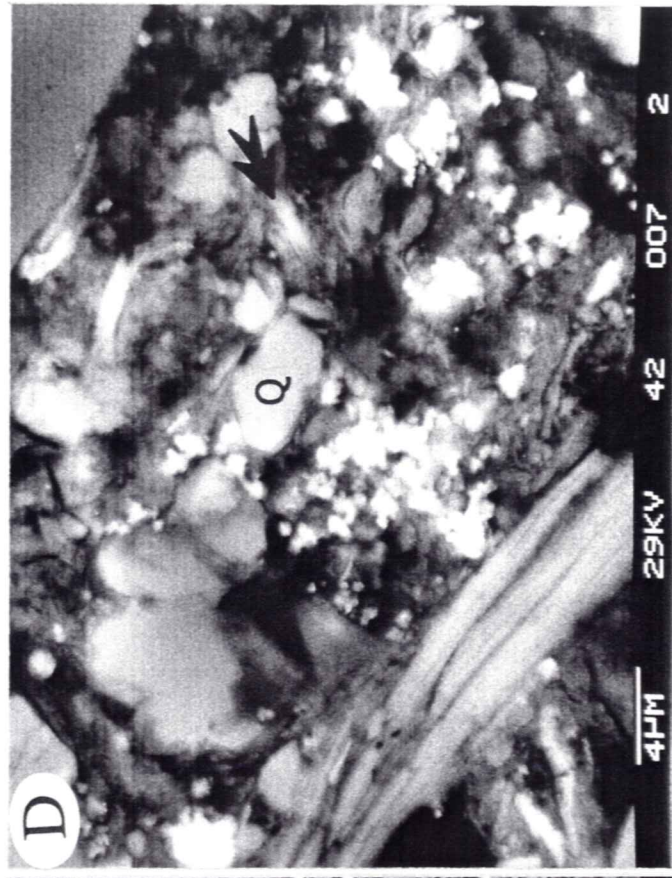
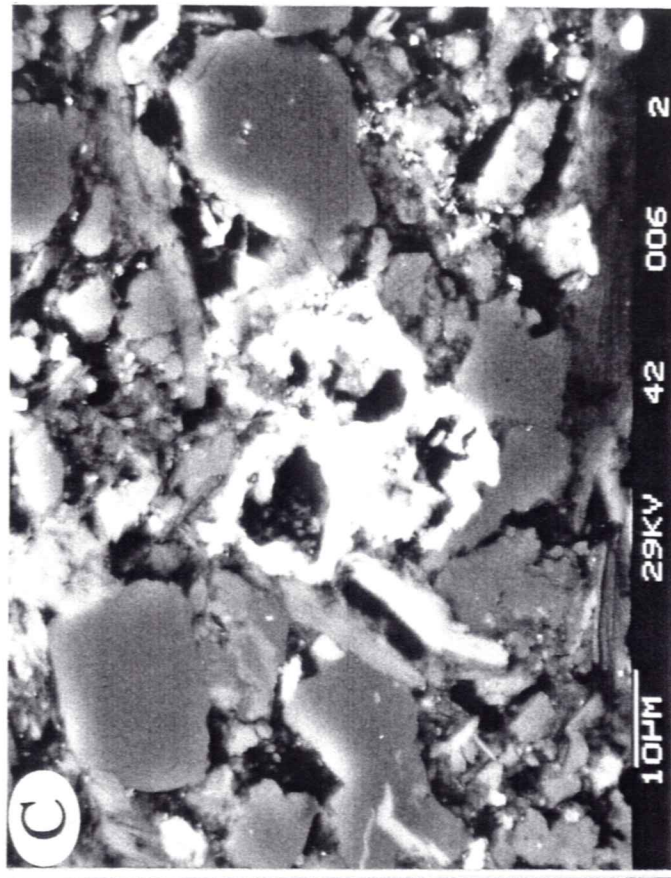
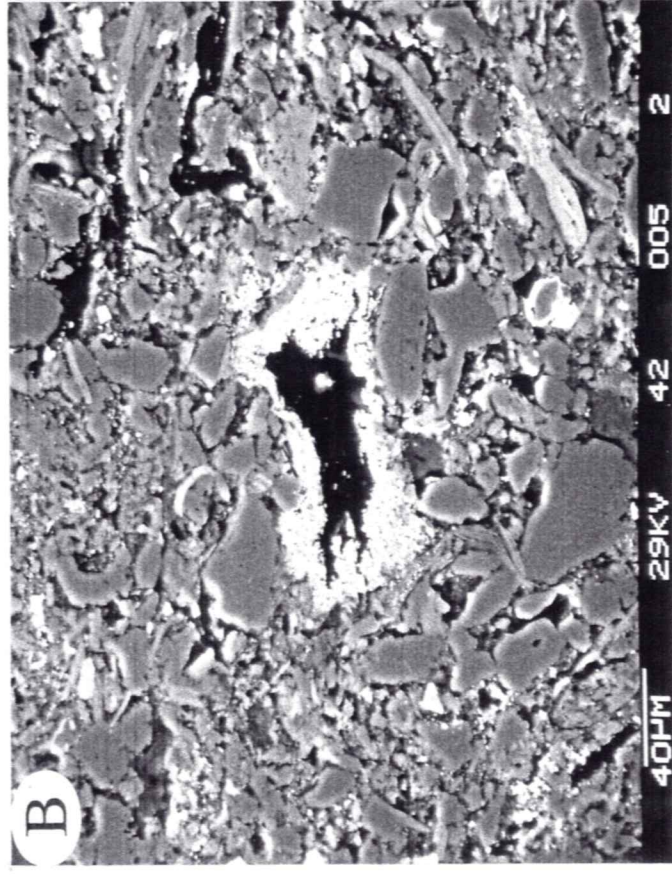
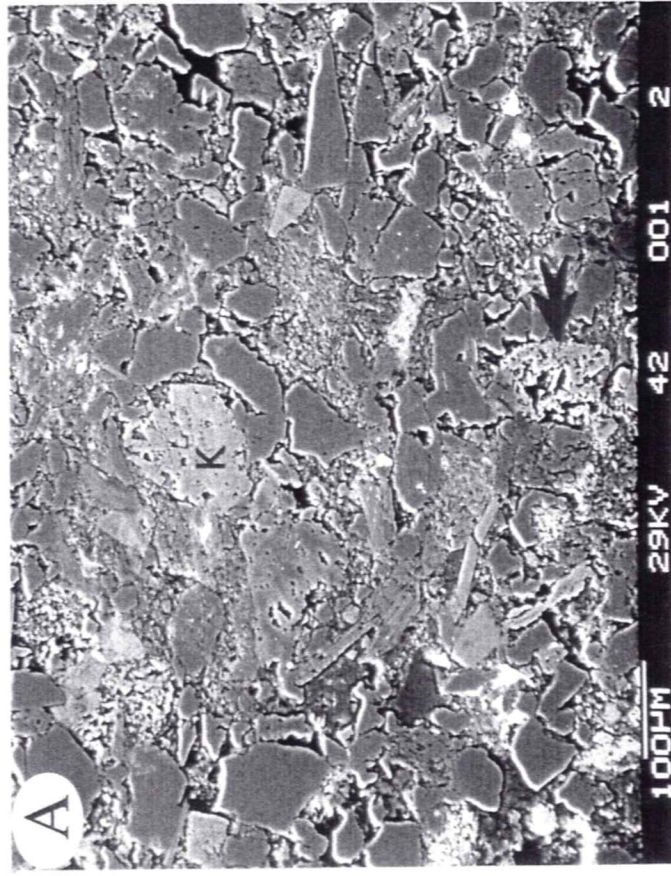


Plate 2. Sample O09031 or BAR-3 - 1765m - normally pressured - 28 - 34% measured porosity - 25-29% sonic porosity - bulk density = 1.78 g/cm³. A) well-polished and plucked areas. B) large organic "clast" in claystone with pyrite inclusions. C) unoriented matrix fabric. Detrital micas have a "dull" reflectance and low K content. D) matrix supported fabric with unoriented micas. Note difference in mica reflectance. Mica in upper left has higher K-content.

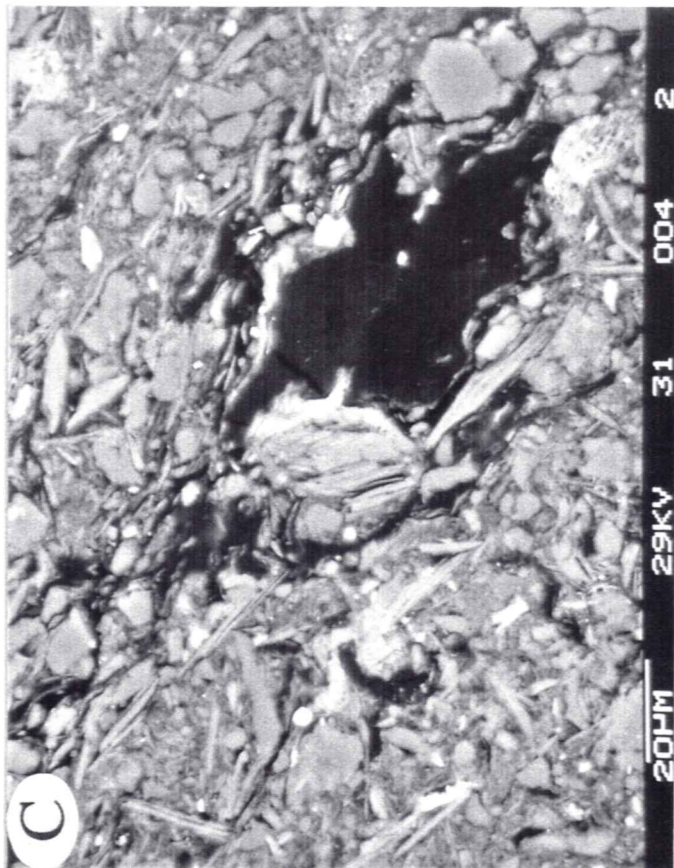
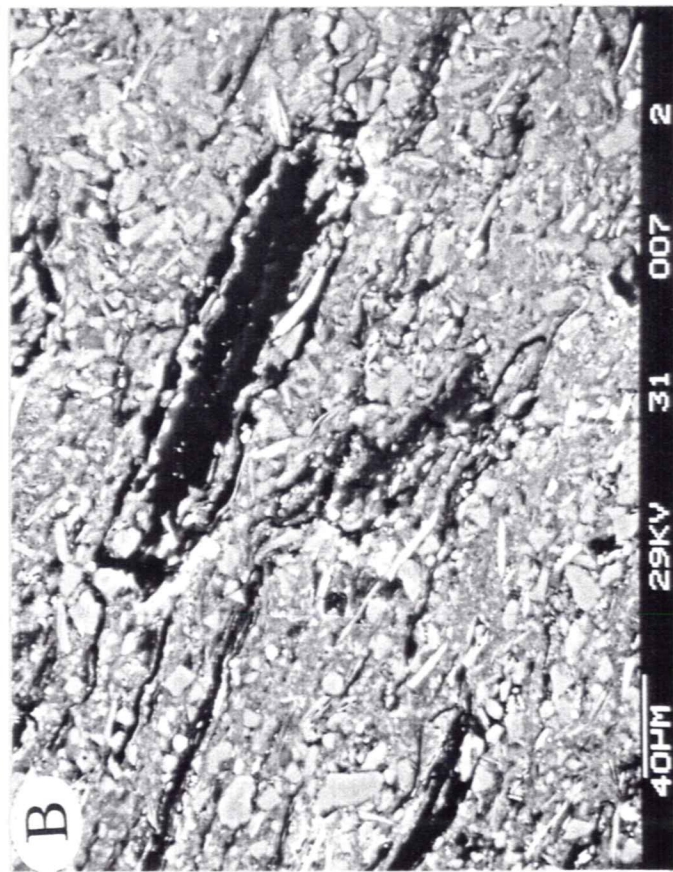
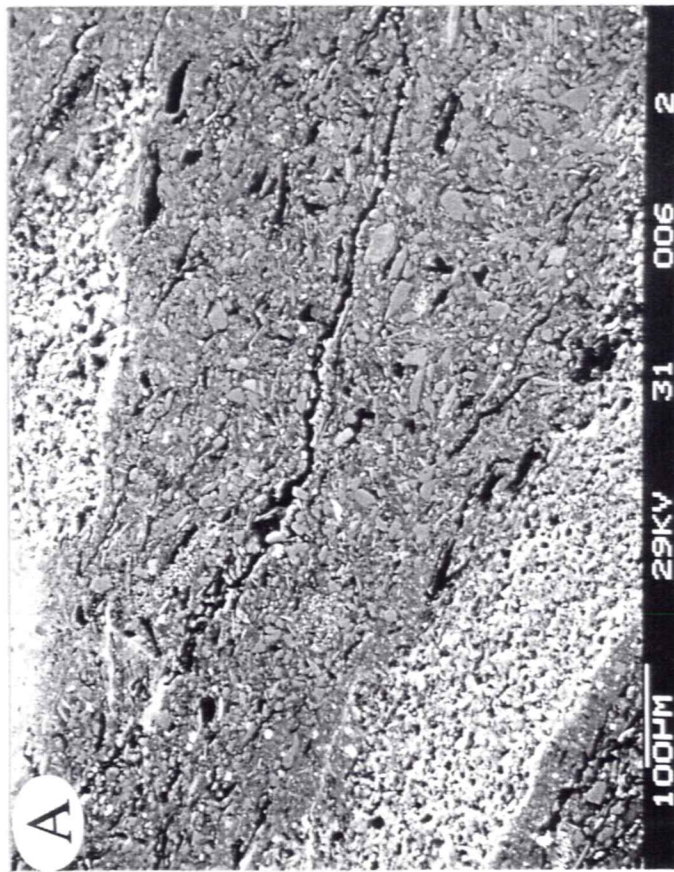


Plate 3. Sample O09031 or BAR-3 - 1765m - normally pressured - 28 - 34% measured porosity - 25-29% sonic porosity - bulk density = 1.78 g/cm³. A) fine silt in a matrix of quartz, illite, K-feldspar, and some mica, primarily "weathered" muscovite. B) high-magnification of claystone matrix. Bright grain is anatase. C) sideritized rootlet. D) high magnification of sideritized rootlet fibers.

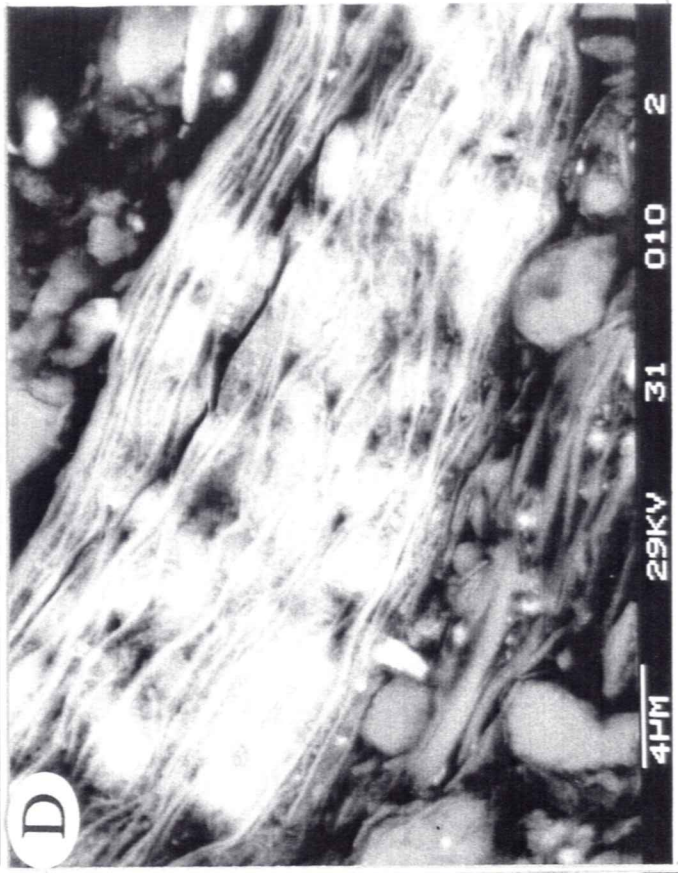
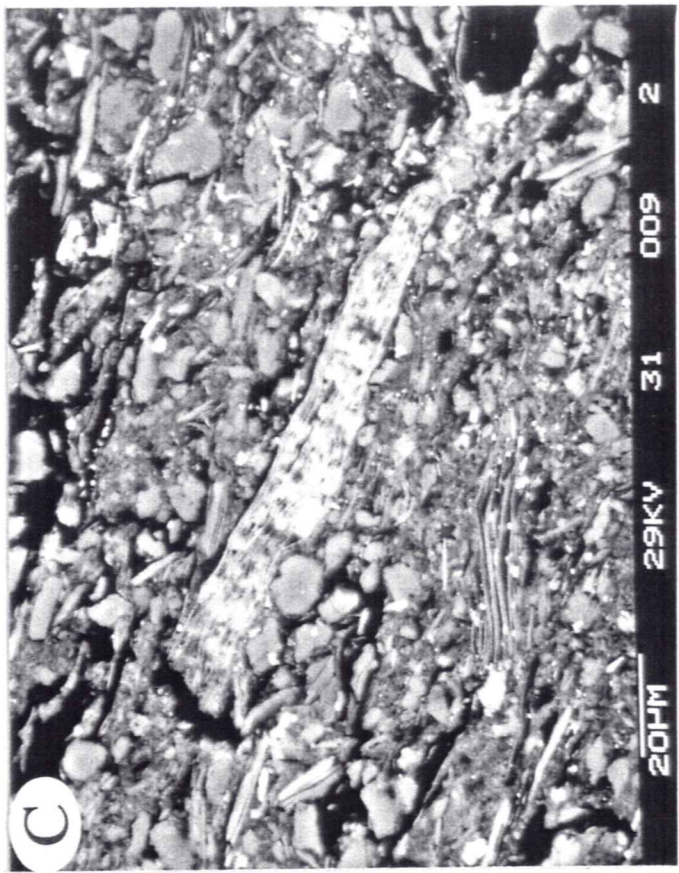
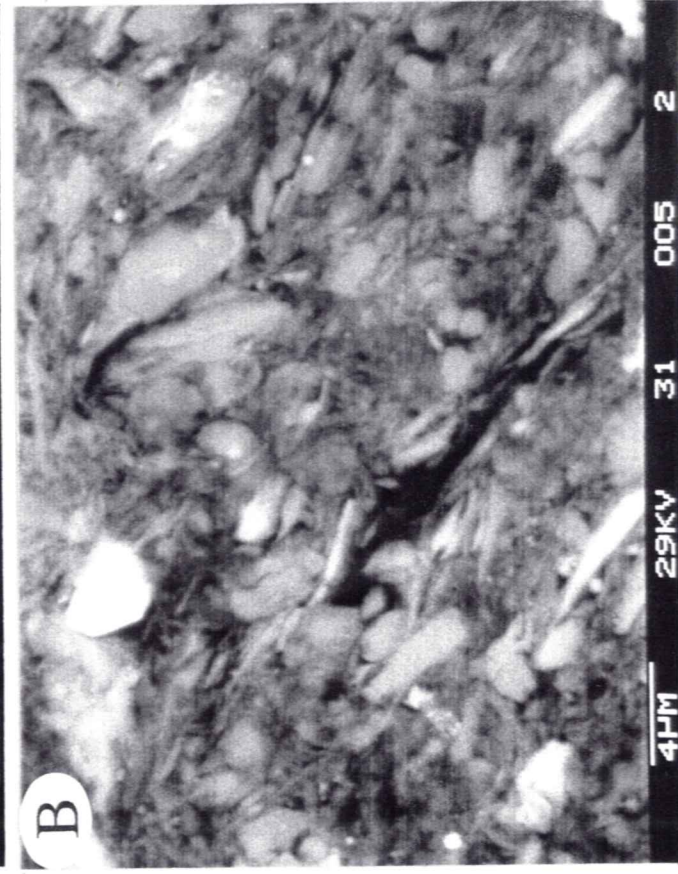
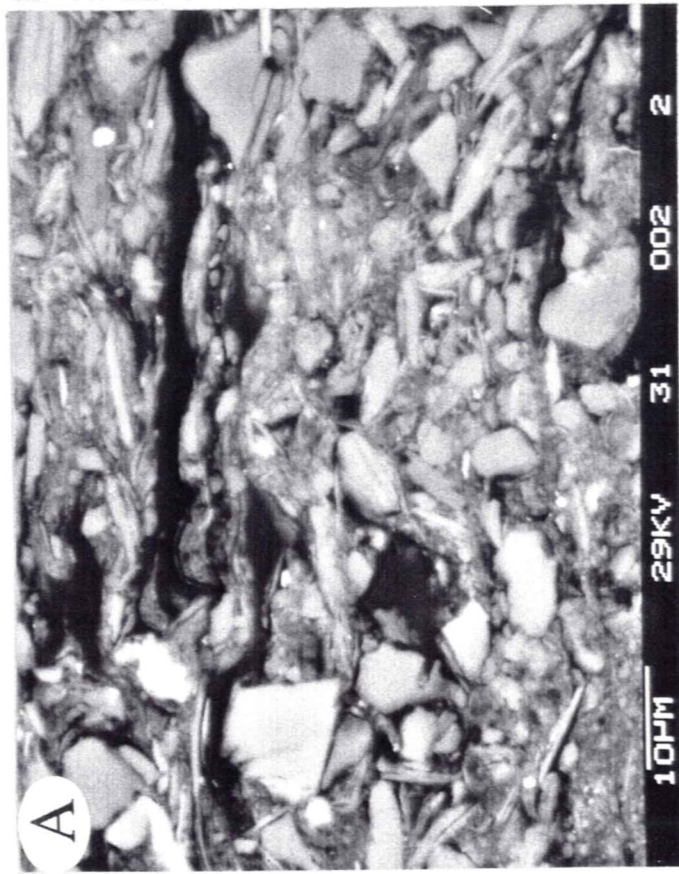


Plate 4 - Sample G33101 or BTG-5 - 2459m - normally pressured - ~ 8% measured porosity - ~12-17 % sonic porosity - bulk density = 2.46 g/cm³. A) Interlaminated silt- and clay-rich laminations showing variable porosity distribution. Bedding plane is diagonal (in direction of arrow). Bright spheres are authigenic pyrite. B) quartz- (upper left) and illite-rich zones with contrasting fabrics. Porosity appears to be greater in phyllosilicate rich matrix. C) framework-supported, silt-rich lamination. Grain contacts are dominantly tangential with little penetration and micas show minimal deformation. Porosity appears to be high. D) compacted matrix showing bedding-parallel fabric.

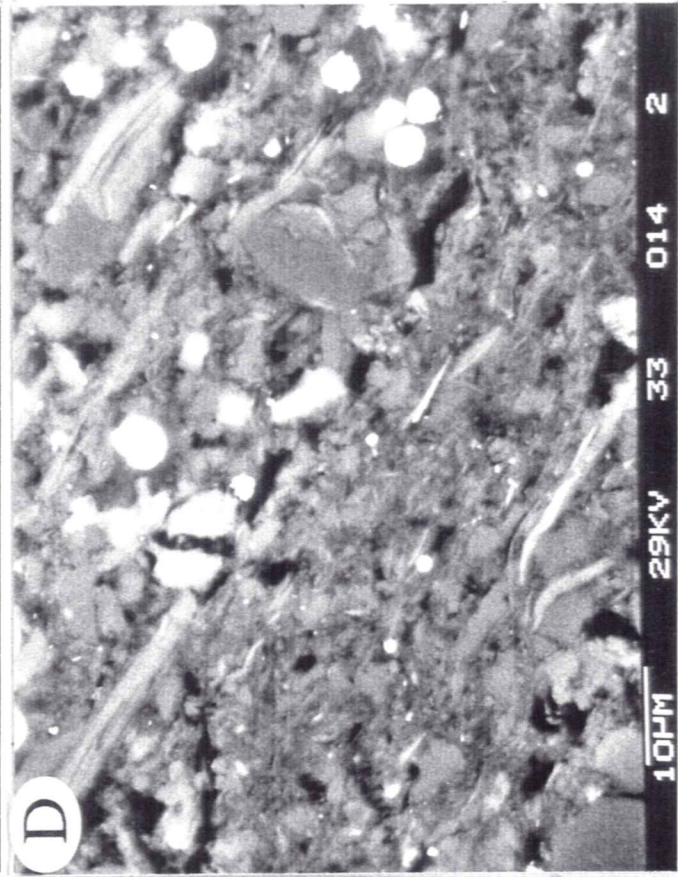
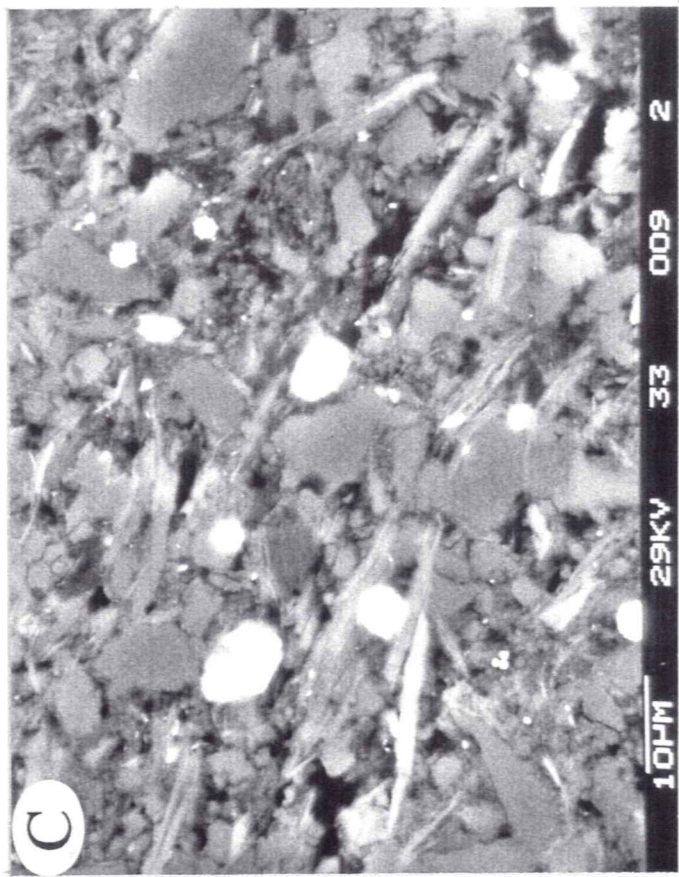
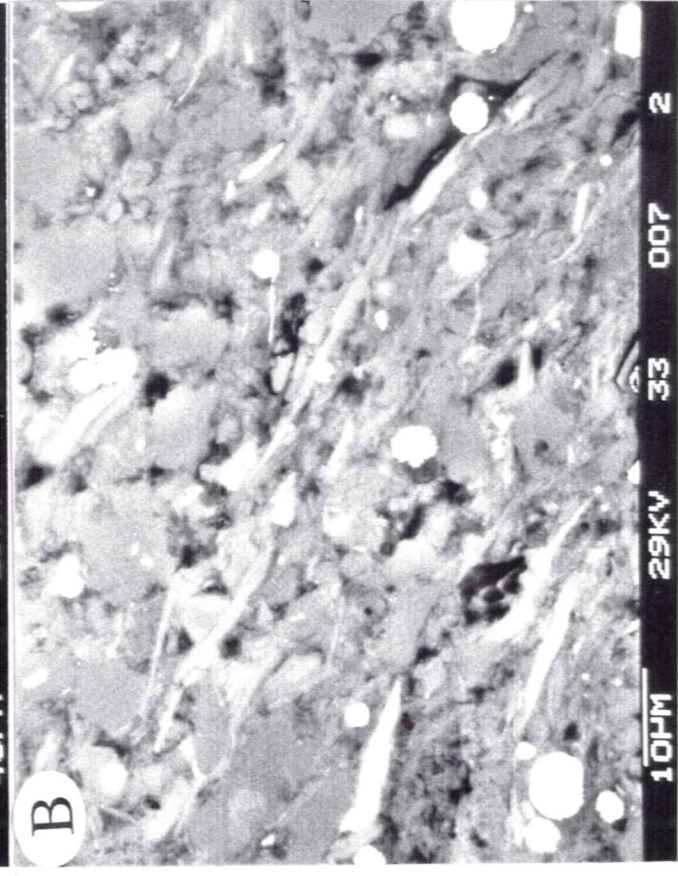
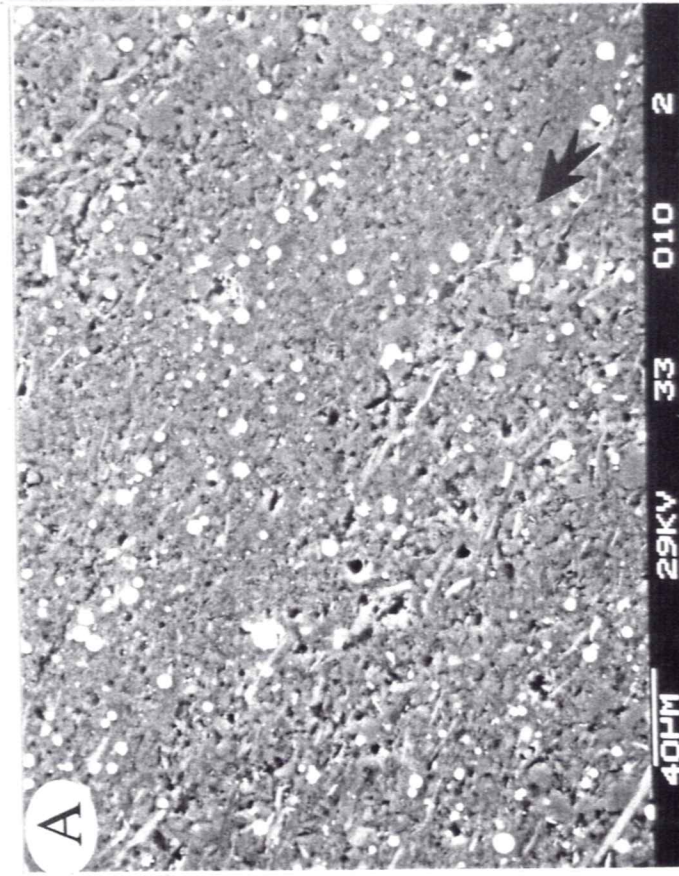


Plate 5 - Sample G33101 or BTG-5 - 2459m - normally pressured - ~ 8% measured porosity - ~12-17 % sonic porosity - bulk density = 2.46 g/cm³. A) starved ripple (?) or burrow with Ca-plagioclase (P), K-feldspar (K) and quartz, partially cemented with kaolinite. Grain contacts are dominantly tangential. B) kaolinite cement (dark area to left) with a matrix of Fe- carbonate or oxide, clay-sized quartz, and detrital illite. C) bedding parallel induced fracture. D) high magnification of fracture in C. The absence of material within the fracture and parallel edges suggest it is recently formed.

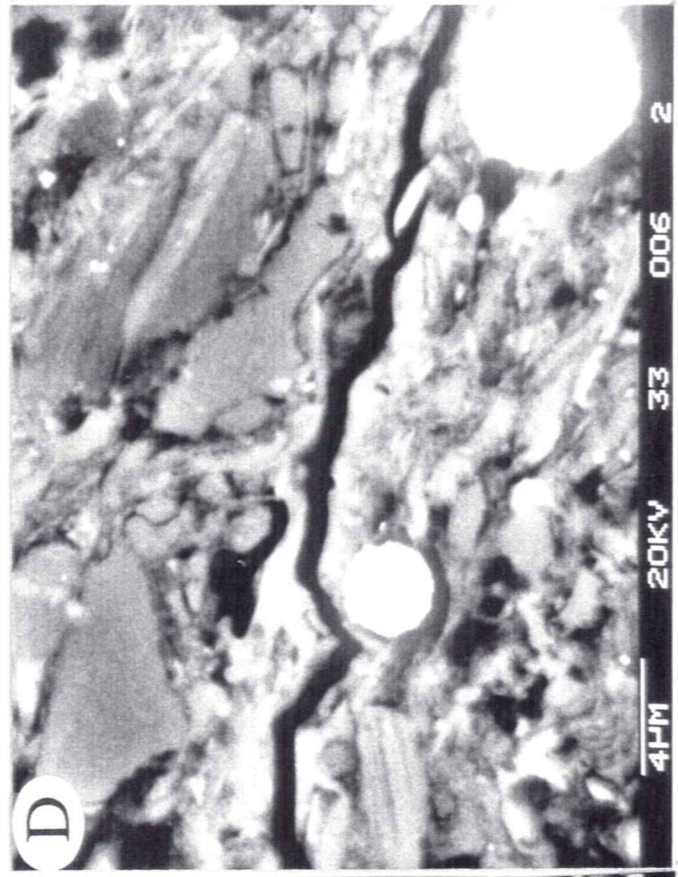
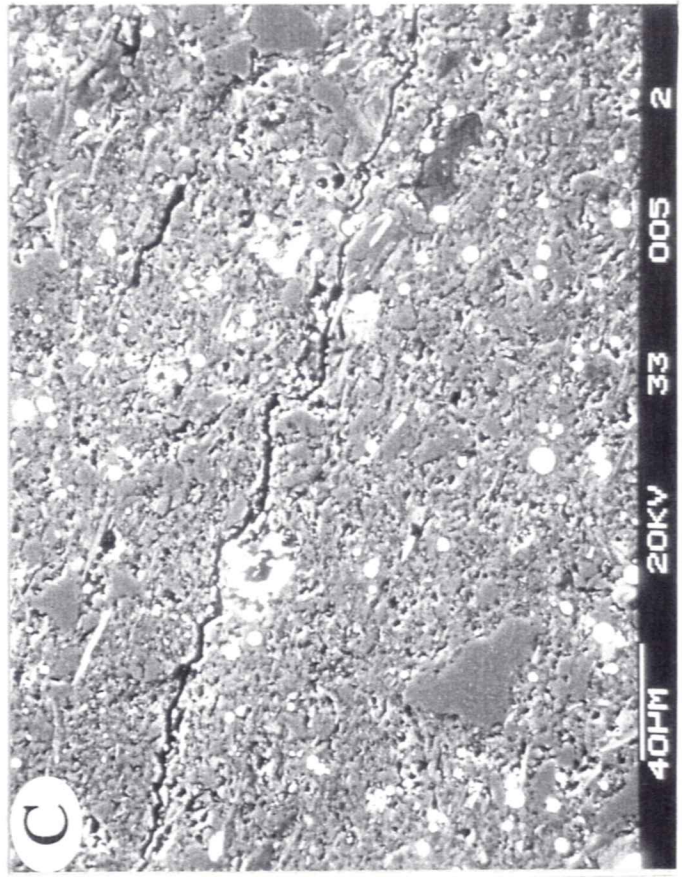
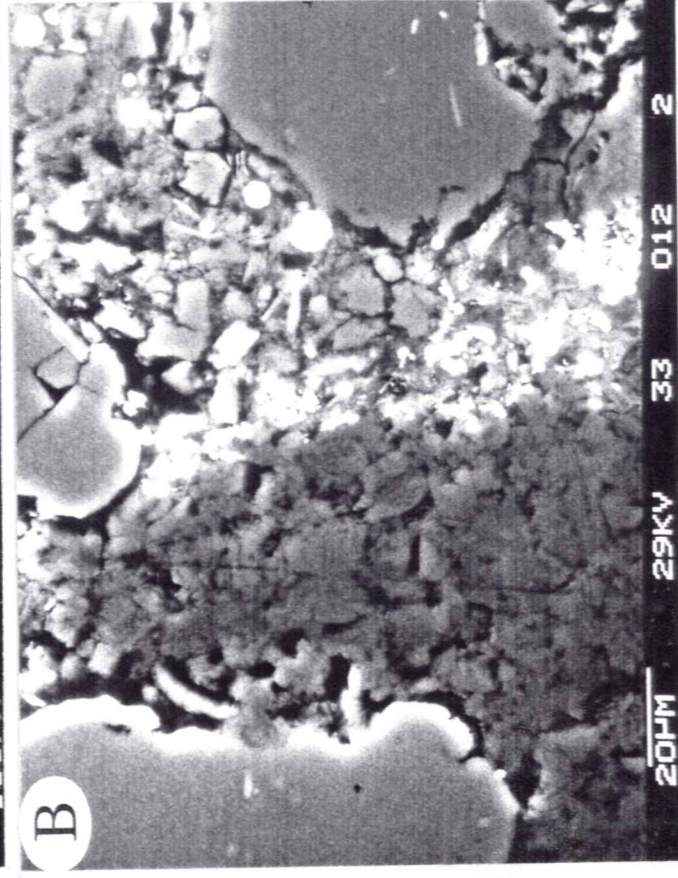
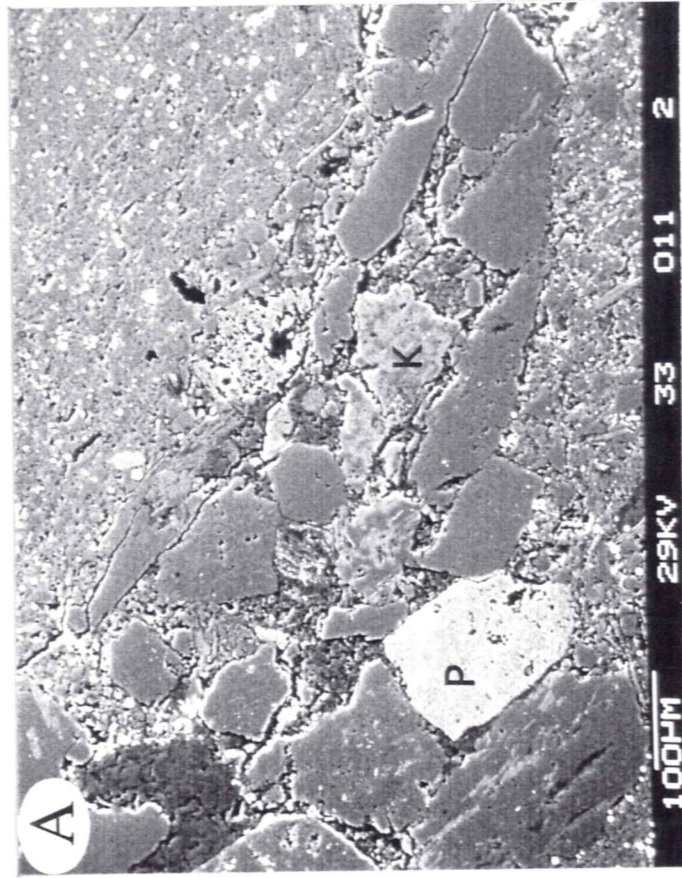


Plate 6 - Sample G33102 or BTG - 6 - 2460m - normally pressured - 7-10% measured porosity - sonic porosity = 12-17% - bulk density = 2.55 g/cm³. This sample is located 1m below G33101 (plates 4 and 5). A) bedding parallel or sub-parallel induced fractures in pyritic claystone. Authigenic pyrite is abundant. B) medium sand-sized quartz grain in claystone matrix. C) compacted organic grain in claystone with small stringer on right side D) very fine-grained matrix comprising clay flocs, quartz and pyrite.

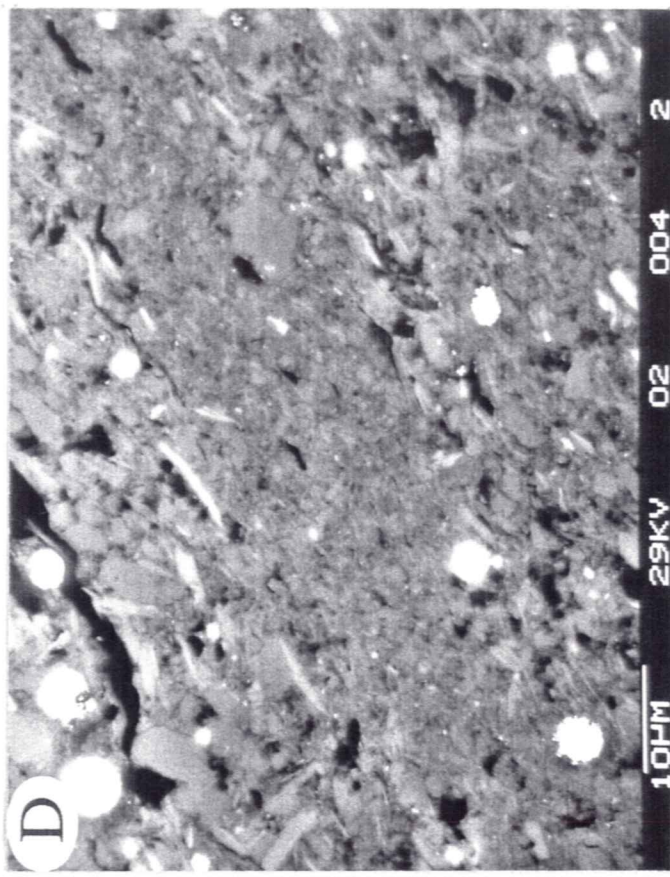
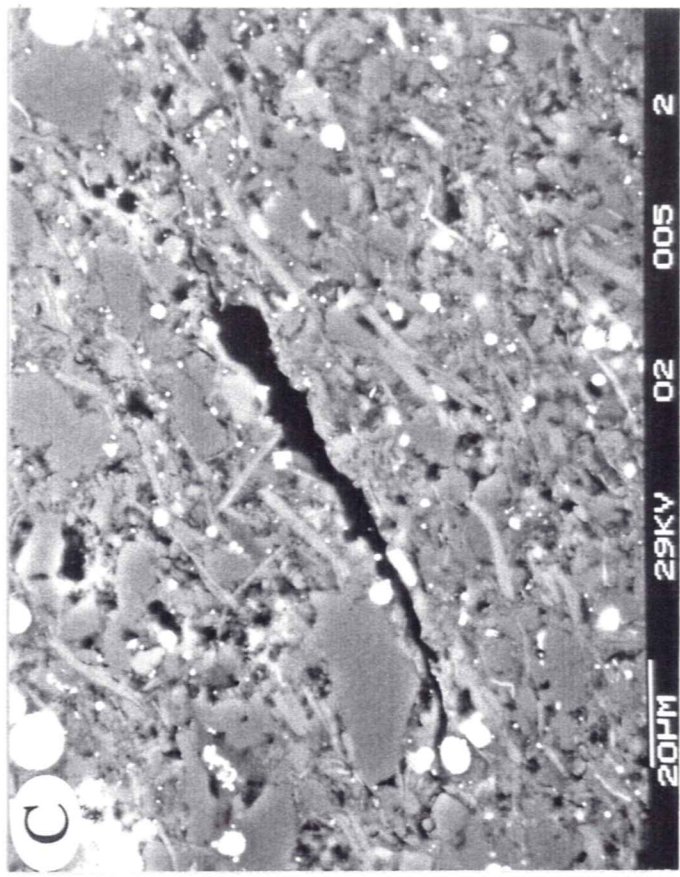
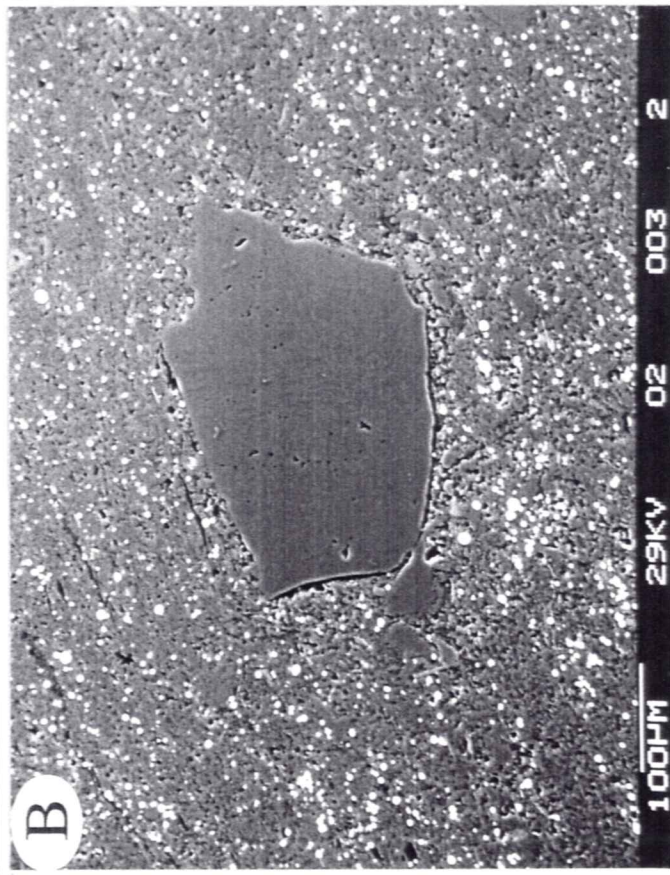
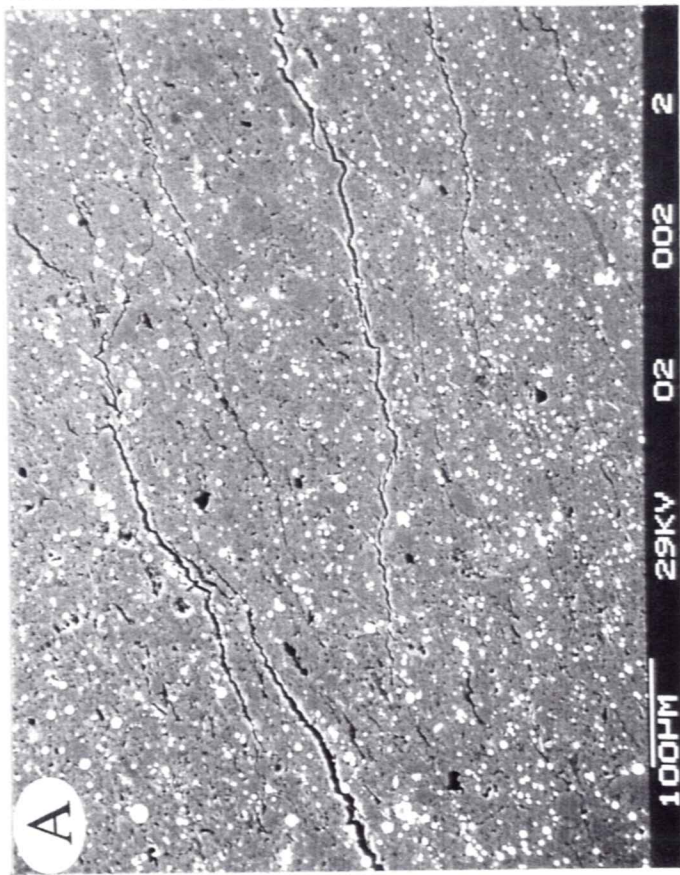


Plate 7 - Sample F24011 or BAM-1 - 3106m true vertical depth (TVD), normally pressured, ~ 10-14% measured porosity, 12 % sonic porosity - bulk density = 2.50 g/cm³. A) well-compacted siltstone with quartz rich matrix. Some illite and chlorite are present. Intergranular porosity appears to be high. B) flattened fecal pellet in siltstone. C) poorly-sorted siltstone with high intergranular porosity. D) poorly-sorted siltstone with rutile (left) and sideritized fecal material (upper left). Note abundant porosity.

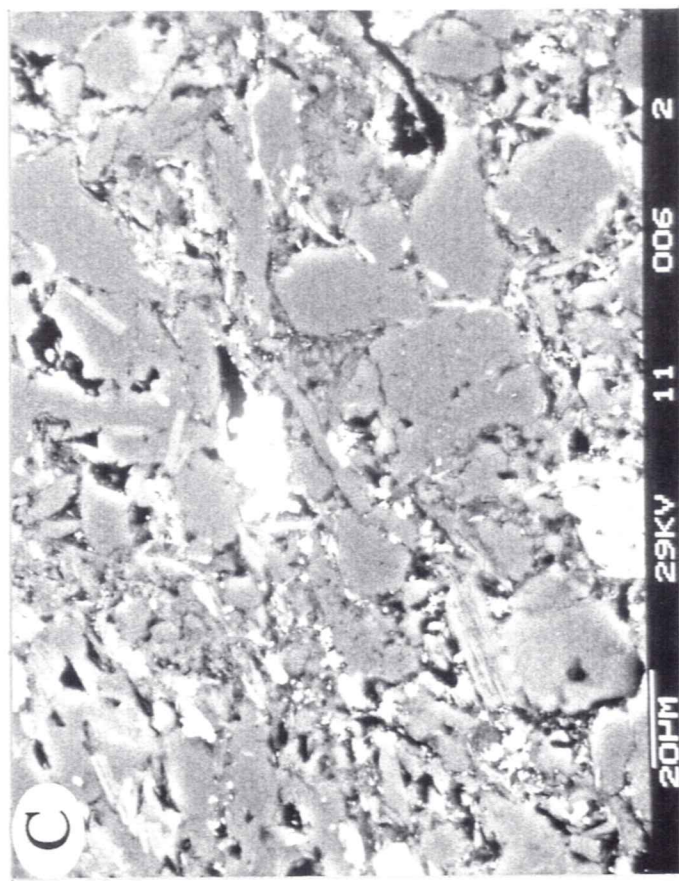
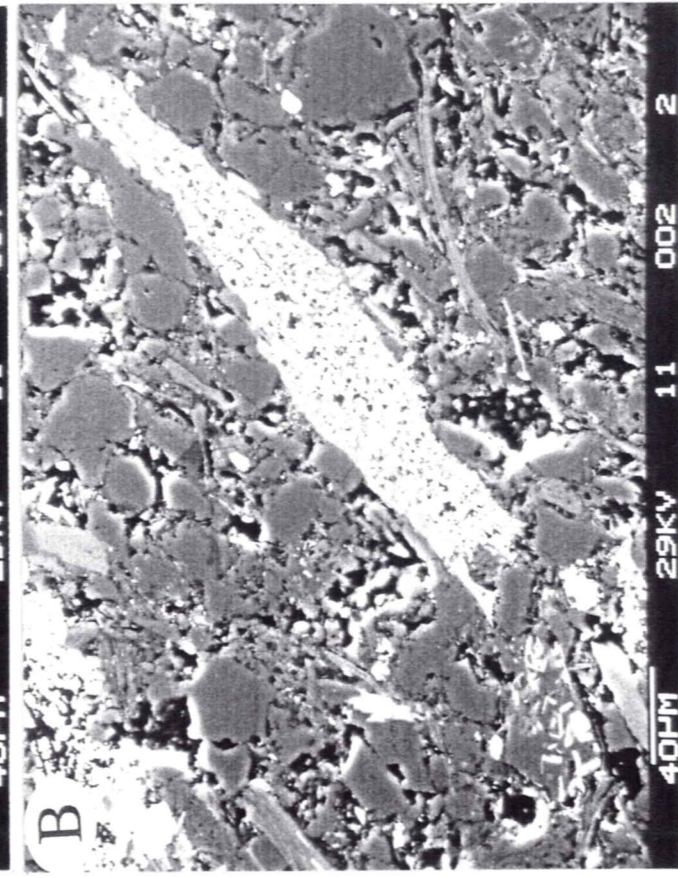
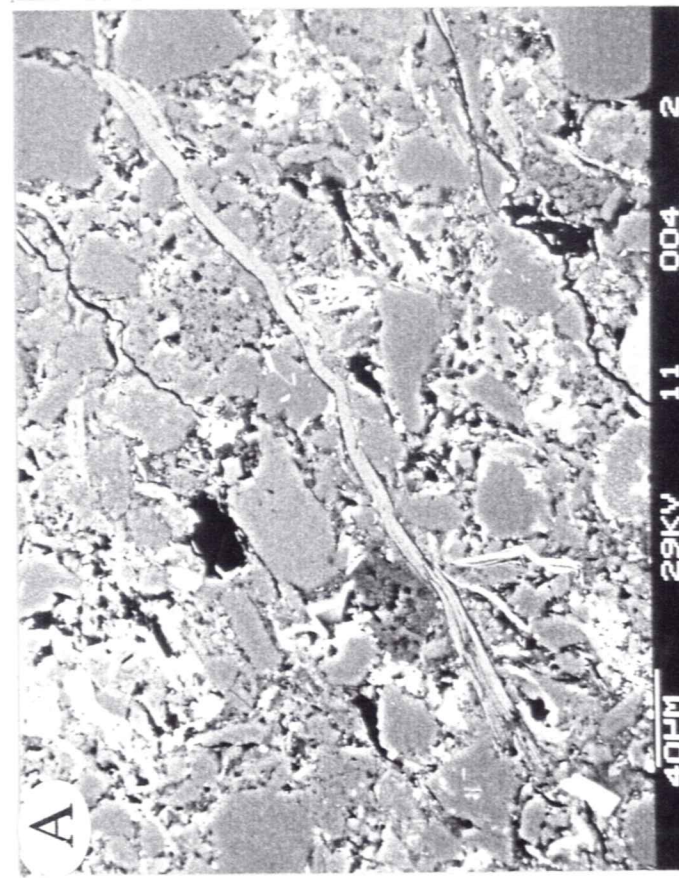


Plate 8 - Sample F24021 or BAM - 2 - 3119m TVD - normally pressured - 11-12% measured porosity, 12% sonic porosity - bulk density = 2.40 g/cm^3 . A) matrix supported, relatively homogeneous fabric. B) induced fracture in fine-grained siltstone. C) sand-sized K-feldspar in bioturbated siltstone matrix. D) a lot of charging at grain edges indicating relief on polished surface. Matrix is dominantly quartz with illite and siderite. Is the quartz in the center authigenic?

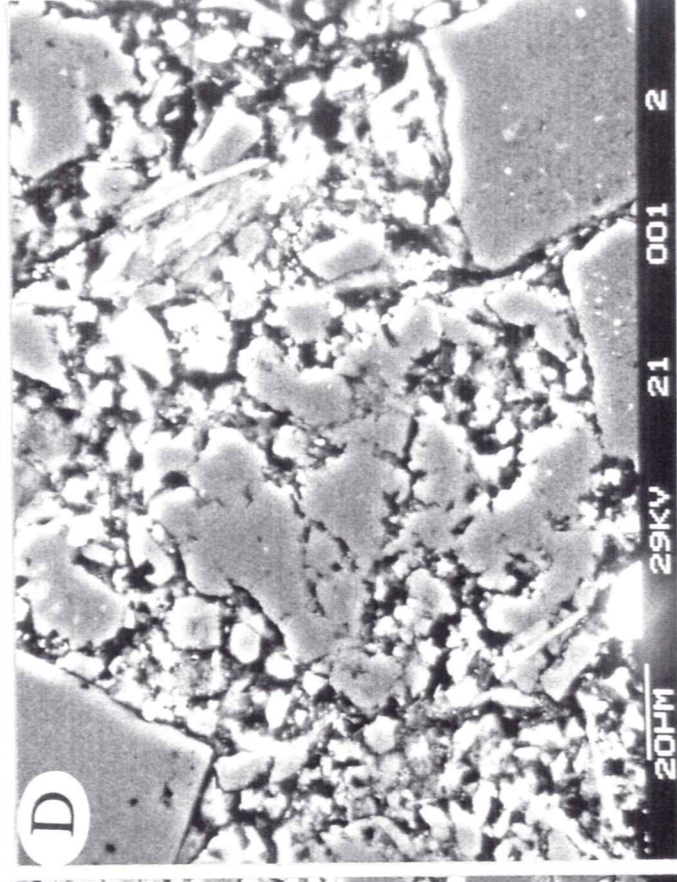
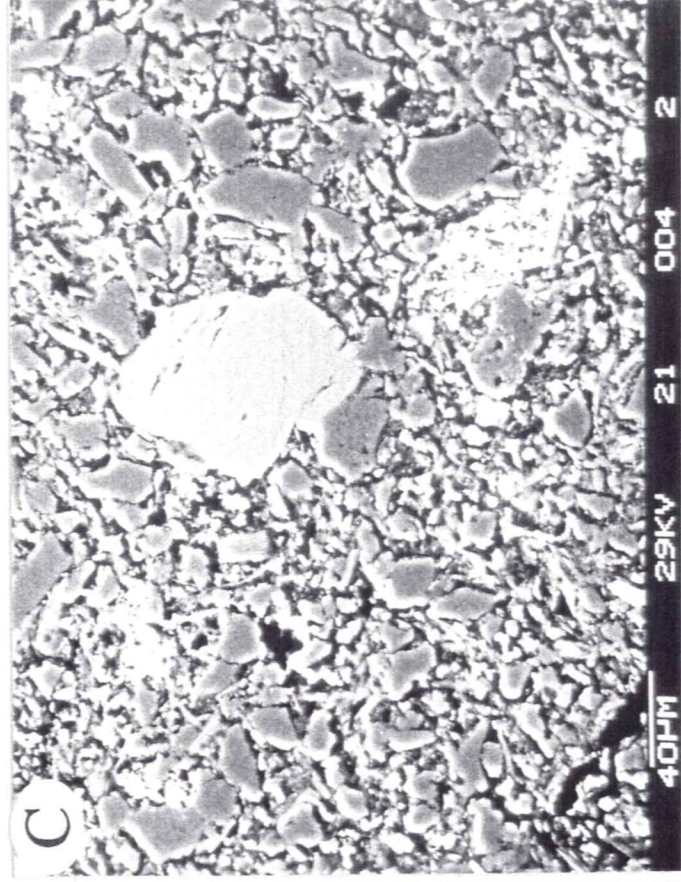
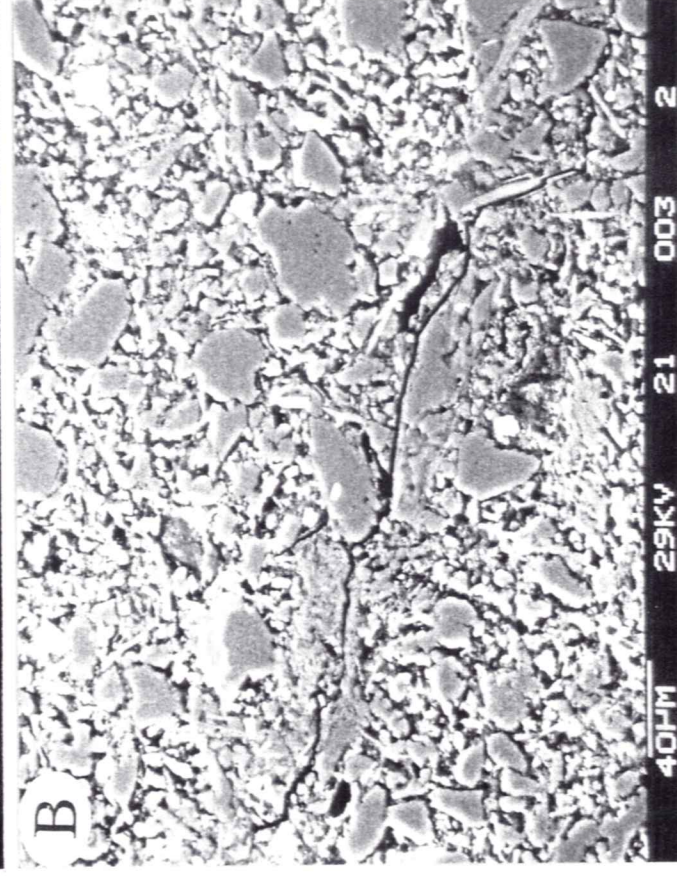
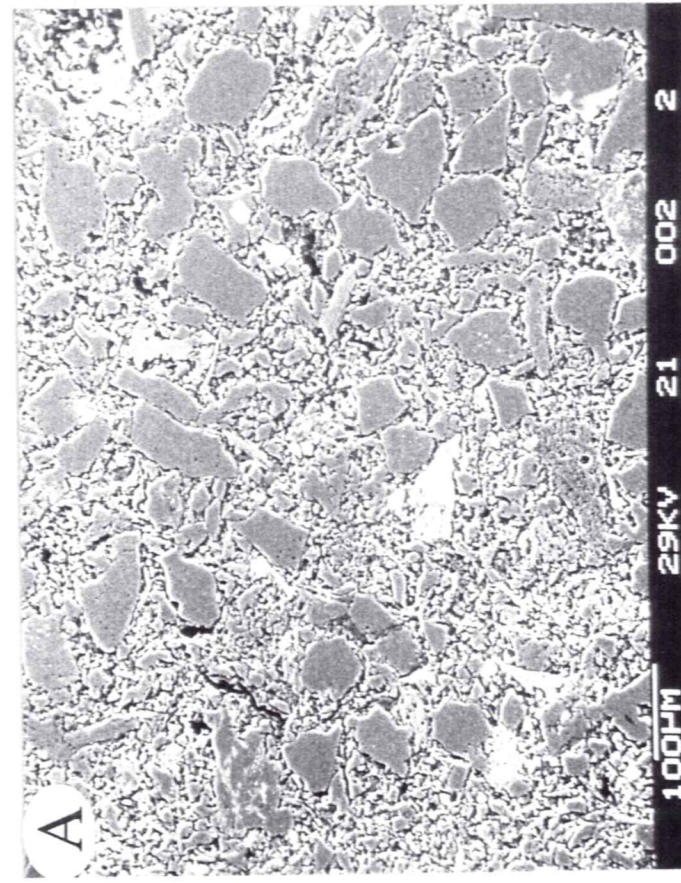


Plate 9 - Sample F24041 - BAM-3 - 3341m TVD - normally pressured - ~9.5 to 10 % measured porosity, sonic porosity = 10-12% - bulk density = 2.44 g/cm³.
A) poorly-sorted quartz siltstone with a lithic fragment (F), fecal pellet (P) and siderite (S) clast. B) Fe-rich K-Al-silicate - probably a sideritized illite-rich zone or possibly glauconite. C) low magnification of silica cement (?), or a partially dissolved chert grain? D) high magnification of C.

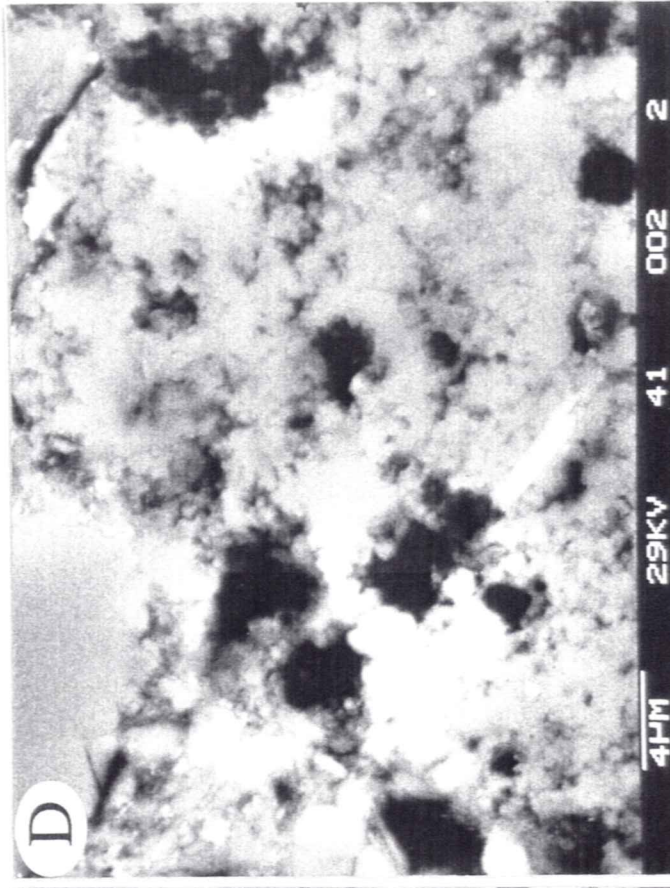
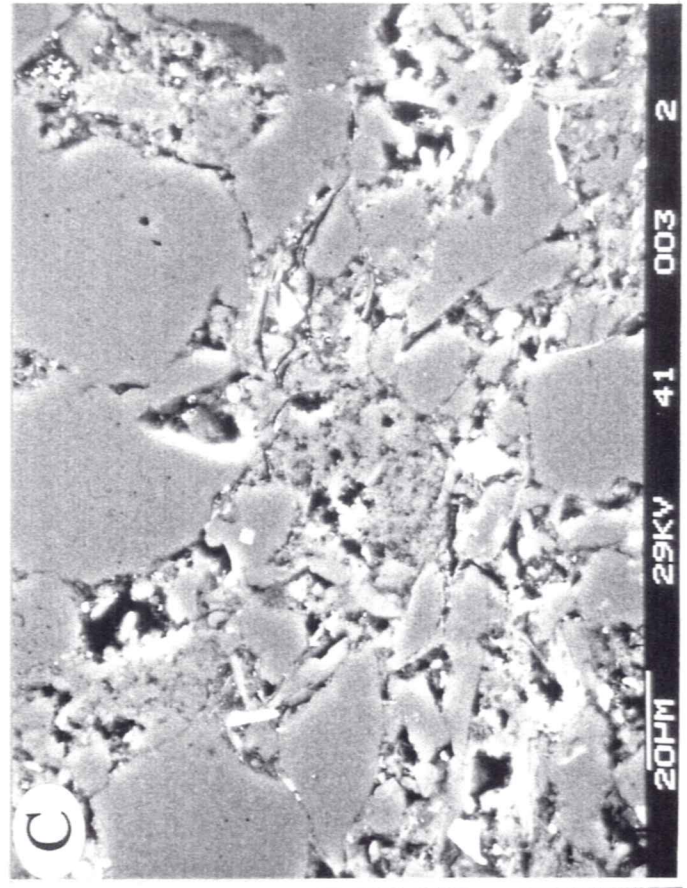
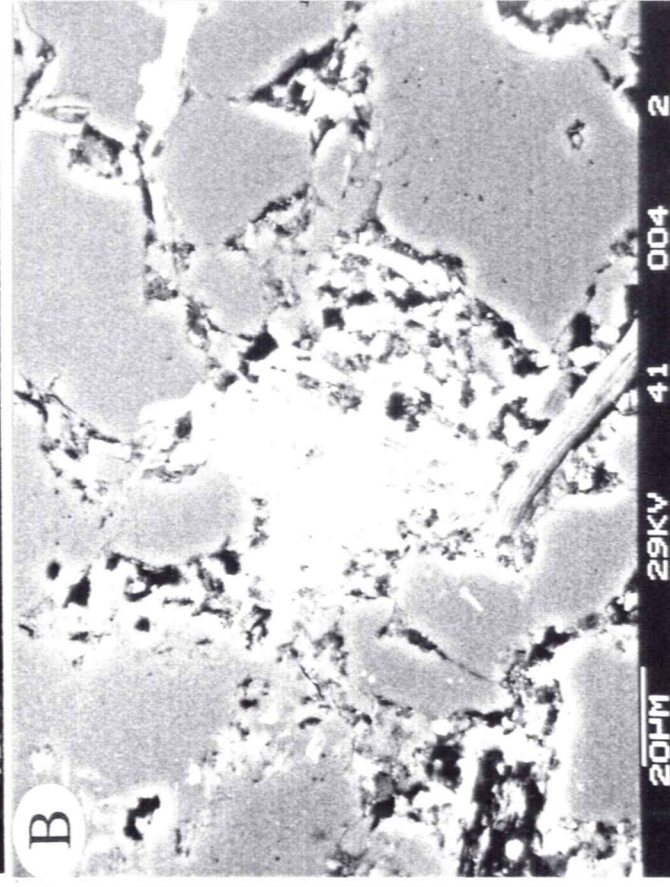
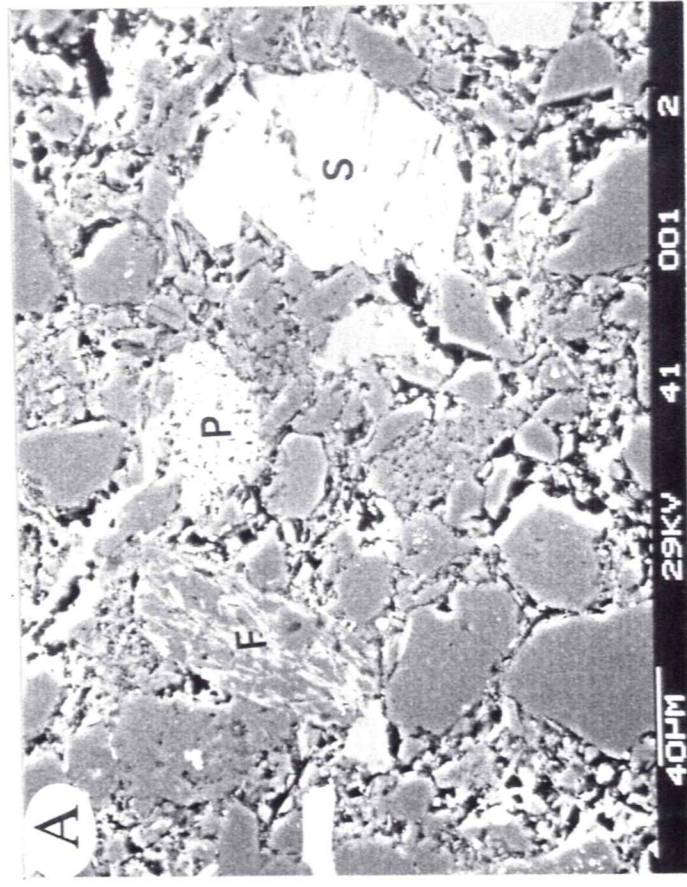


Plate 10 - Sample D27141 or BRE-8 - 2421m - overpressured - ~ 8% measured porosity - 11-13% sonic porosity - bulk density = 2.48 g/cm³. A) bitumen-filled fracture network in matrix supported silt-rich lamination. B) matrix supported silt grains, primarily quartz. C) fairly well-sorted, angular to sub-angular, matrix supported quartz silt. D) abundant matrix porosity in fine-grained siltstone. Matrix fabric is chaotic.

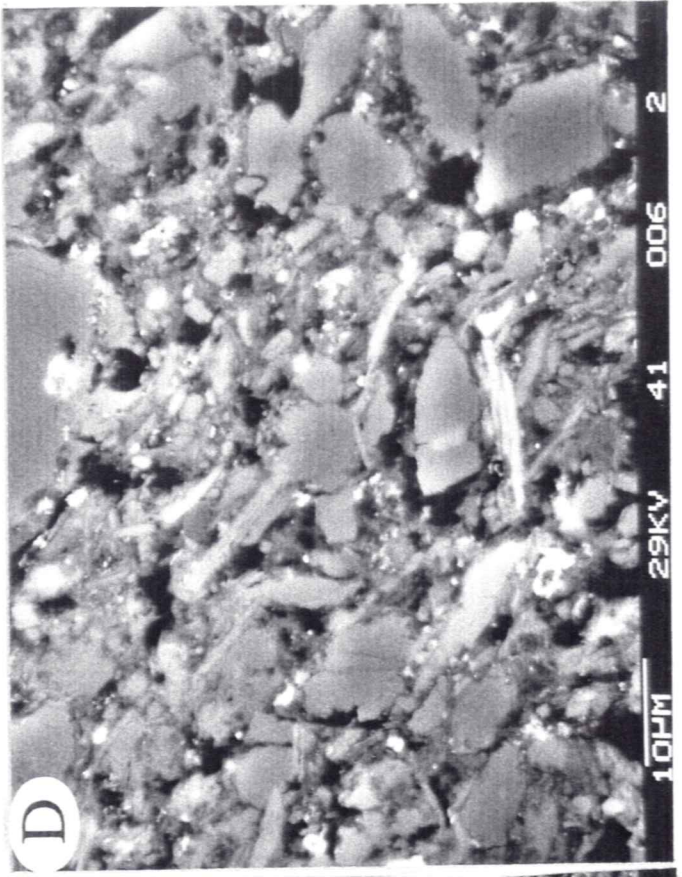
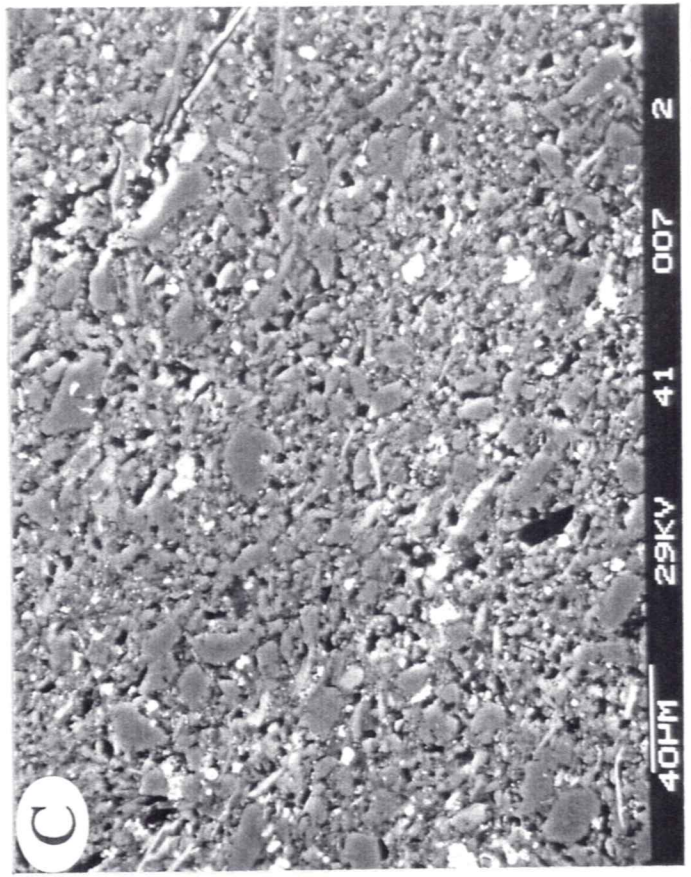
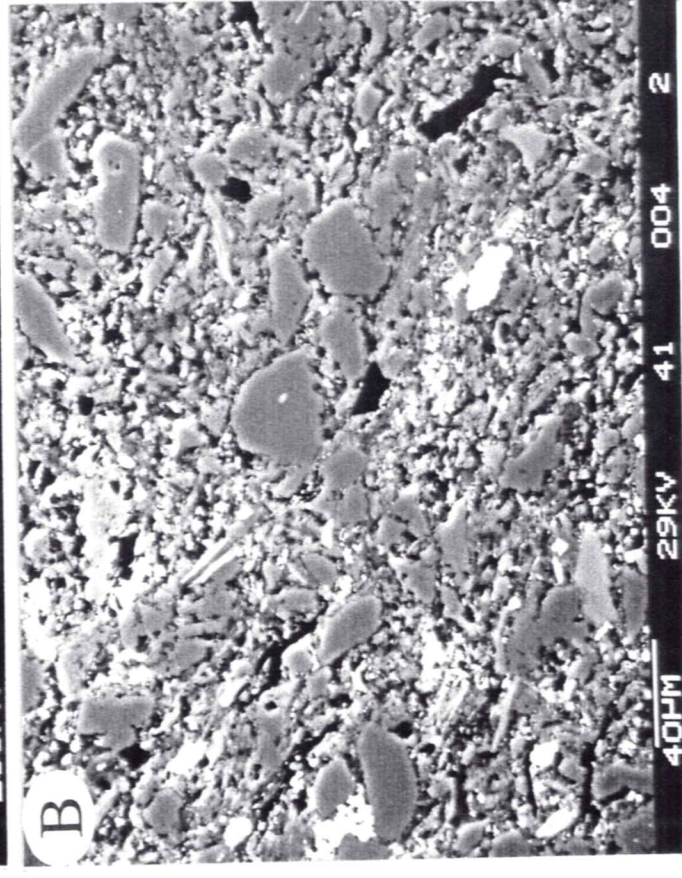
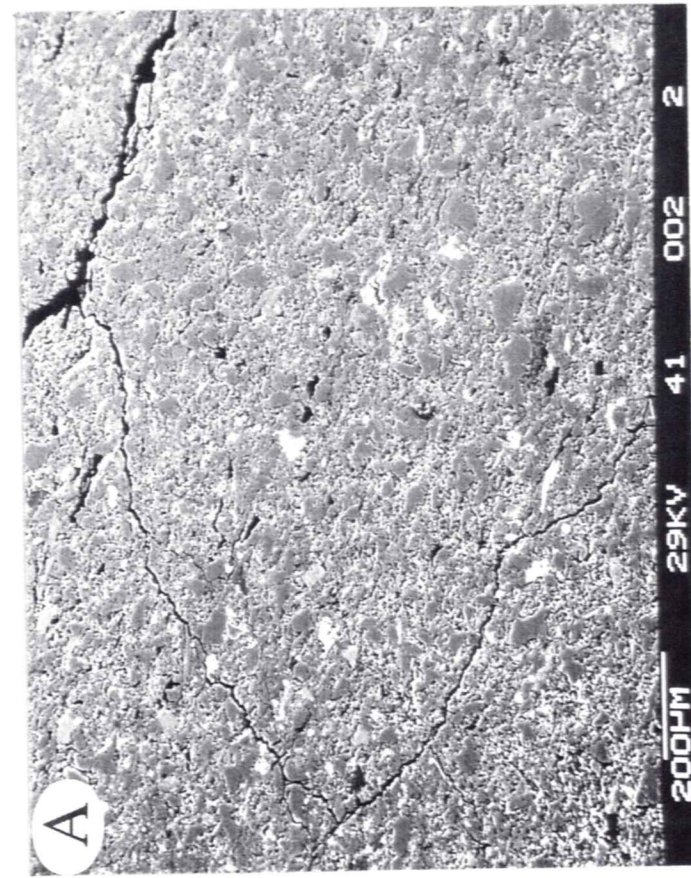


Plate 11 - Sample D27141 or BRE-8 - 2421m - overpressured - ~ 8% measured porosity - 11-13% sonic porosity - bulk density = 2.48 g/cm³. A) very low magnification of organic clasts and stringer. B) organic "clast" with a stringer of organic matter that works along a bedding parallel plane. C) mechanical compaction - note deflected mica that is penetrating quartz grain. D) high-magnification of a portion of the organic stringer shown in B. Note porosity restriction below fractured quartz grain.

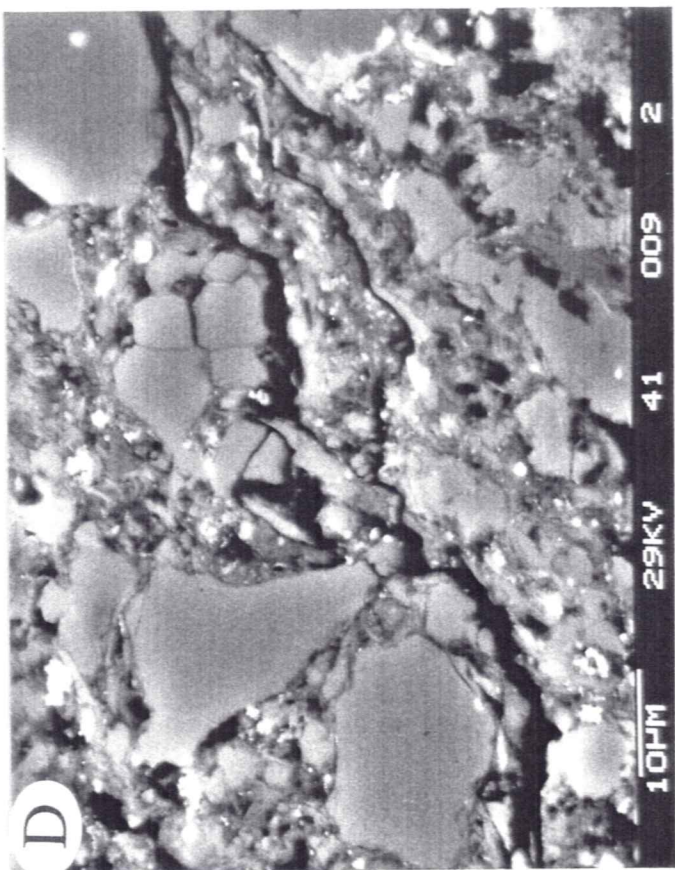
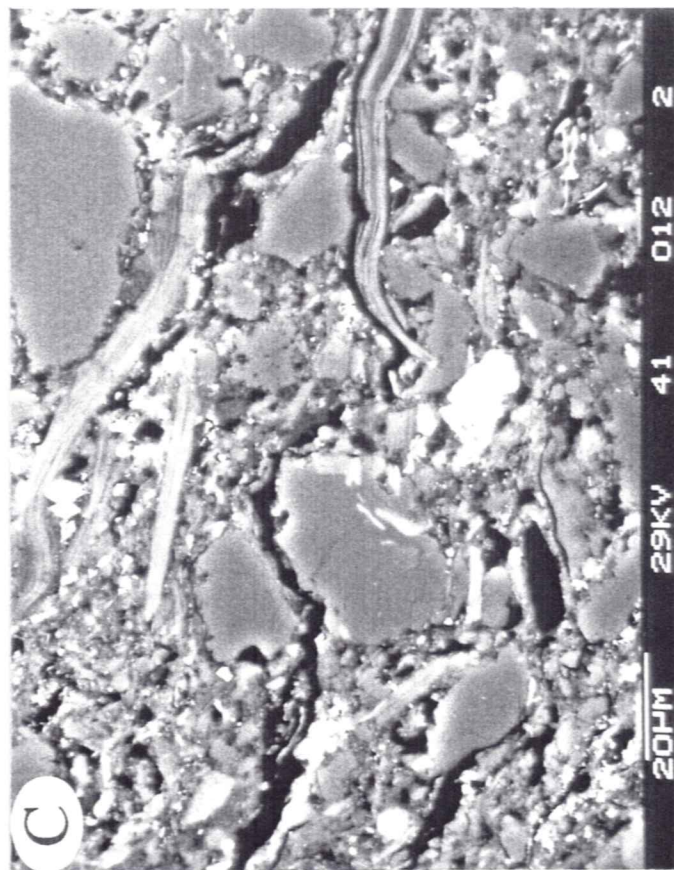
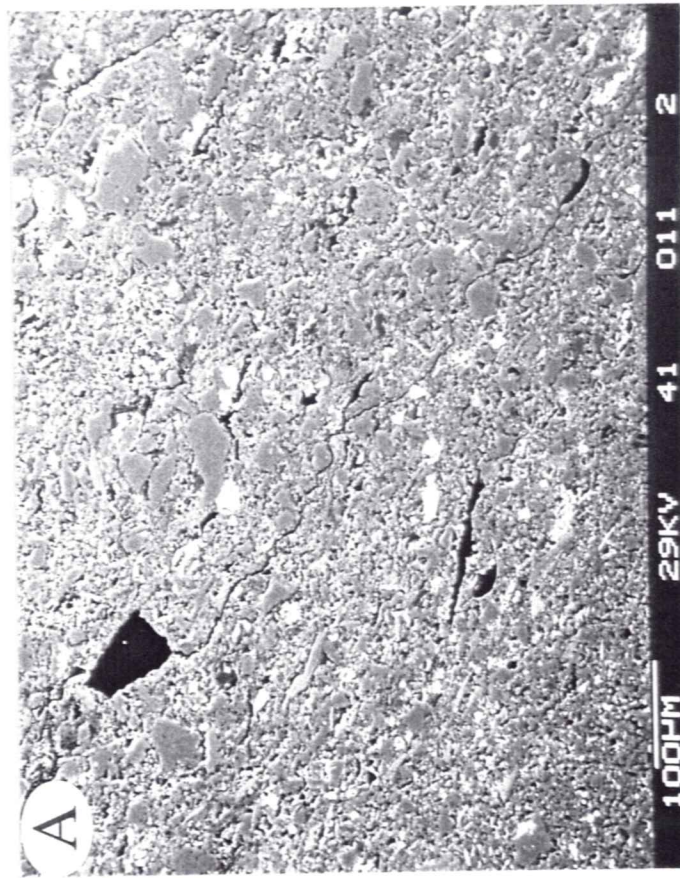


Plate 12 - Sample D27141 or BRE-8 - 2421m - overpressured - ~ 8% measured porosity - 11-13% sonic porosity - bulk density = 2.48 g/cm³. A) bedding sub-parallel organic stringer connects with a vertical, cross-bed oriented stringer (at lower arrow. B) bitumen filled sub-parallel (to bedding) fracture with pyrite inclusions. C) mechanically induced restriction along organic stringer resulting in reduced permeability. This is a high magnification image of the area in A indicated by the upper arrow. D) another constriction (pore throat) in an organic stringer. This is a high magnification image of the area in A indicated by the lower arrow.

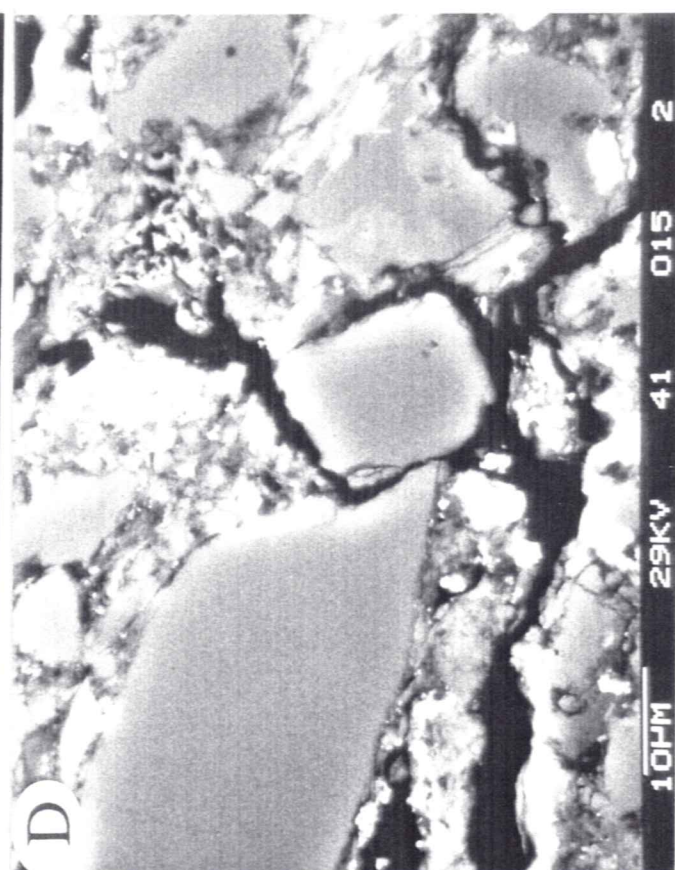
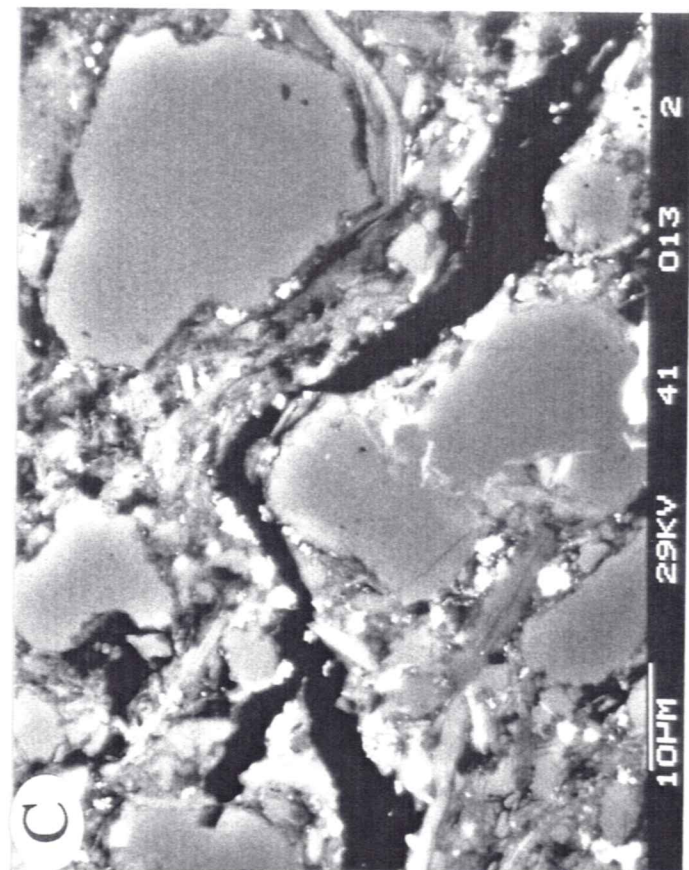
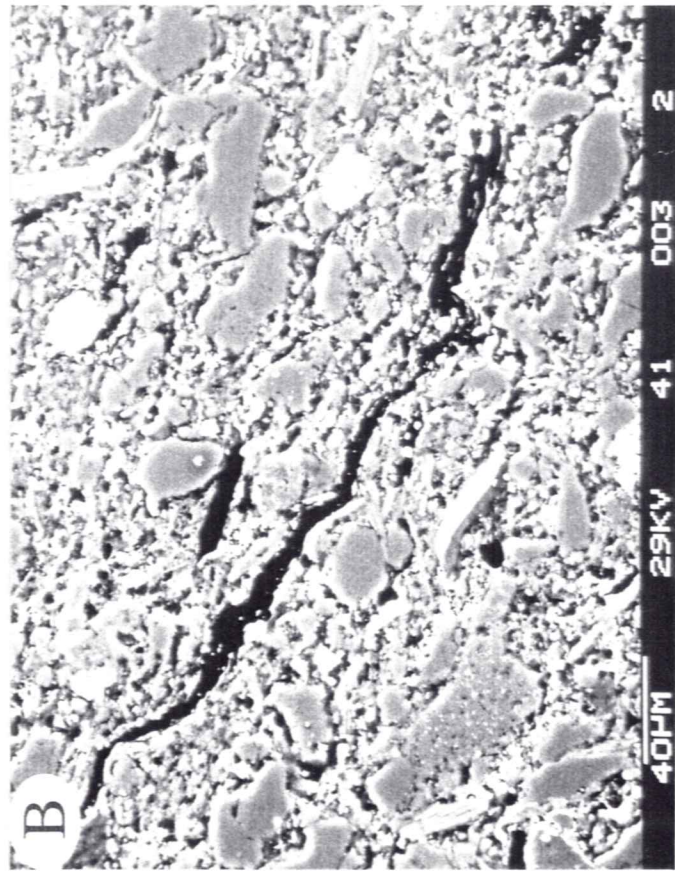
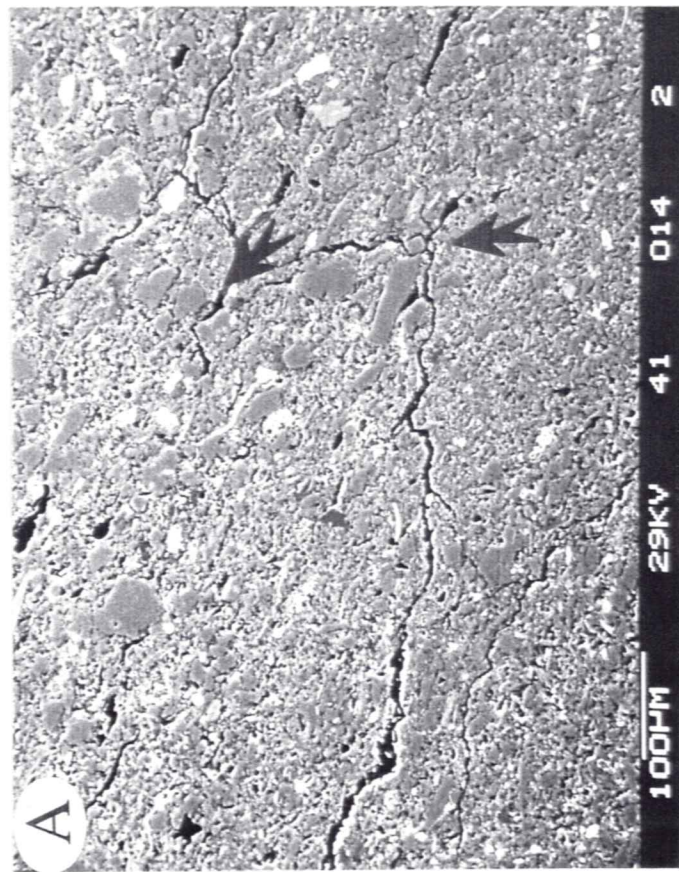


Plate 13 - Sample D27161 or B-RE-10 - 2725m - overpressured - ~10-11% measured porosity - ~ 15% sonic porosity - bulk density = 2.48 g/cm³. A) poorly sorted, matrix supported siltstone. B) high magnification of clay-rich zone (arrow) in center of A. Clay aggregates are laced with finely disseminated apatite and pyrite. Individual clay particles are blocky and lath shaped and aggregate boundaries are distinct. Compaction effects appear minimal. C) poorly sorted quartz grains with muscovite and disseminated pyrite and siderite. Pore-sizes are variable and appear poorly connected. Clay, or near-clay sized, particle fabric is particularly chaotic. D) poorly sorted, framework-supported silt grains of quartz, K-feldspar (K), K-leached biotite and/or chlorite and muscovite with intergrown siderite (S).

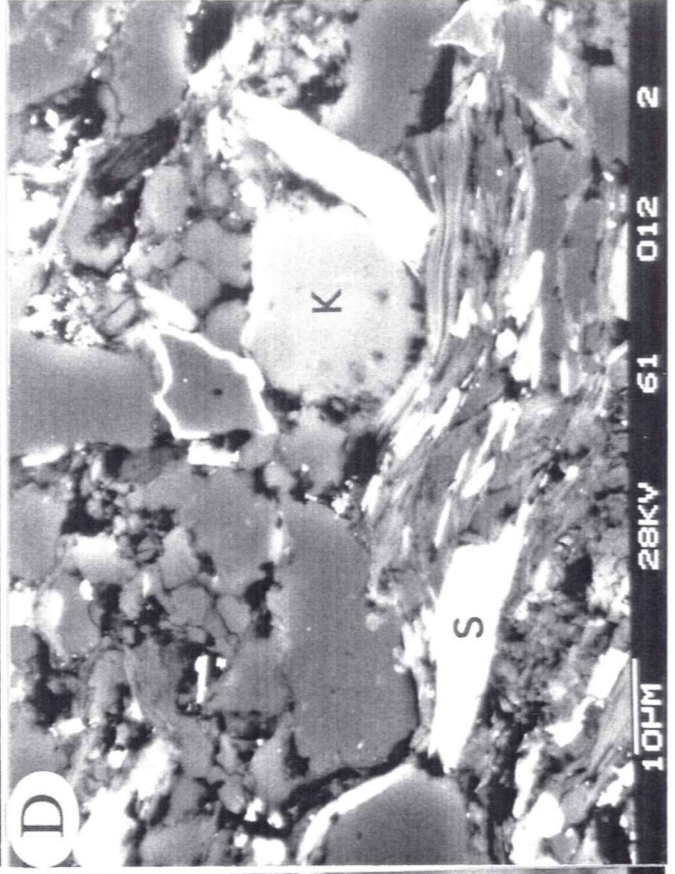
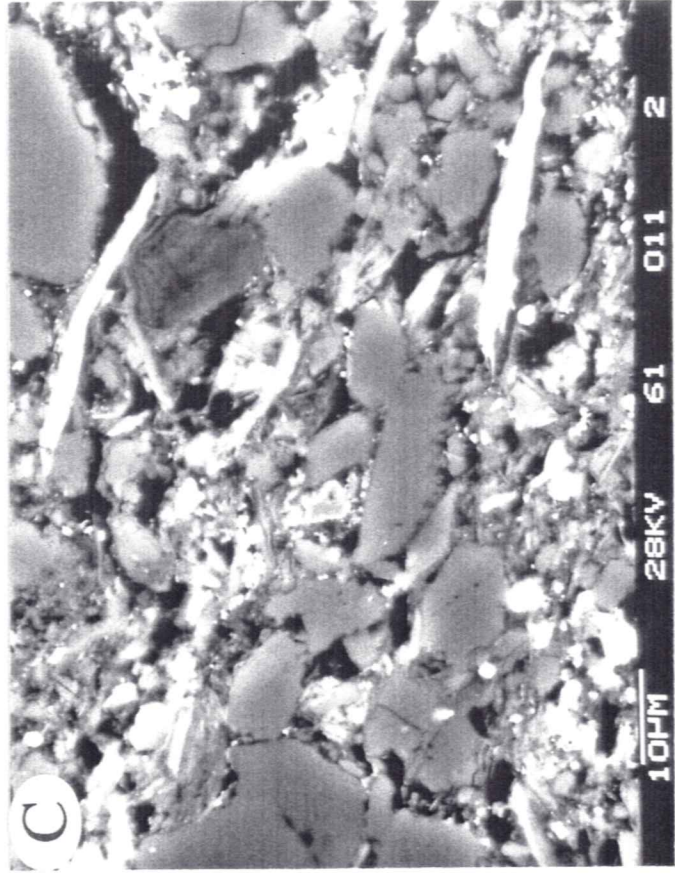
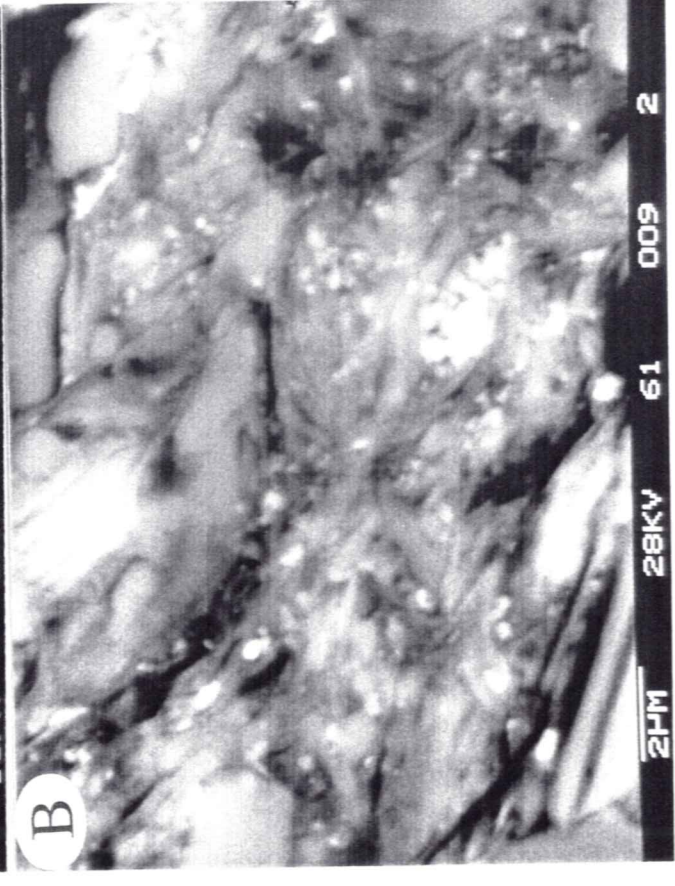
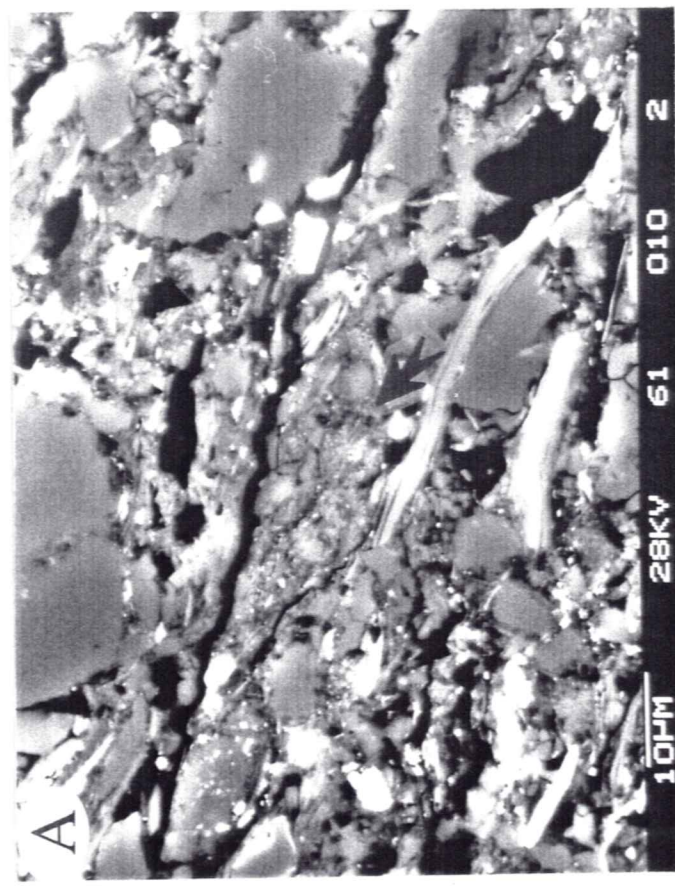


Plate 14 - Sample D27161 or B-RE-10 - 2725m - overpressured - ~10-11% measured porosity - ~ 15% sonic porosity - bulk density = 2.48 g/cm³. A) medium sand-sized quartz and chert (C) grains in mudstone matrix. Matrix fabric appears to "flow" around grains. B) medium sand-sized, unaltered quartz grain in mudstone matrix. C) kaolinized mica and unaltered muscovite in illitic and apatite-rich (sub-micron disseminated bright spots) matrix. Note aggregate of fibrous, fuzzy clay particles (arrow). This morphology is distinct from the blocky euhedral habit of detrital illite. Quartz grains in upper right corner (Q) show a triple junction suggesting that quartz overgrowths are present. D) chaotic matrix fabric characteristic of high-energy, episodic deposition. Note vertical, thin mica lathes that penetrate quartz grains.

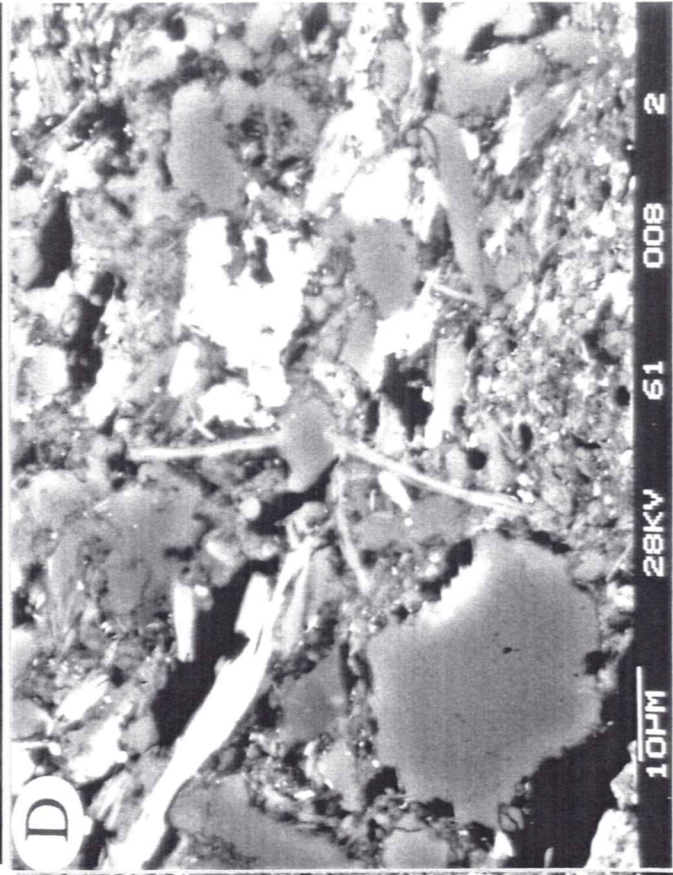
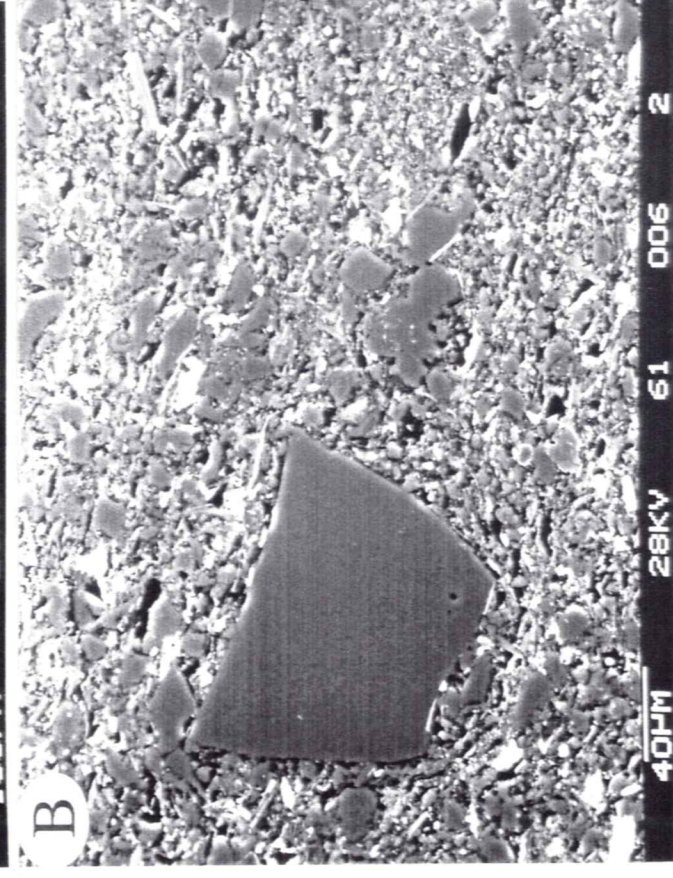
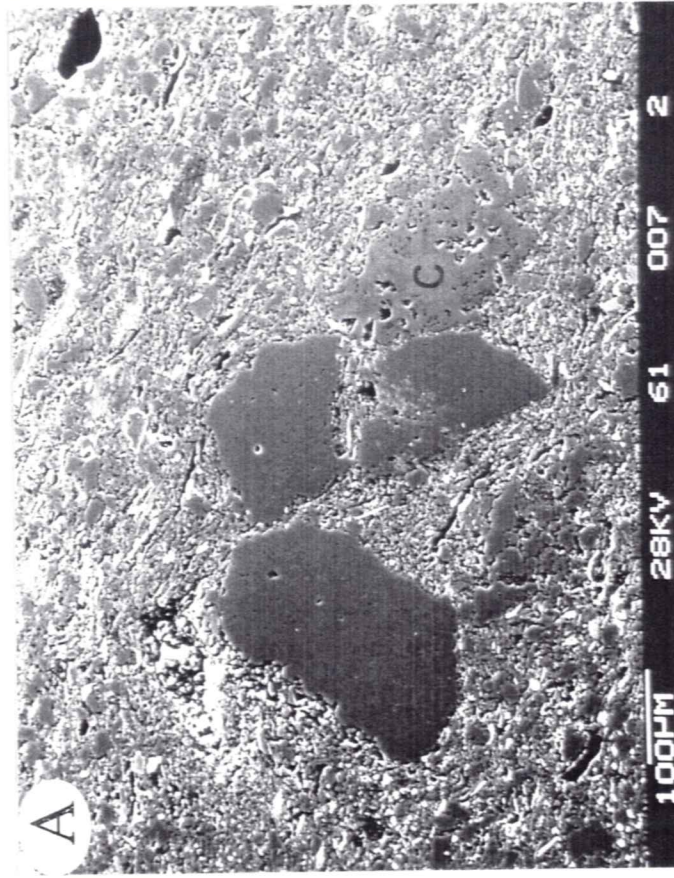


Plate 15 - Sample D27161 or B-RE-10 - 2725m - overpressured - ~10-11% measured porosity - ~ 15% sonic porosity - bulk density = 2.48 g/cm³. A) Siltstone with quartz, muscovite, K-feldspar (K) and chert (C). B) poorly sorted silt-sized quartz and muscovite with abundant clay-sized quartz. Again, note euhedral, blocky clay particles, primarily illite, of detrital origin. C) silt-sized detrital chlorite. EDX indicates high-Fe content. D) high - magnification of illitic matrix with quartz. Note euhedral, well-crystallized clay particles. These are interpreted as detrital and suggest that much of the matrix is composed of detrital illite.

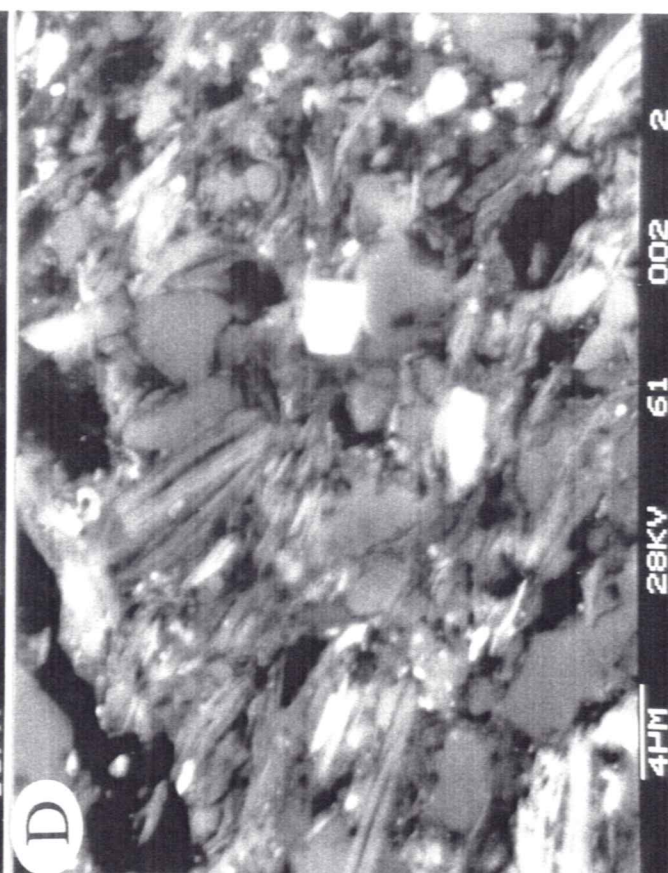
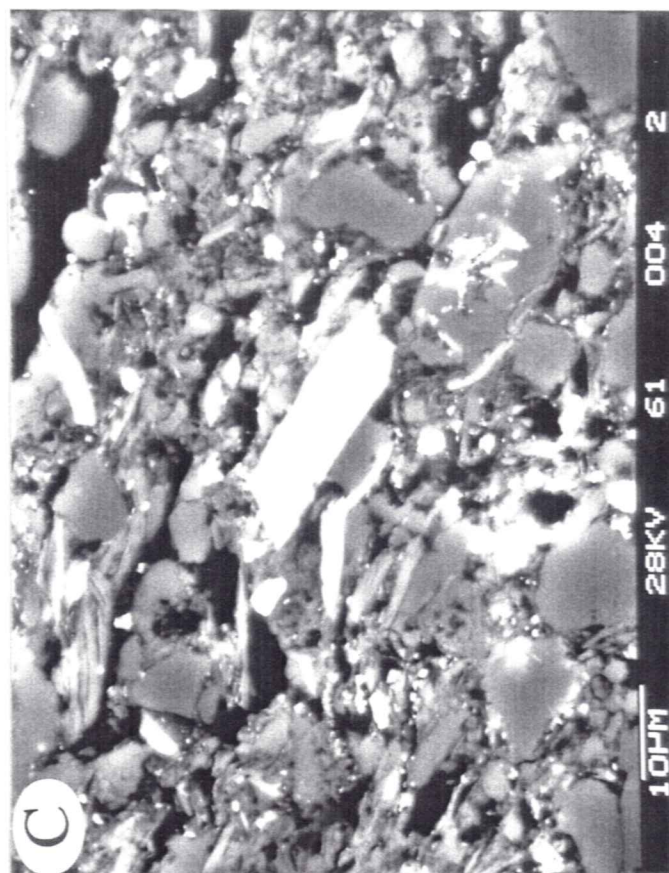
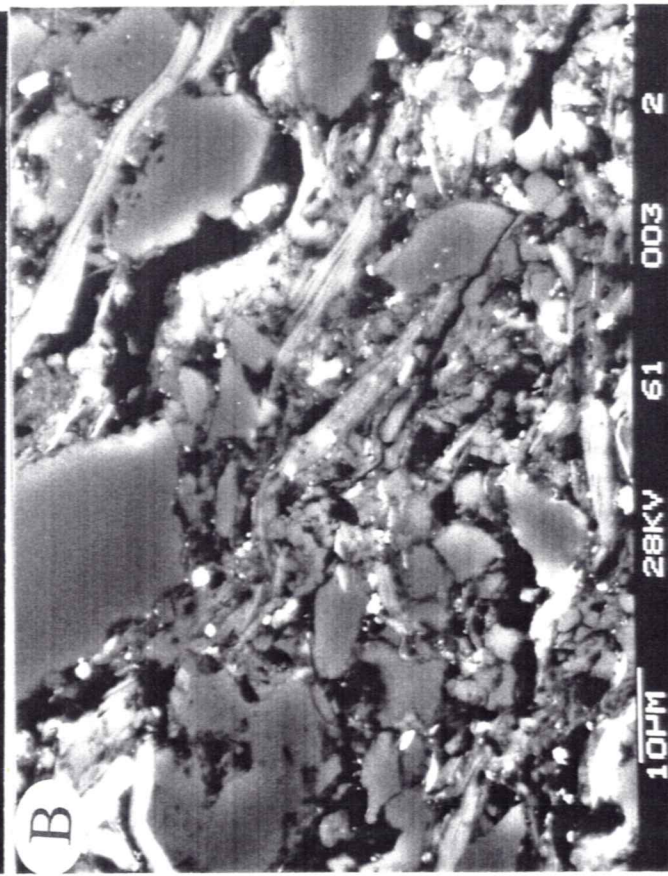
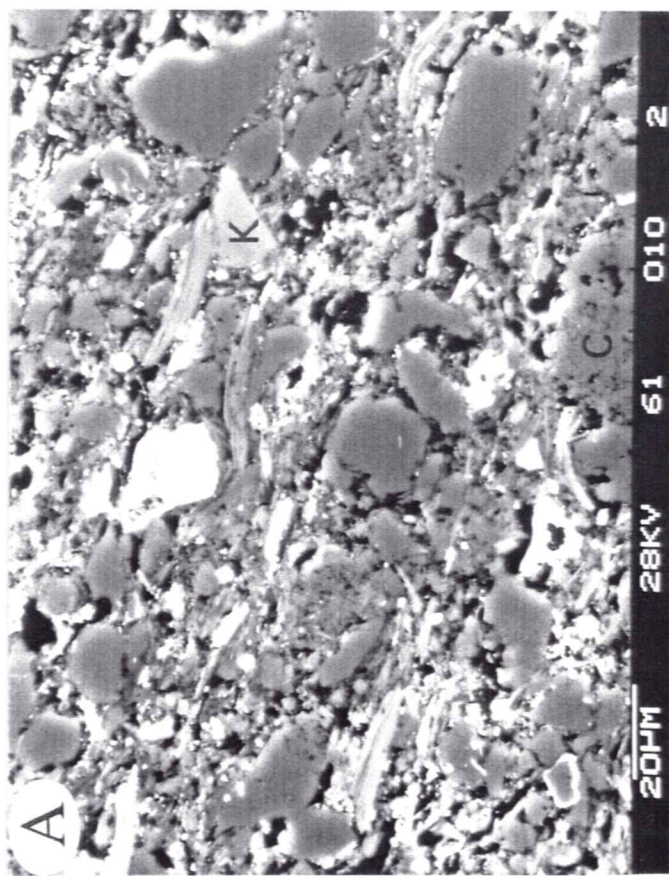


Plate 16 - Sample A06071 or BML-2 - 3176m TVD - overpressured - ~5-7% measured porosity, 2 % sonic porosity, bulk density = 2.61 g/cm³. A) poorly sorted, bioclastic, well-compacted siltstone with localized disseminated siderite cement. Bioclasts have Fe-rich rims (arrows). B) carbonate (C) and quartz grains with abundant intergranular, disseminated siderite. C) compacted fecal pellet with abundant weathered, detrital mica. D) pore-filling authigenic siderite with matrix quartz and illite.

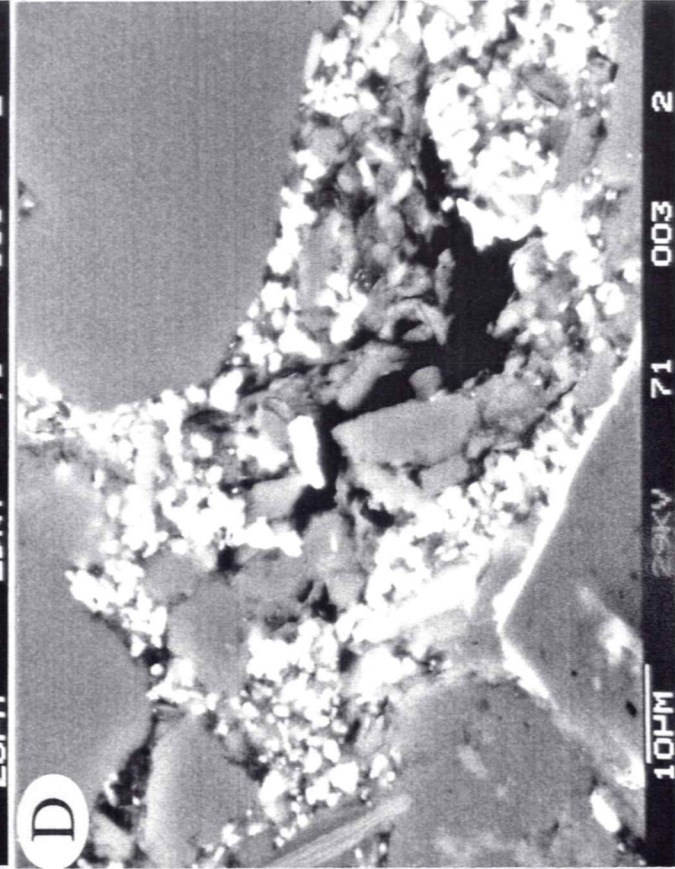
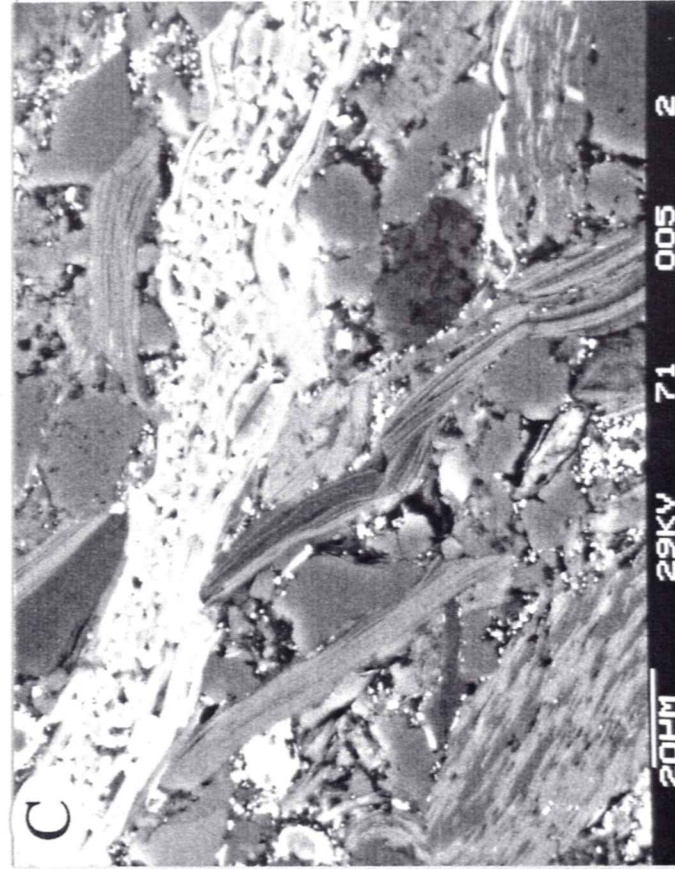
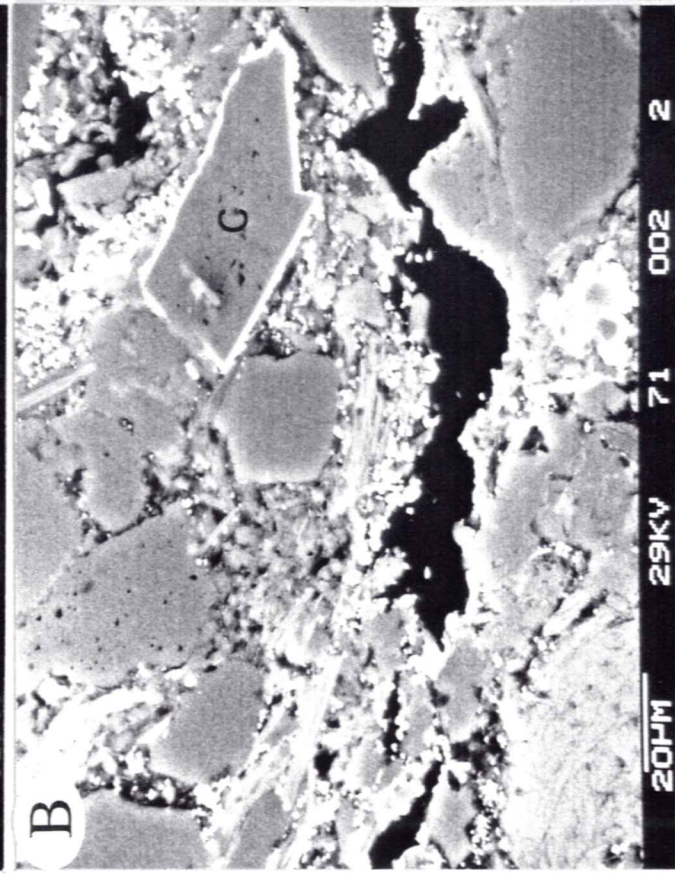
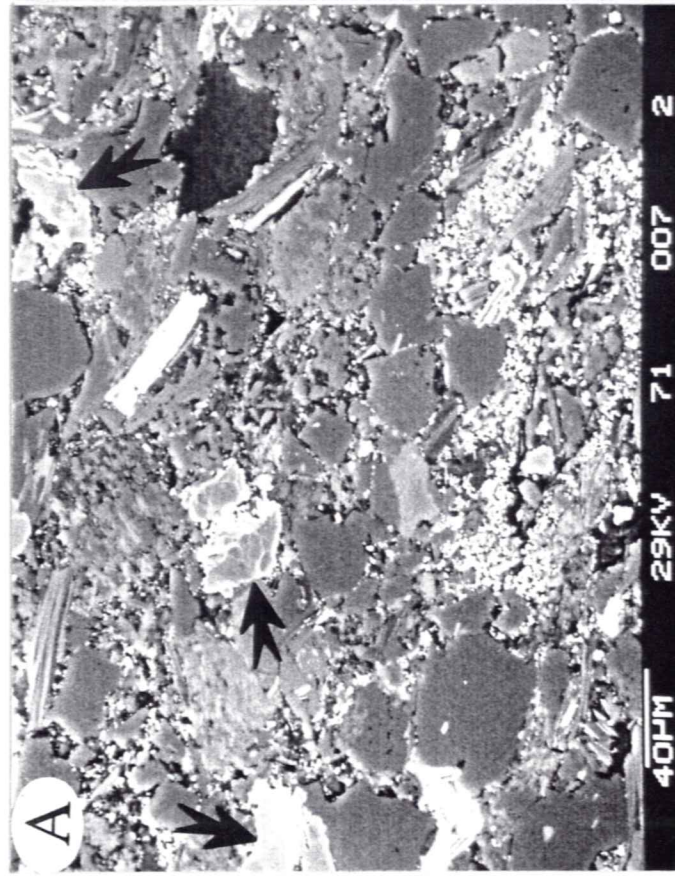


Plate 17 - Sample E90011 or BAK-1 - 3452m - overpressured - 13-14% measured porosity, 21% sonic porosity, bulk density = 2.40 g/cm³. A) siltstone (bottom) and claystone (top) laminations. Siltstone has a high matrix content and poor grain orientation. B) matrix supported mudstone lamination. Silt grains show some preferred orientation. C) poorly sorted, matrix supported mudstone. Matrix shows little evidence of compaction. D) apparently high matrix porosity in mudstone matrix comprising illite, quartz and chlorite (C).

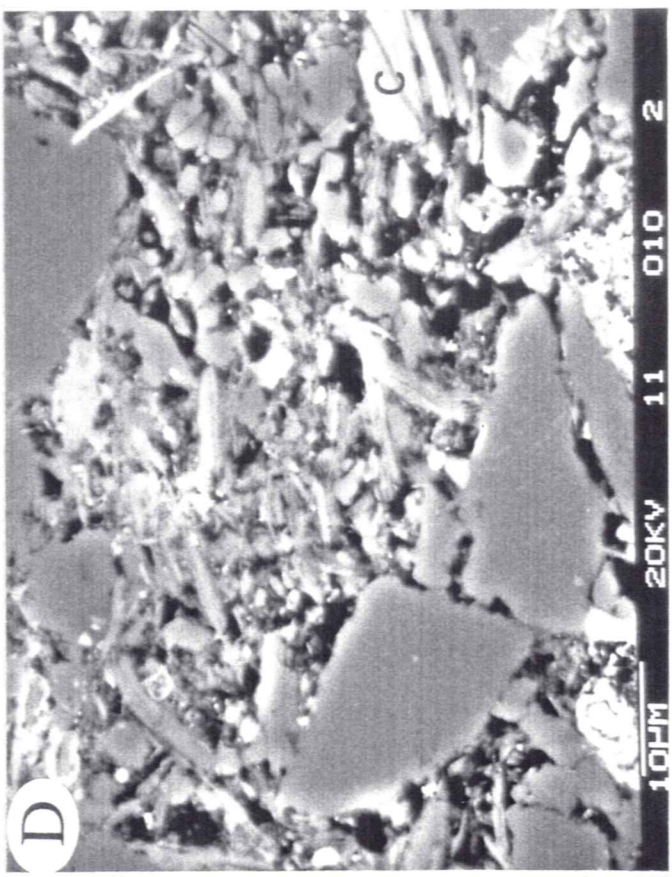
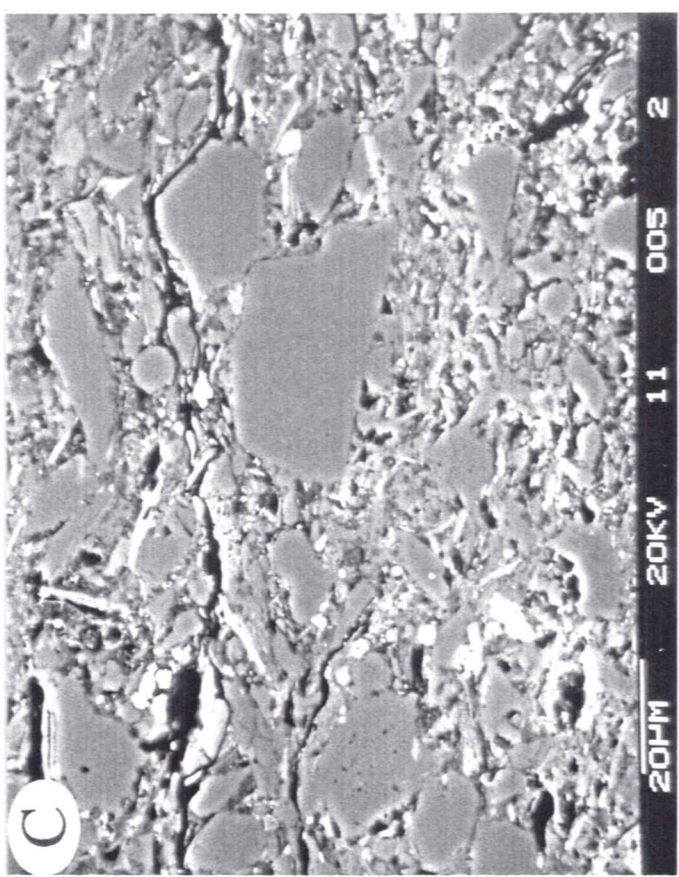
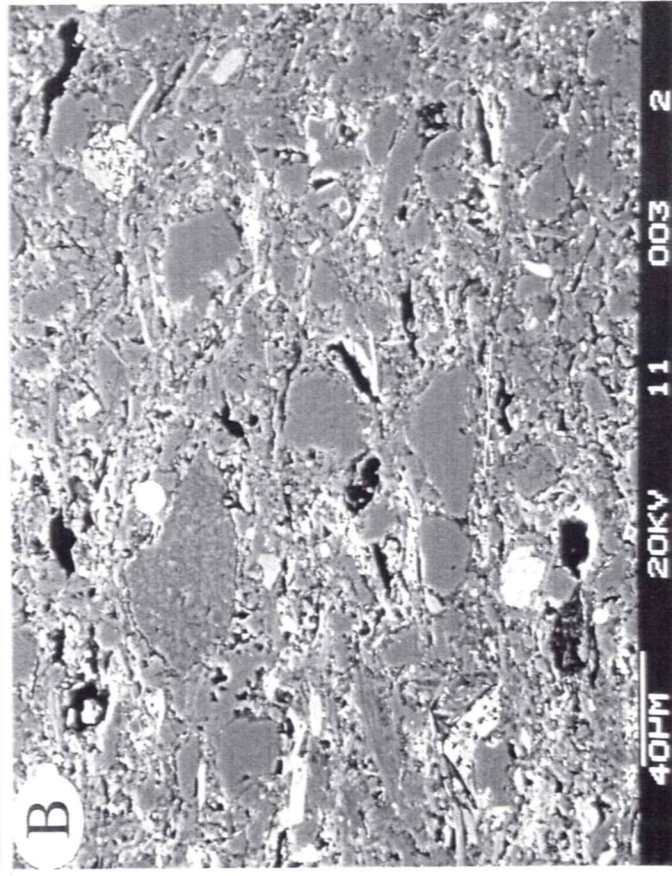
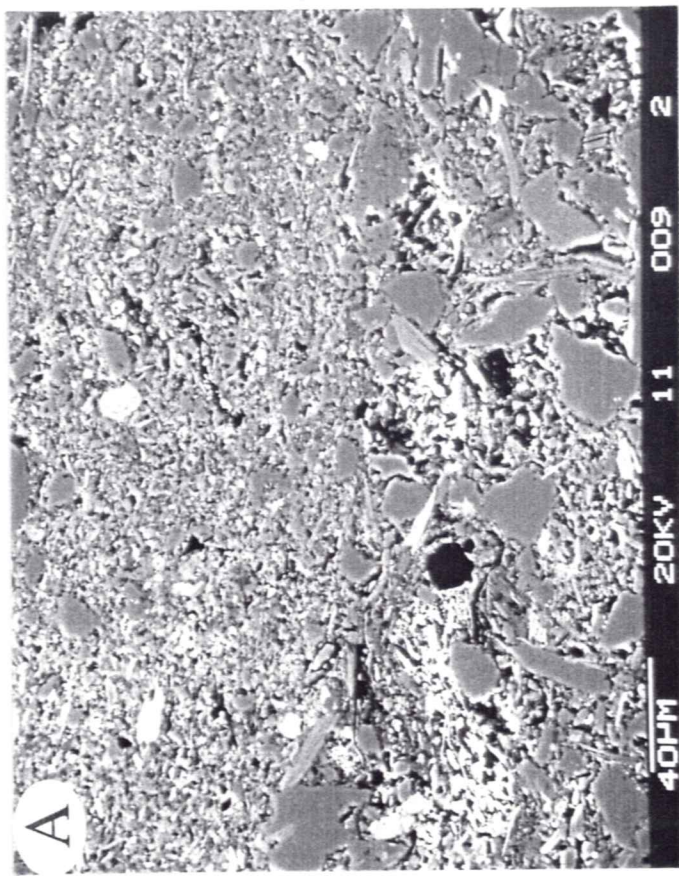


Plate 18 - Sample E90011 or BAK-1 - 3452m - overpressured - 13-14 % measured porosity, 21% sonic porosity, bulk density = 2.40 g/cm³. A) authigenic botryoidal siderite and a large detrital mica(?) with intergrown siderite. B) mechanical secondary porosity - biotite compacted perpendicular to ab plane, with siderite intergrowths. C) poorly sorted micaceous siltstone with muscovite (M), biotite (arrow), and minor siderite. Note carbonate clast with Fe-rich carbonate rim (center). Grain contacts are largely tangential. D) claystone matrix porosity does not appear to be as high as in Plate 17D.

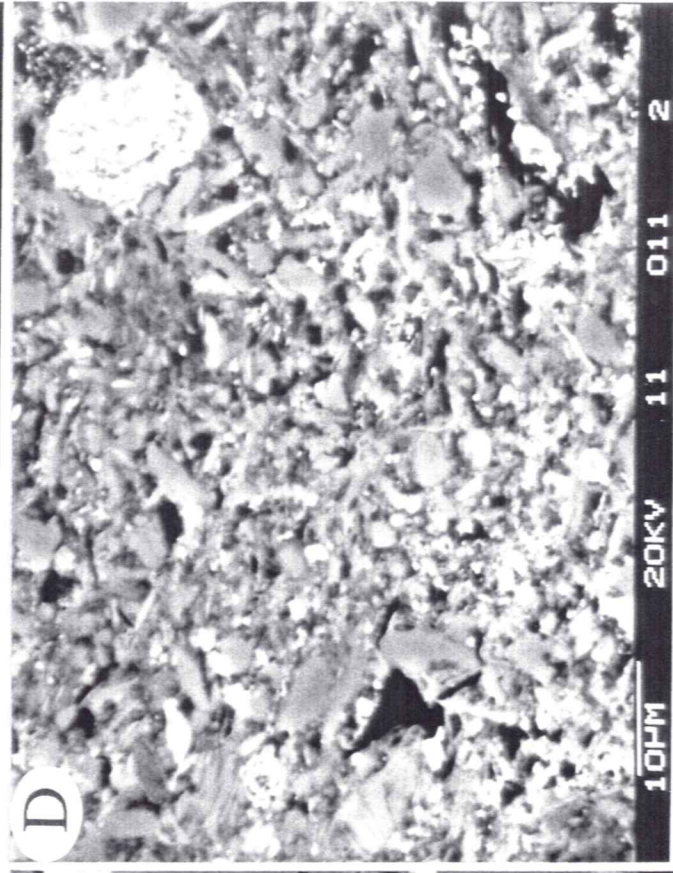
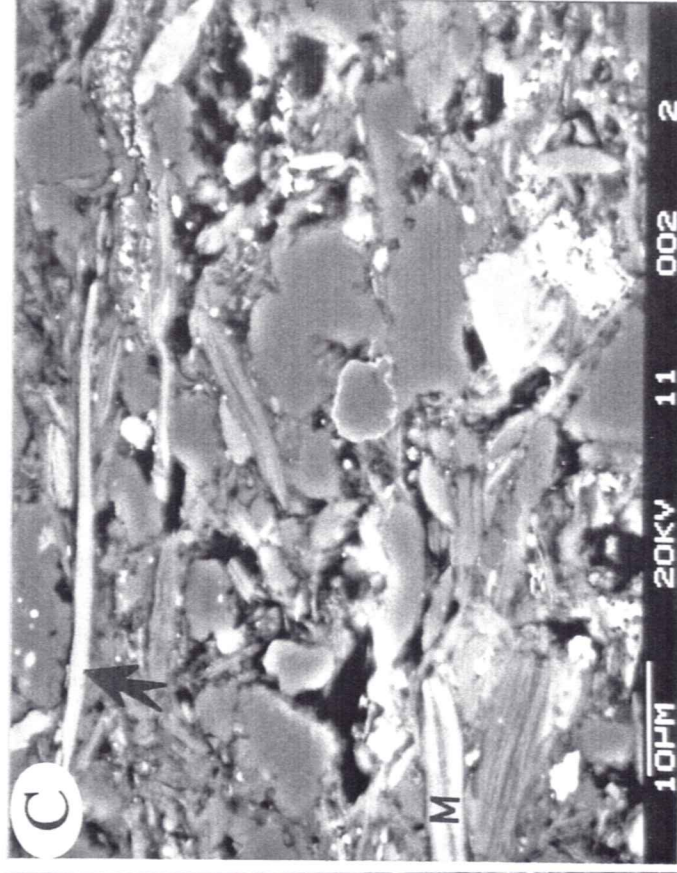
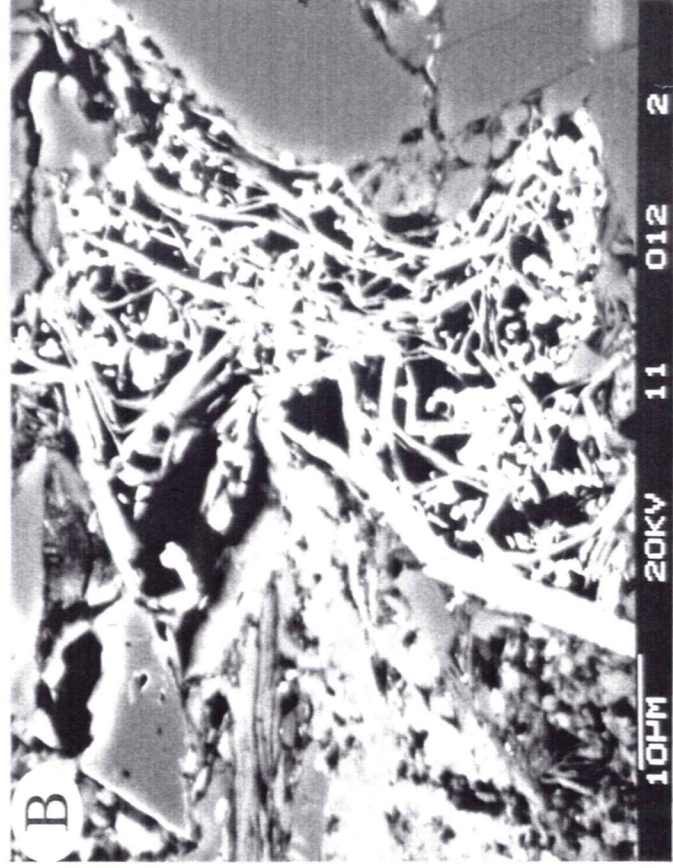
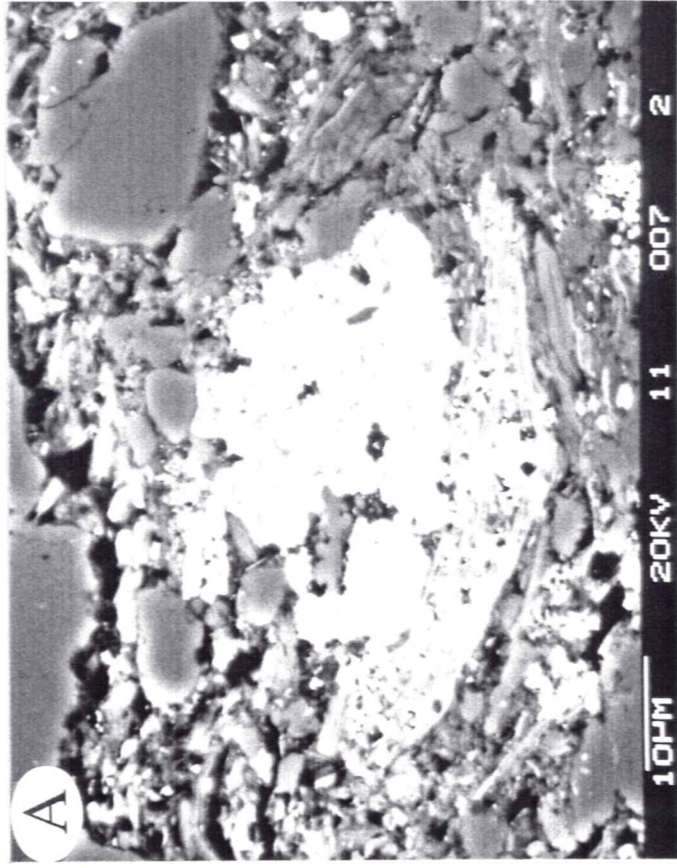


Plate 19 - Sample A06081 or BML-3 - 3547m TVD- overpressured - ~ 6 % measured porosity - ~5 % sonic porosity- bulk density = 2.61 g/cm³. A) well-compacted siltstone fabric. Dominantly concavo-convex grain contacts. Bright clast is siderite. B) Matrix supported siltstone with abundant disseminated very fine-grained siderite and pyrite. Note sideritized fecal pellet at bottom. C) volcanic clast with high and low K zones and a "poikilotopic" texture characteristic of rhyolites; with muscovite, quartz and sideritized fecal material (bright areas). D) compacted clay matrix between quartz, K-feldspar (K) and carbonate (C) grains. Carbonate grain is calcite (gray) and siderite (white).

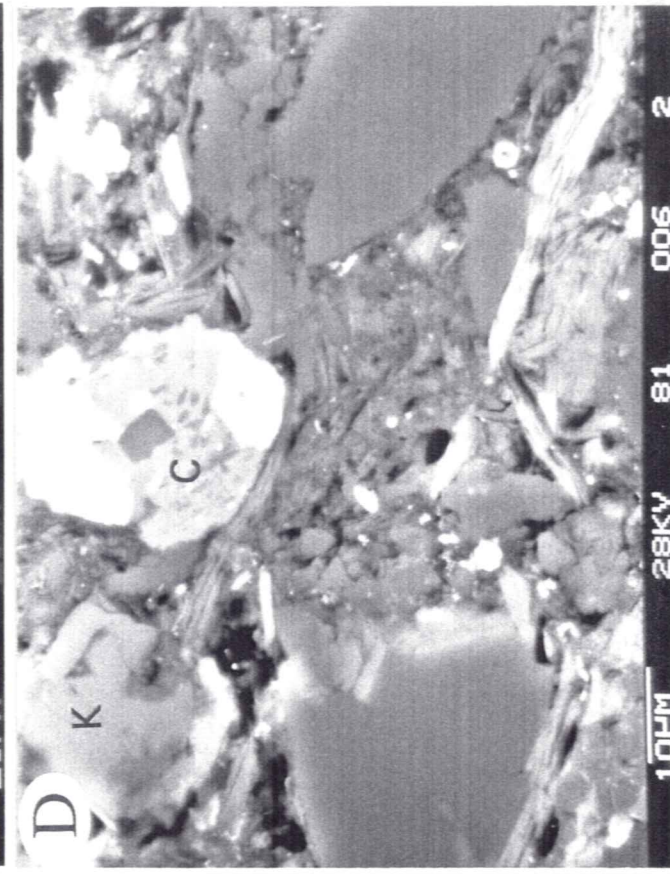
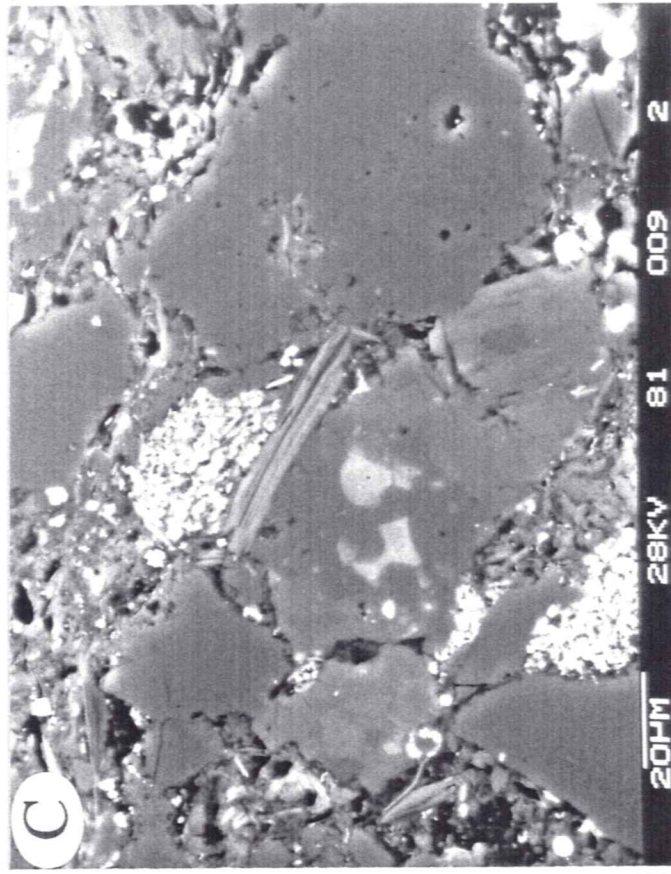
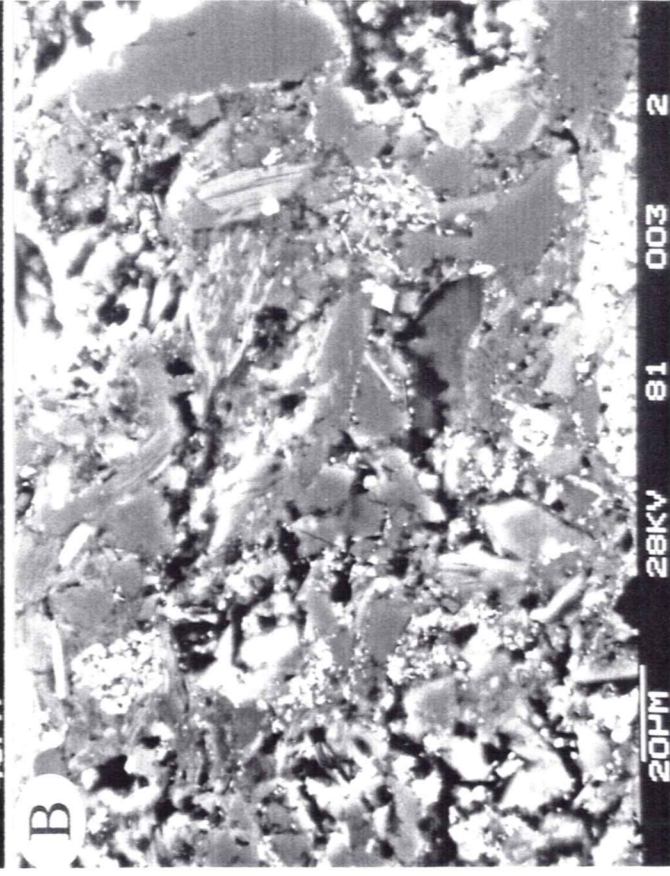
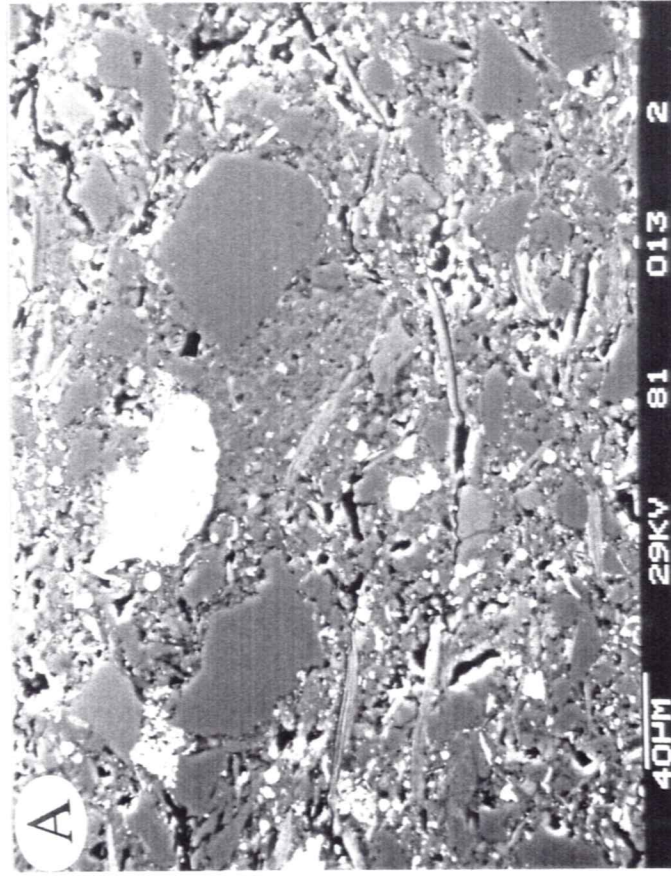


Plate 20 - Sample A06081 or BML-3 - 3547m TVD- overpressured - ~ 6 %
measured porosity - ~5 % sonic porosity- bulk density = 2.61 g/cm³. A) fine-
sand lamination in poorly sorted siltstone matrix - chert, quartz and muscovite.
B) fine-sand sized grains of quartz, muscovite and partially dissolved K-feldspar
(K). C) mechanically deformed muscovite between sub-rounded quartz grains.
D) unaltered K-feldspar (K) in an illitic matrix. Compare this texture to that of the
K-feldspar in B.

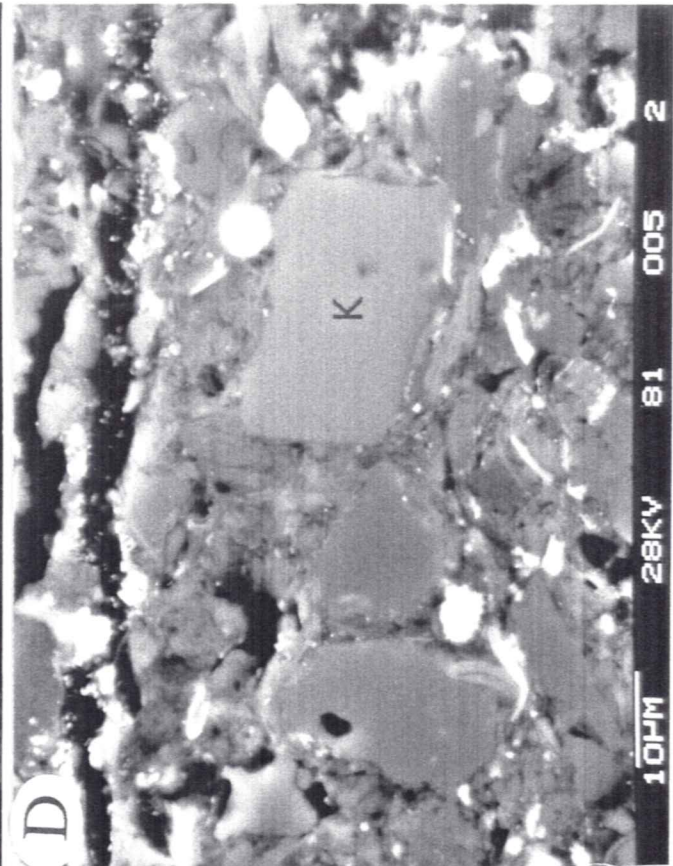
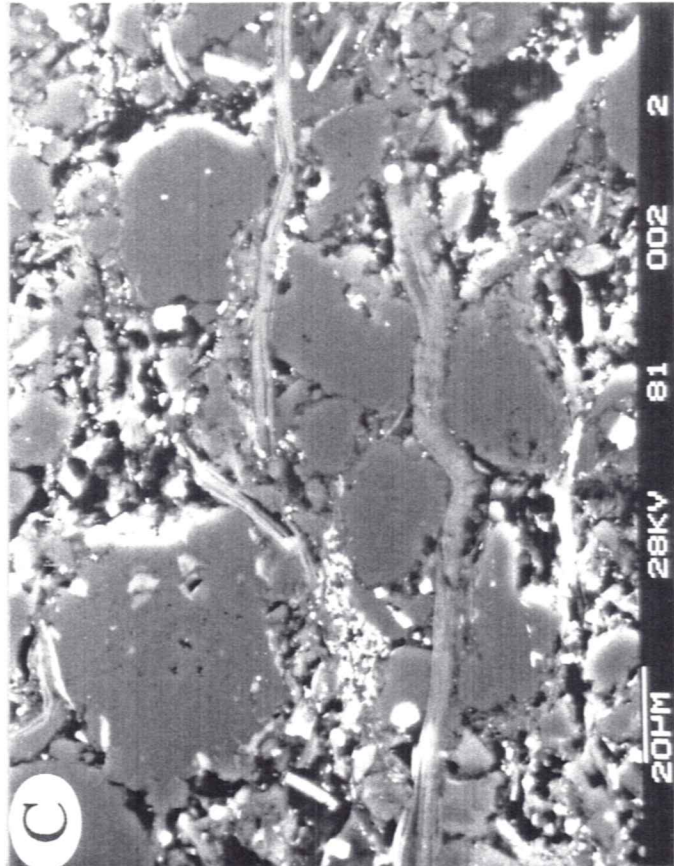
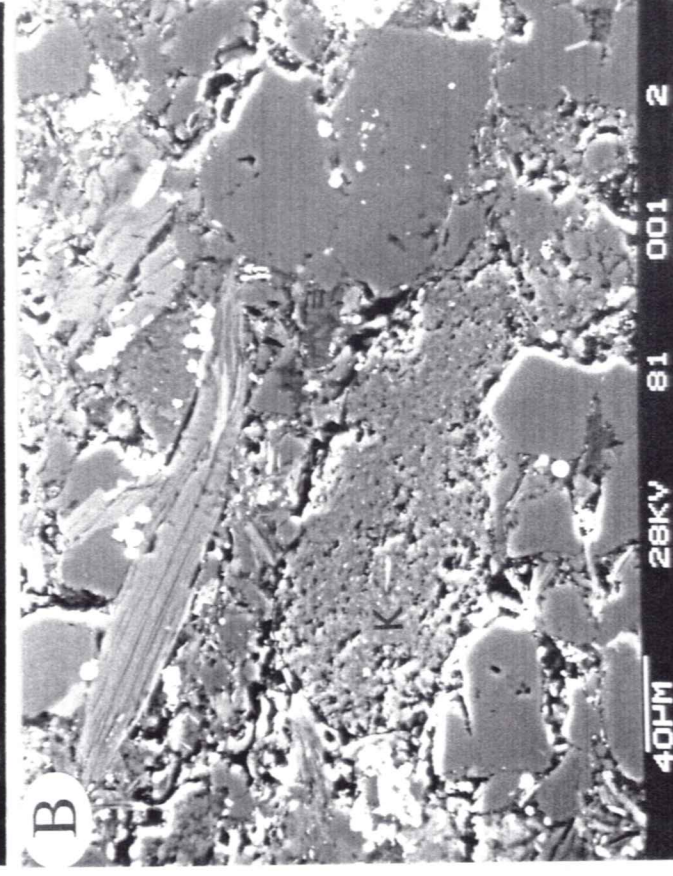
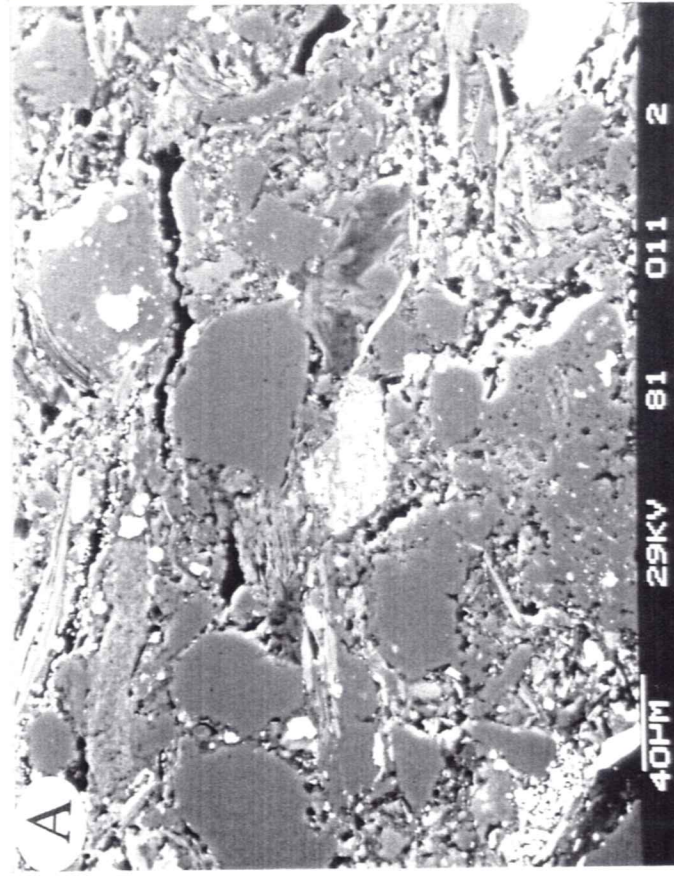


Plate 21 - Sample A06081 or BML-3 - 3547m TVD- overpressured - ~ 6 % measured porosity - ~5 % sonic porosity- bulk density = 2.61 g/cm³. A) muscovite and quartz with sideritized fecal material (arrow). B) fine-silt and clay-sized quartz and clay mineral particles with siderite and pyrite. Note matrix porosity, even at this depth. C) matrix shows abundant microporosity. D) quartz (authigenic?), illite aggregates and muscovite in "pore" between quartz grains. Matrix fabric within the "pore" is uncompacted.

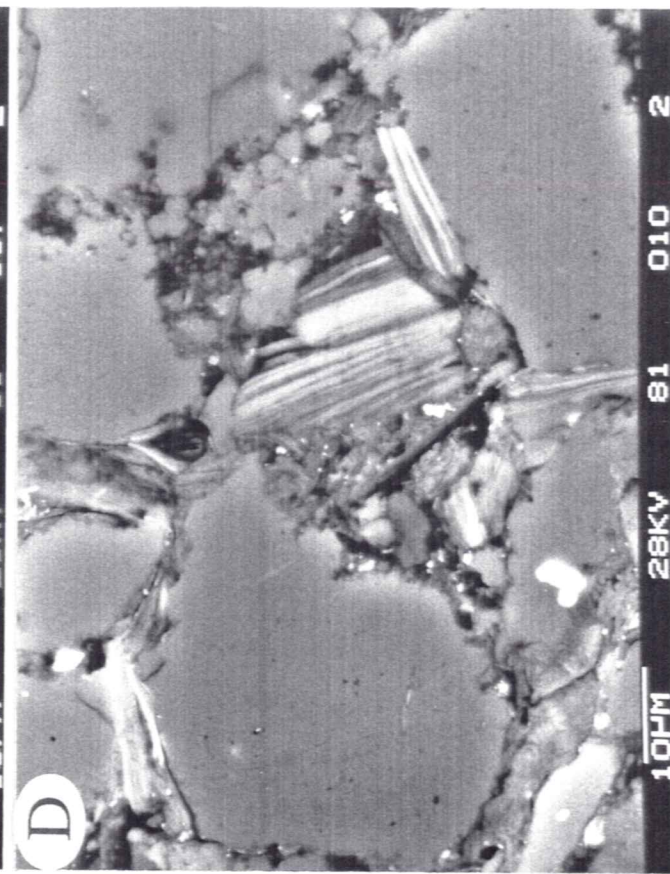
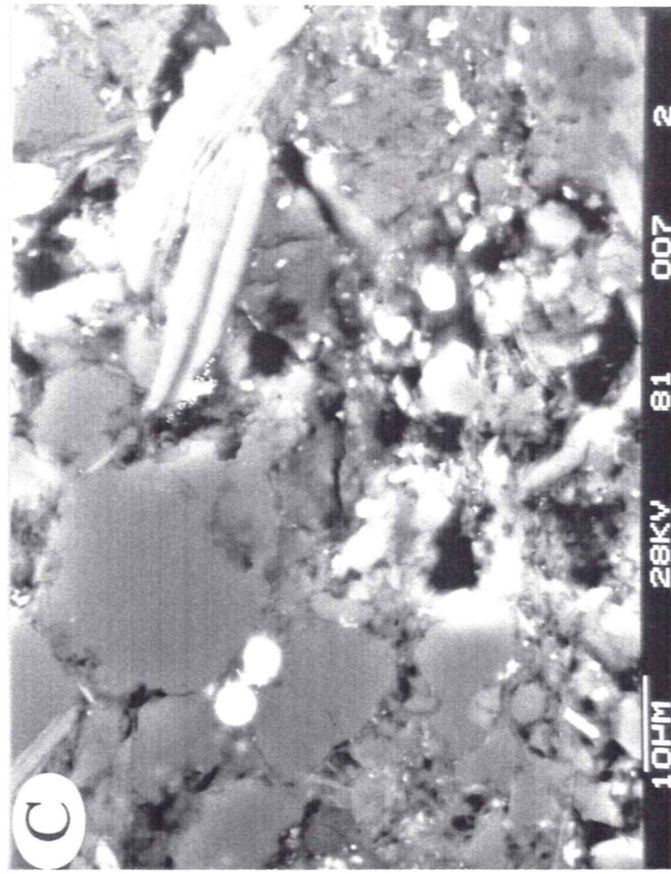
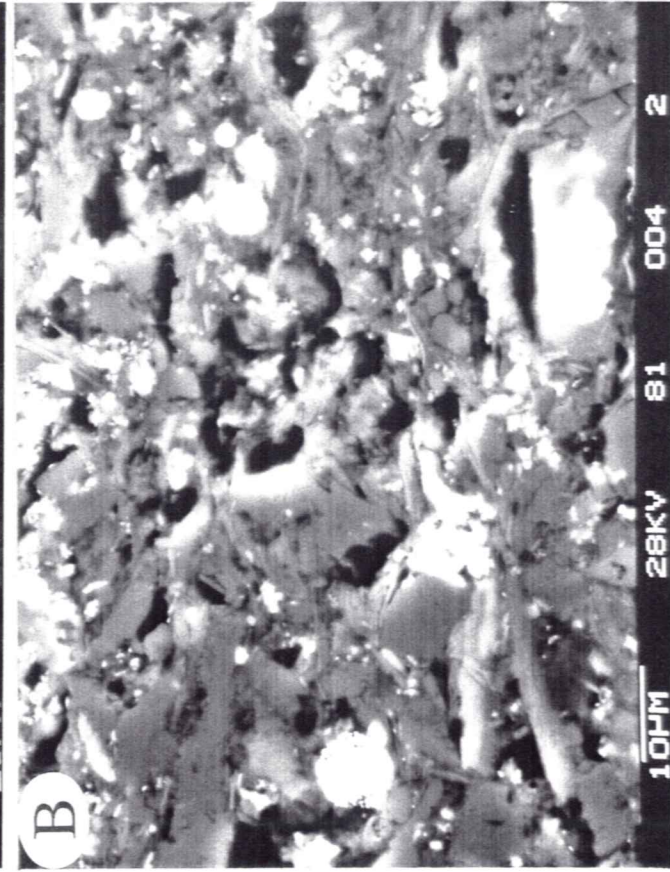
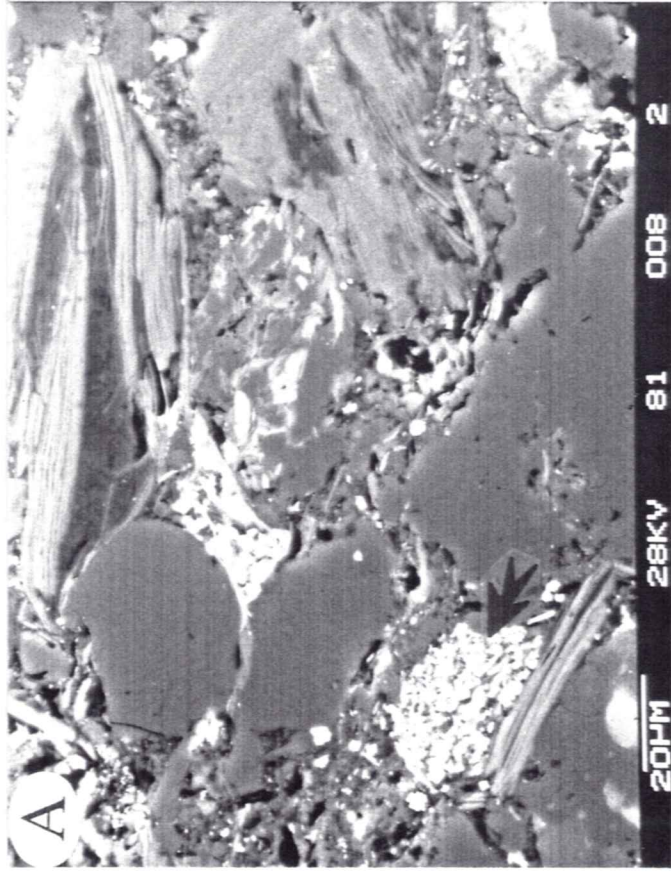


Plate 22 - Sample O09091 or BAR-7 - 4861m - overpressured - 8-12% measured porosity - 10% sonic porosity- bulk density = 2.50 g/cm^3 . A) fractures (induced?) in siltstone. B) induced microfracture in siltstone. C) low magnification of organic stringer in poorly sorted siltstone. D) sutured grain boundaries along an organic stringer.

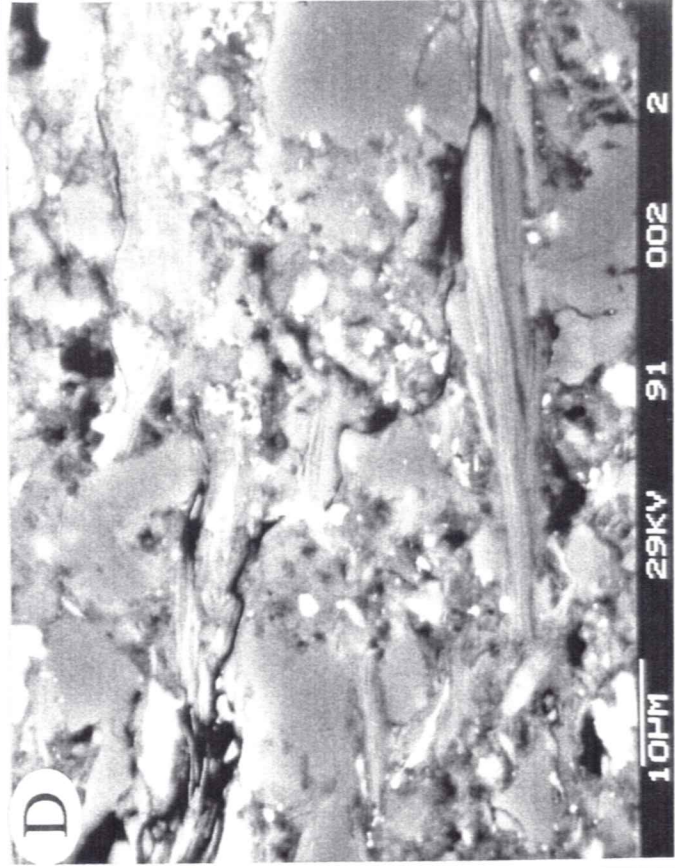
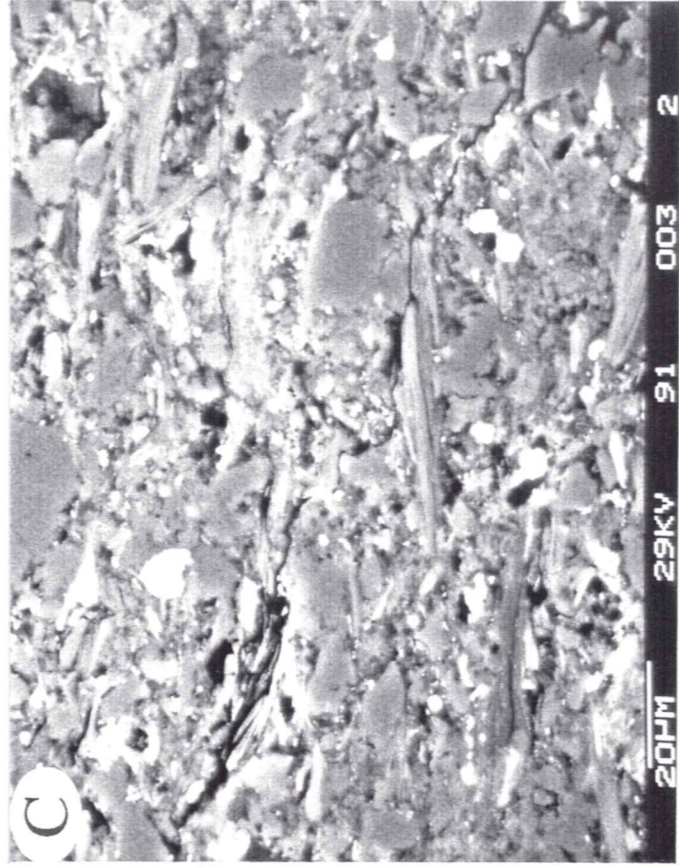
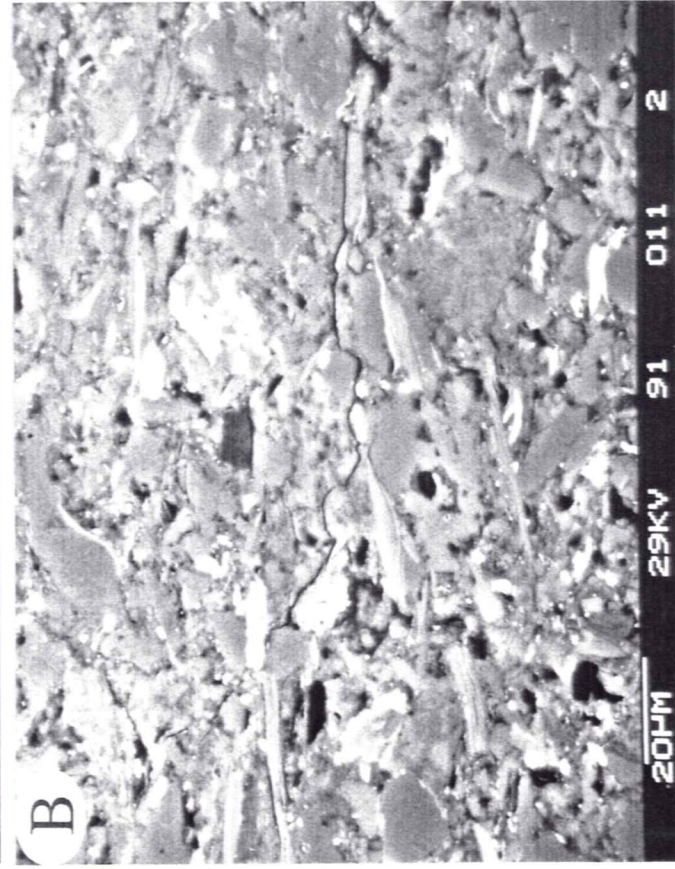
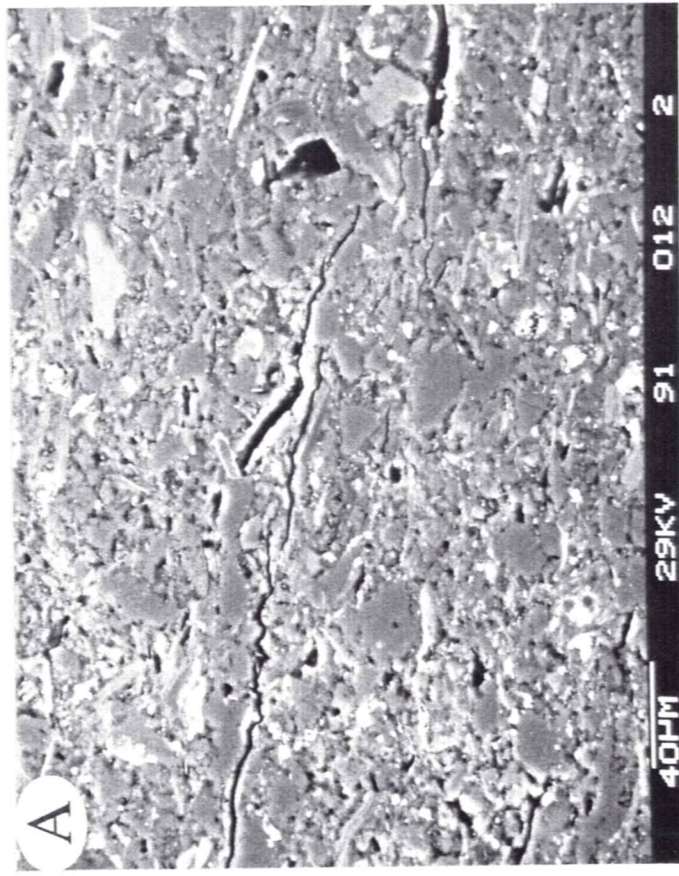


Plate 23 - Sample O09091 or BAR-7 - 4861m - overpressured - 8-12% measured porosity - 10% sonic porosity- bulk density = 2.50 g/cm³. A) low matrix porosity in relatively well-compacted mudstone. B) fairly well-compacted matrix with organic clast. C) well compacted matrix with quartz, muscovite and chlorite. D) matrix comprises quartz, illite and disseminated siderite and rutile.

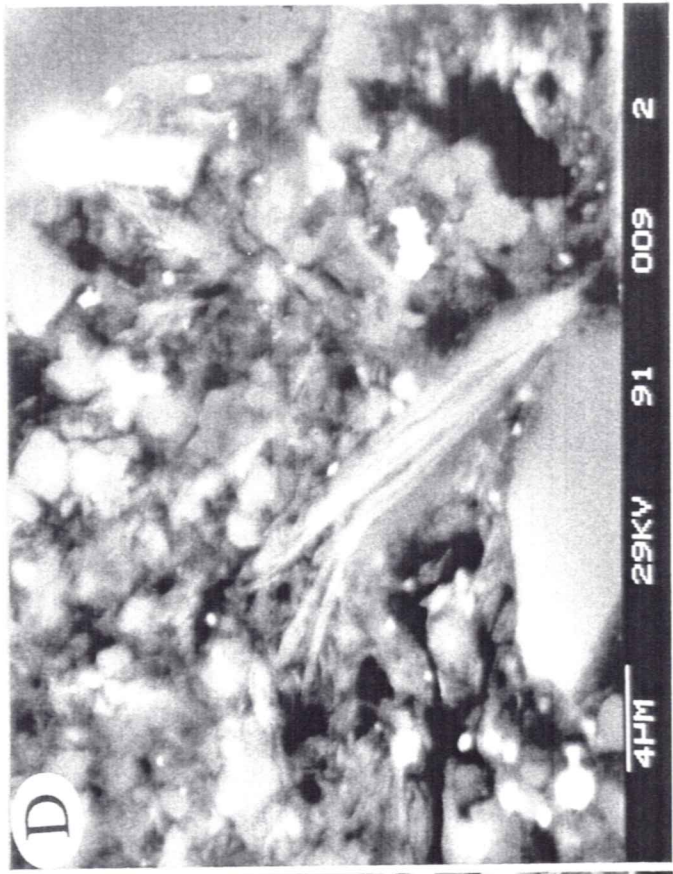
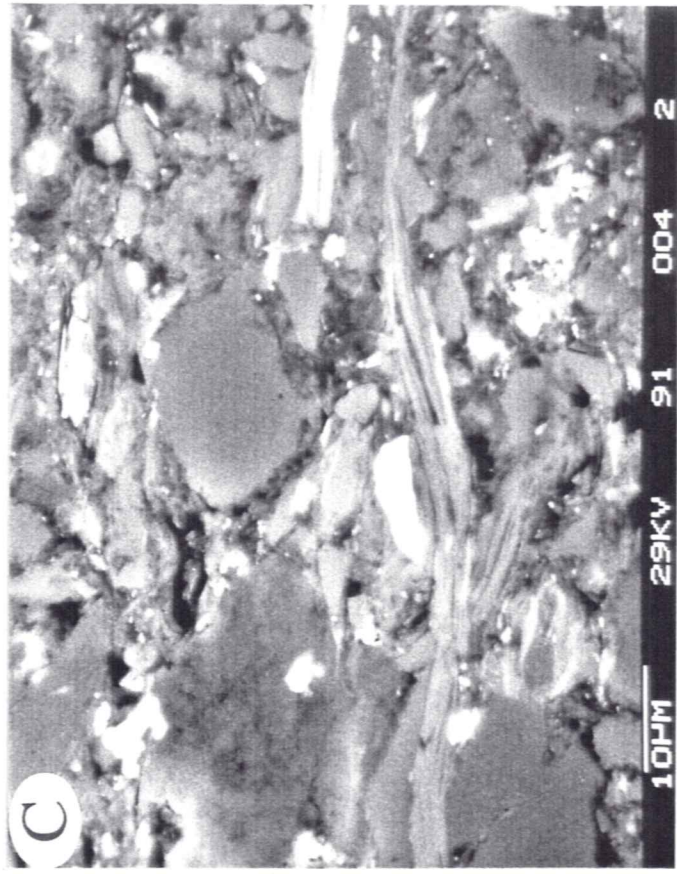
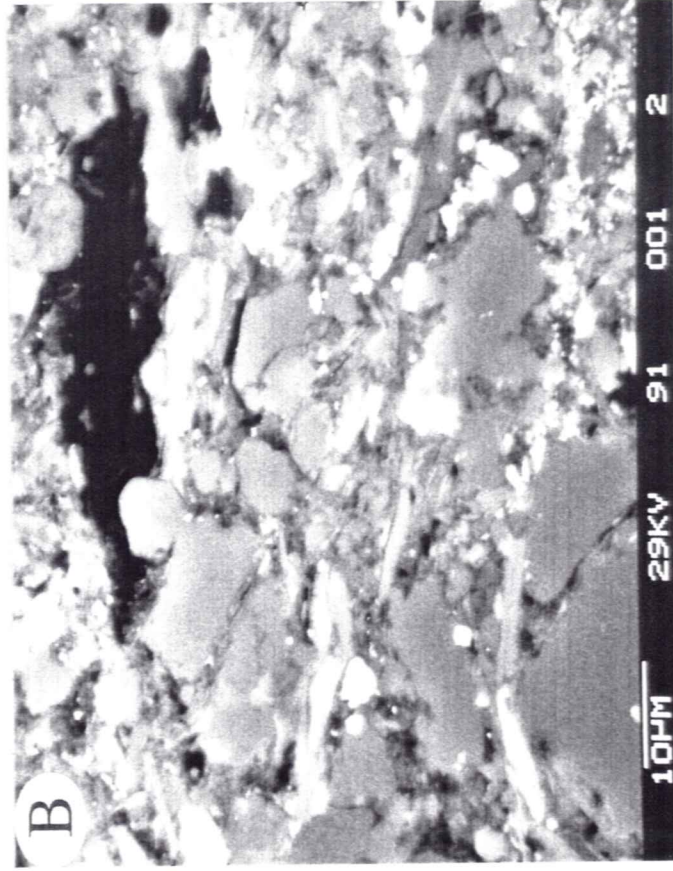
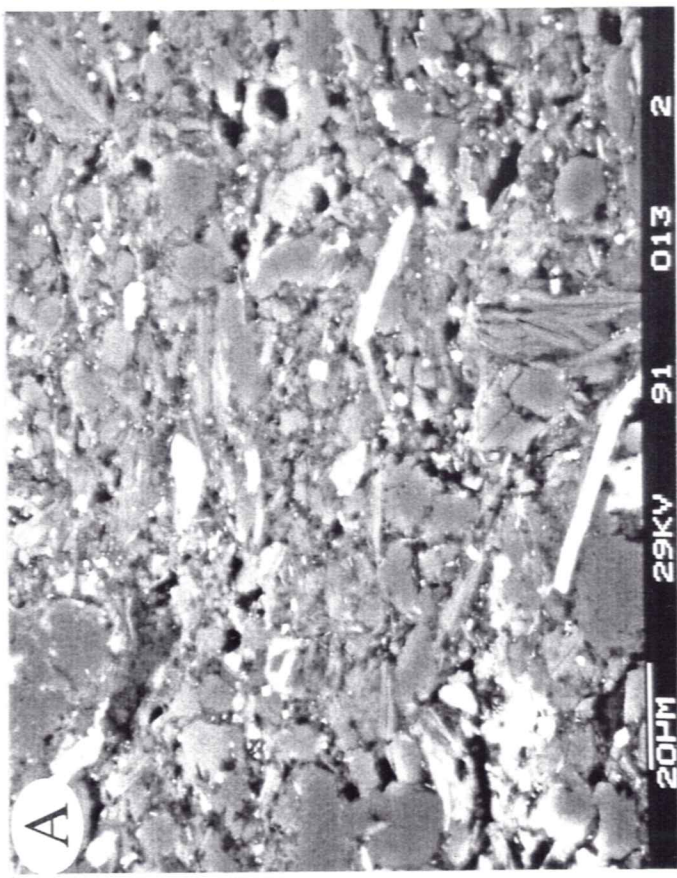
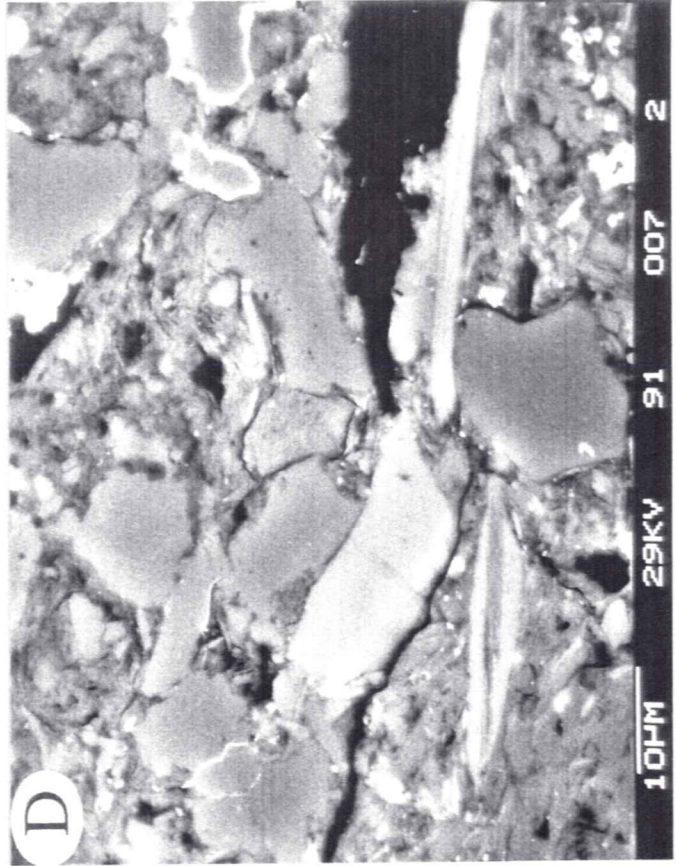
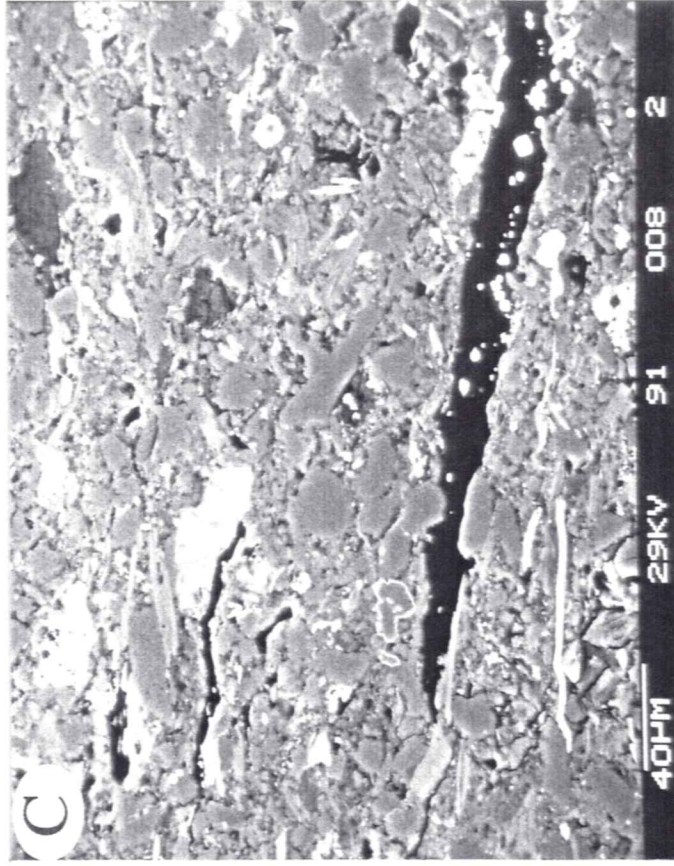
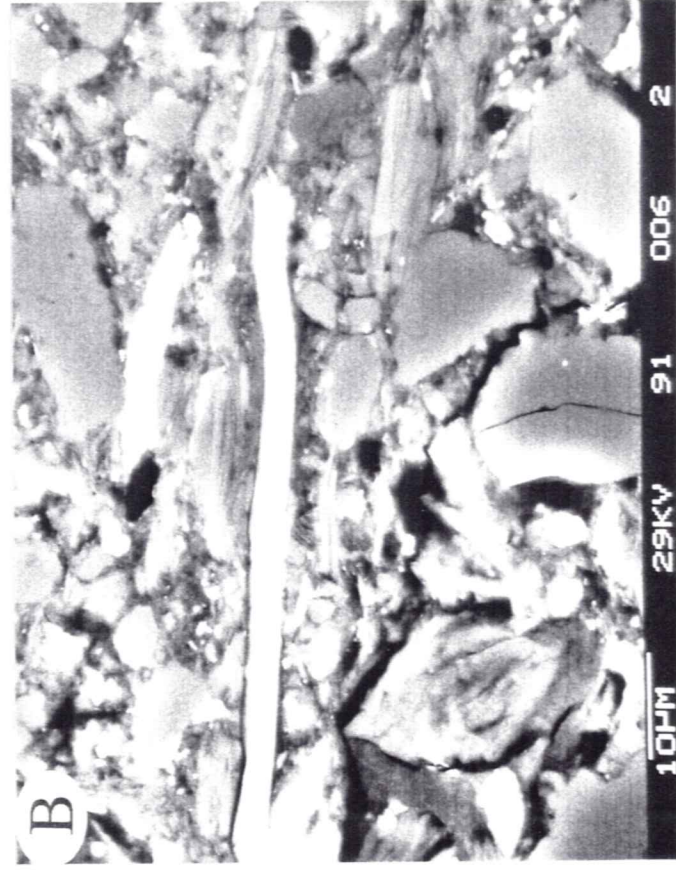
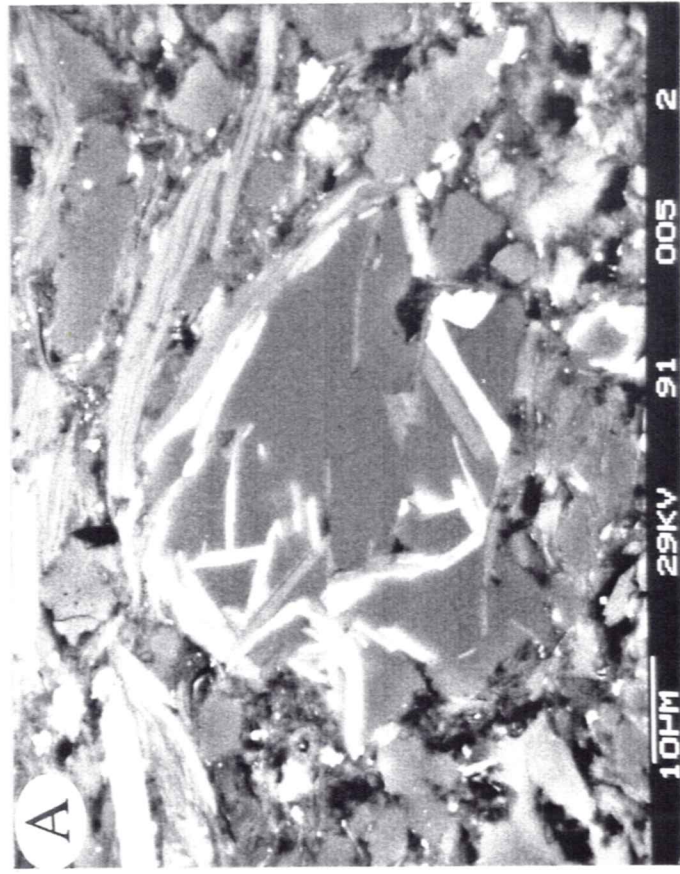


Plate 24 - Sample O09091 or BAR-7 - 4861m - overpressured - 8 -12%
measured porosity - 10% sonic porosity- bulk density = 2.50 g/cm³. A) occluded
"compaction" porosity - dismembered chamosite is cemented with silica. B)
well-compacted siltstone. C) large organic clast with authigenic pyrite
inclusions. D) sutured grains above a thin organic stringer at left end of clast in
C.



APPENDIX B

Tables 1 - 6

TABLE 1 - ROCK-EVAL DATA										
SAMPLE #	DEPTH	CORRECTED	Tmax	S 1	S 2	S 3	P I	TOC	H I	O I
	(m)	DEPTH (m)	(°C)					(wt%)	(mgHC/gOC)	(mgCO2/gOC)
A06031	1362	1762	429	0.06	0.57	1.59	0.09	1.03	55	154
A06071*	3215	3576	432	0.04	0.2	1.16	0.17	0.5	40	234
A06081*	3609	3947	431	0.12	0.72	1.05	0.14	0.92	78	115
C42021	2881	2881	430	0.26	2.1	2.55	0.11	2.06	102	124
D27041	1458	2108	431	0.01	0.25	0.86	0.04	0.72	35	119
D27042	1469	2119	433	0.03	0.52	2.16	0.06	1.22	42	178
D27091	2022	2672	427	0.09	1.31	4.1	0.06	1.96	67	209
D27101	2092	2742	424	0.16	0.98	3.64	0.14	1.55	63	234
D27111	2099	2749	428	0.07	0.86	4	0.07	1.58	54	253
D27121	2213	2863	424	0.15	1.04	3.54	0.13	1.56	67	227
D27131	2389	3039	431	0.11	1.23	5.05	0.09	1.94	63	260
D27141	2421	3071	429	0.08	0.83	3.2	0.09	1.37	61	234
D27151	2551	3201	432	0.13	0.74	2.46	0.15	1.27	58	194
D27161	2725	3375	431	0.13	0.84	3.93	0.14	1.31	63	300
D27171	2923	3573	433	0.12	0.93	3.95	0.12	1.64	57	242
D27191	3153	3803	432	0.06	0.42	0.66	0.12	0.87	48	76
D27211	3481	4131	438	0.35	3.01	0.37	0.1	1.84	164	20
D27221	3628	4278	439	0.2	1.03	0.53	0.16	1.21	85	43
E90011	3452	3452	427	0.42	1.08	3.43	0.29	1.25	86	275
E90021	3938	3938	435	0.35	1.3	1.56	0.21	1.3	100	119
F24011**	4376	3106	422	0.71	1.39	3.23	0.34	1.31	106	246
F24021**	4395	3119	426	0.94	1.48	3.95	0.39	1.36	109	292
F24041**	4695	3341	427	0.13	1.27	3.02	0.09	1.17	109	259
F43011	3247	3247	430	0.11	0.35	1.08	0.24	0.55	64	197
G33141	2533	2533	423	0.27	0.48	1.53	0.36	0.61	78	251
G33102	2460	2460	414	0.03	0.24	0.66	0.1	0.87	27	76
G33101	2459	2459	415	0.03	0.35	0.7	0.08	1.01	34	69
G33051	2075	2075	417	0.05	0.55	1.65	0.08	0.76	72	219
G33031	1640	1640	426	0.81	0.87	3.66	0.49	1.15	75	318
G33021	1350	1350	428	0.71	0.89	11.5	0.45	1.06	84	1089
G33011	952	952	412	1.48	1.64	2.68	0.48	1.63	101	164
O09091	4861	4861	436	0.2	0.68	0.29	0.23	0.79	85	36
O09081	4606	4606	435	0.32	1.74	0.35	0.16	1.06	164	32
O09071	4375	4375	425	0.11	0.83	0.49	0.12	0.94	88	52
O09061	3866	3866	433	0.13	0.93	3.19	0.12	1.16	80	276
O09031	1765	1765	420	0.33	4	6.46	0.08	4.51	88	143
O09021	1533	1533	419	0.05	0.46	3.84	0.09	1	46	385
O09011	1317	1317	409	0.12	0.62	2.5	0.16	1.32	47	190
J67021**	4358	4006	428	0.06	0.81	6.57	0.07	1.06	76	620
J67012**	3962	3673	430	0.09	0.81	6.78	0.1	1.21	67	562
J67011**	3945	3658		0.06	0.99	5.7	0.06	1.2	82	475
* - deviated hole; corrected depth is true vertical depth plus 400m (A06) and 650m (D27)										
** - deviated hole with no erosion correction (see Issler, 1992)										

TABLE 2 - X-RAY FLUORESCENCE ANALYSIS OF <2 MICROMETER FRACTION (in wt%)															
I.D.	SiO2	Al2O3	Fe2O3	MGO	CAO	MNO	BAO	TiO2	K2O	NA2O	P2O5	LOI*	TOTAL		
A06031	47.48	24.71	6.43	3.18	0.70	0.02	0.05	0.87	4.07	0.66	0.13	11.70	100.00		
C42021	47.41	23.84	5.71	4.01	0.57	0.05	0.14	0.91	4.17	1.26	0.21	11.72	100.00		
D27041	48.81	23.53	5.86	3.44	0.86	0.03	0.16	1.06	3.62	0.37	0.22	12.04	100.00		
D27091	46.23	23.98	7.08	3.05	0.80	0.03	0.13	1.10	3.47	1.24	0.47	12.43	100.01		
D27111	47.36	23.75	7.35	2.79	0.82	0.02	0.08	1.07	3.58	1.20	0.34	11.66	100.02		
D27141	47.91	23.15	7.13	3.12	0.92	0.06	0.12	1.15	3.80	0.85	0.36	11.43	100.00		
D27161	47.33	23.12	6.83	3.34	0.96	0.06	0.11	1.03	4.24	0.78	0.39	11.82	100.01		
D27191	47.17	23.90	7.10	3.52	0.78	0.04	0.09	1.23	4.35	0.72	0.18	10.93	100.01		
D27211	46.22	22.06	8.61	3.79	0.91	0.06	0.05	1.10	5.10	1.92	0.32	9.87	100.01		
E90011	46.60	23.95	7.82	4.12	0.70	0.05	0.25	1.29	4.82	0.18	0.23	10.01	100.02		
G33011	48.43	23.98	6.14	3.43	0.49	0.03	0.12	1.12	3.85	0.88	0.14	11.38	99.99		
G33031	47.79	21.68	8.83	3.26	0.85	0.03	0.06	1.08	4.02	1.30	0.17	10.93	100.00		
G33141	45.95	20.52	9.68	3.76	1.06	0.07	0.08	1.09	3.57	0.95	0.29	12.98	100.00		
J67021	49.50	22.52	6.88	3.73	0.72	0.03	0.16	1.24	4.36	0.58	0.25	10.02	99.99		
O09021	46.84	21.97	8.87	2.67	0.85	0.02	0.08	1.21	3.90	0.76	0.17	12.66	100.00		
O09031	48.52	22.66	6.42	3.61	0.71	0.03	0.16	1.15	4.12	0.45	0.20	11.98	100.01		
O09061	45.12	23.20	8.06	3.71	0.74	0.02	0.20	1.20	4.50	1.64	0.24	11.37	100.00		
O09091	49.82	24.17	5.52	3.27	0.48	0.01	0.09	1.06	4.65	1.04	0.17	9.73	100.01		
* - loss on ignition by thermogravimetric analysis															

TABLE 3 - WHOLE ROCK CHEMICAL DATA (in wt%)*															
I.D.	SiO ₂	Al ₂ O ₃	Fe ₂ O ₃	MgO	CaO	MnO	BAO	TiO ₂	K ₂ O	Na ₂ O	P ₂ O ₅	LOI	TOTAL	S	TIC
A06031	66.34	14.58	4.45	1.40	0.46	0.03	0.11	0.87	2.48	0.68	0.20	8.40	100.00	0.168	1.03
C42021	59.11	15.75	7.40	1.80	0.57	0.12	0.21	0.86	3.00	0.66	0.24	10.28	100.00	0.074	2.06
D27041	67.61	15.22	4.16	1.48	0.67	0.03	0.19	0.84	2.65	0.50	0.27	6.38	100.00	0.140	0.72
D27091	60.13	15.17	7.45	1.48	1.01	0.07	0.22	0.96	2.56	0.66	0.43	9.87	100.01	0.071	1.96
D27111	61.87	14.42	6.83	1.53	1.16	0.06	0.17	0.90	2.34	0.61	0.37	9.76	100.02	0.095	1.58
D27141	65.12	13.68	5.96	1.42	1.01	0.08	0.15	0.85	2.23	0.54	0.37	8.59	100.00	0.104	1.37
D27161	61.66	13.77	8.65	1.63	1.14	0.06	0.16	0.83	2.38	0.67	0.41	8.64	100.00	0.326	1.31
D27191	60.84	16.76	7.10	1.89	0.79	0.05	0.15	0.94	2.73	0.89	0.27	7.61	100.02	0.750	0.87
D27211	59.16	16.55	7.54	2.25	0.90	0.05	0.15	0.98	3.52	0.72	0.47	7.71	100.00	0.915	1.84
E90011	64.53	14.71	6.41	1.63	0.64	0.05	0.20	0.88	2.55	0.64	0.33	7.45	100.02	0.083	1.25
G33011	69.13	13.54	3.98	1.41	0.42	0.04	0.15	0.88	2.35	0.53	0.20	7.38	100.01	0.111	1.63
G33031	59.31	16.94	6.92	1.97	0.92	0.03	0.14	0.90	2.97	0.77	0.34	8.79	100.00	0.149	1.15
G33141	64.09	13.92	7.20	1.65	1.02	0.09	0.17	0.86	2.52	0.68	0.44	7.37	100.01	0.079	0.61
J67021	65.11	13.45	6.90	1.58	0.84	0.04	0.18	0.83	2.49	0.61	0.36	7.60	99.99	0.070	1.06
O09021	75.89	9.24	3.91	0.96	0.75	0.02	0.18	0.68	1.84	0.39	0.19	5.95	100.00	0.381	1.00
O09031	57.39	16.04	6.15	1.81	0.73	0.07	0.20	0.90	2.78	0.77	0.31	12.87	100.02	0.641	4.51
O09061	61.14	15.13	7.06	1.70	0.85	0.04	0.43	0.95	2.69	0.79	0.45	8.77	100.00	0.150	1.16
O09091	63.93	17.45	4.79	1.63	0.33	0.02	0.17	1.00	3.22	0.61	0.21	6.64	100.00	0.414	0.79
* - major elements by XRF, sulphur (S) and total inorganic carbon (TIC) by combustion, total organic carbon (TOC) by pyrolysis.															
Loss on ignition (LOI) by thermogravimetric analysis. See Bloch (1994) for details.															

TABLE 4 - CALCULATED "MIXED-LAYER" CLAY COMPOSITIONS AND STRUCTURAL FORMULAE*																
I/S Compositions			Structural Formulae													
I.D.	SiO ₂	Al ₂ O ₃	Fe ₂ O ₃	MgO	CaO	Na ₂ O	K ₂ O	TOTAL	Tetrahedral			Octahedral			Interlayer	
									Si	Al		Al	Fe ³⁺	Mg	Ca	Sum
A06031	46.5	22.4	6.30	4.00	.77	.96	5.80	86.73	3.49	0.51	1.47	0.36	0.11	0.06	2.00	0.14
C42021	46.5	22.4	6.00	5.00	.40	1.76	5.70	87.76	3.48	0.52	1.46	0.34	0.14	0.03	1.96	0.26
D27041	46.5	22.4	5.50	3.80	.80	.52	5.00	84.52	3.53	0.47	1.54	0.31	0.11	0.07	2.03	0.08
D27091	46.5	22.4	7.50	3.80	.27	1.86	5.20	87.53	3.46	0.54	1.42	0.42	0.11	0.02	1.97	0.27
D27111	46.5	22.4	7.70	3.50	.54	1.75	5.20	87.59	3.45	0.55	1.41	0.43	0.10	0.04	1.98	0.25
D27141	46.5	22.4	7.20	3.50	.62	1.17	5.20	86.59	3.48	0.52	1.45	0.41	0.10	0.05	2.00	0.17
D27161	46.5	22.4	6.00	4.00	.63	1.09	5.90	86.52	3.50	0.50	1.48	0.34	0.11	0.05	1.98	0.16
D27191	46.5	22.4	7.00	4.20	.73	.98	5.90	87.71	3.47	0.53	1.43	0.39	0.12	0.06	2.00	0.14
D27211	46.5	22.4	7.50	3.80	.61	2.40	5.50	88.71	3.43	0.57	1.38	0.42	0.10	0.05	1.95	0.34
E90011	46.5	22.4	7.70	4.70	.52	.23	6.10	88.15	3.46	0.54	1.43	0.43	0.13	0.04	2.03	0.03
G33011	46.5	22.4	6.80	4.40	.46	1.31	5.30	87.17	3.48	0.52	1.45	0.38	0.12	0.04	1.99	0.19
G33031	46.5	22.4	8.00	3.50	.79	1.63	5.00	87.82	3.44	0.56	1.40	0.45	0.10	0.06	2.00	0.23
G33141	46.5	22.4	7.40	3.50	.88	1.23	4.60	86.51	3.47	0.53	1.44	0.42	0.10	0.07	2.03	0.18
J67021	46.5	22.4	7.40	4.20	.53	.79	5.70	87.52	3.47	0.53	1.44	0.42	0.12	0.04	2.01	0.11
O09021	46.5	22.4	7.90	2.90	.87	1.05	5.40	87.02	3.46	0.54	1.42	0.44	0.08	0.07	2.01	0.15
O09031	46.5	22.4	6.90	4.30	.61	.61	5.60	86.92	3.48	0.52	1.46	0.39	0.12	0.05	2.02	0.09
O09061	46.5	22.4	7.50	4.10	.51	1.97	5.40	88.38	3.44	0.56	1.40	0.42	0.11	0.04	1.97	0.28
O09091	46.5	22.4	6.90	4.30	.40	1.61	7.00	89.11	3.45	0.55	1.40	0.38	0.12	0.03	1.94	0.23

* - calculated compositions are a mixture of discrete illite and mixed-layer I/S. SiO₂ and Al₂O₃ values are from Ko (1992). See text for details.

TABLE 5 - CALCULATED MINERAL ABUNDANCES IN CLAY FRACTION								
I.D.#	DEPTH (m)	QTZ	KAO	CHL	I/S	ANA	APA	SUM
	(corrected)							
A06031	1762	4	20	6	70	0.87	0.31	101.18
C42021	2881	5	18	4	71	0.91	0.50	99.41
D27041	2108	8	21	7	62	1.06	0.52	99.58
D27091	2672	5	22	10	59	1.10	1.11	98.21
D27111	2749	7	23	5	61	1.07	0.80	97.87
D27141	3071	7	18	7	65	1.15	0.85	99.00
D27161	3375	5	14	6	72	1.03	0.92	98.95
D27191	3803	3	15	8	74	1.23	0.42	101.65
D27211	4131	2	4	4	87	1.10	0.76	98.86
E90011	3452	1	9	10	82	1.29	0.54	103.83
G33011	952	6	20	7	66	1.12	0.33	100.45
G33031	1640	8	12	7	69	1.08	0.40	97.48
G33141	2533	8	8	19	61	1.09	0.68	97.77
J67021	4006	7	11	8	74	1.24	0.59	101.83
O09021	1533	8	19	3	61	1.21	0.40	92.61
O09031	1765	7	14	7	70	1.15	0.47	99.62
O09061	3866	1	11	9	77	1.20	0.57	99.77
O09091	4861	5	16	1	79	1.06	0.40	102.46
QTZ = quartz, KAO = kaolinite, CHL = chlorite, I/S = mixed-layer illite/smectite plus discrete illite, KSP = K-feldspar, ANA = anatase, APA = apatite								

TABLE 6 - CALCULATED WHOLE ROCK MINERALOGY (in wt%)														
I.D.#	DEPTH (m) corrected	QTZ	KAO	CHL	ALB+	I/S#	PYR	APA	ANA	SID	CAL	DOL	TOC	SUM
A06031	1762	39	9	4	1	40	0.3	0.5	0.9	0.7		0.7	1.03	96.82
C42021	2881	29	7	4		47	0.1	0.6	0.9	5.6	0.5		2.06	97.28
D27041	2108	41	9	4		40	0.3	0.6	0.8	0.9		1.0	0.72	98.56
D27091	2672	32	10	4	1	41	0.1	1.0	1.0	5.5	0.8		1.96	97.79
D27111	2749	36	11	3	1	37	0.2	0.9	0.9	6.0	0.8	0.7	1.58	98.01
D27141*	3071	40	10	2	0	36	0.2	0.9	0.9	4.9	0.6	0.7	1.37	98.29
D27161*	3375	36	9	2	1	38	0.6	1.0	0.8	7.8		2.1	1.31	99.50
D27191*	3803	30	11	5	2	44	1.4	0.6	0.9	4.0	0.8		0.87	99.47
D27211*	4131	27	2	6		55	1.7	1.1	1.0	3.4	0.5		1.84	99.50
E90011*	3452	37	8	5	1	41	0.2	0.8	0.9	3.6	0.4		1.25	98.70
G33011	952	44	9	3		37	0.2	0.5	0.9	1.7	0.3		1.63	98.28
G33031	1640	27	9	6	1	47	0.3	0.8	0.9	3.7	0.8		1.15	98.13
G33141	2533	38	7	3	1	40	0.2	1.0	0.9	6.3	0.3	0.9	0.61	99.03
J67021*	4006	40	6	4	0	40	0.1	0.9	0.8	5.0	0.7		1.06	98.51
O09021	1533	58	3	3		29	0.7	0.5	0.7	0.2		1.6	1.00	98.00
O09031	1765	27	8	7	1	44	1.2	0.7	0.9	0.0		1.1	4.51	96.34
O09061*	3866	32	8	4	2	43	0.3	1.1	1.0	5.2	0.5		1.16	97.62
O09091*	4861	34	8	3	1	48	0.8	0.5	1.0	2.5		0.2	0.79	98.90
+ - 0 indicates calculated trace amount (< 0.5 wt%) rounded off; blank indicates calculated zero value.														
# - I/S is a mixture of discrete illite and I/S.														
* - overpressured samples. All others are normally pressured (see Issler and Katsube, 1993).														